Design and Prototype Validation of a Laterally Mounted Powered Hip Joint for Hip Disarticulation Prostheses

Sarah Mroz

Thesis submitted to the Faculty of Engineering
in partial fulfillment of the requirements for the degree of

MASTER OF APPLIED SCIENCE

in Biomedical Engineering

University of Ottawa

Ottawa, Ontario

April 2023

Abstract

Powered prostheses are at the forefront of prosthetic technology, improving functionality by providing positive power to joints in the absence of native anatomy. Currently, there is no commercially available powered solution for hip-level amputees, and most hip prostheses are mounted to the front of the prosthetic socket. This thesis designed, fabricated, and tested a novel Laterally Mounted Powered Hip Joint (LMPHJ) that augments user gait to promote improved walking patterns. The LMPHJ attaches to the lateral side of the prosthetic socket, locating the hip centre of rotation closer to the anatomical location while ensuring user safety and stability. The new design locates the motor and all electronics in the thigh area, thereby maintaining a low profile while transmitting the required hip moments to the joint centre of rotation. A prototype was designed and manufactured to evaluate LMPHJ performance. Mechanical testing followed the ISO 15032:2000 standard and successfully demonstrated the joint's resistance to everyday loading conditions. Functional testing involved integrating the LMPHJ, Ossur Rheo Knee, and Ossur Pro-Flex XC with a prosthesis simulator that allowed three able-bodied participants to walk with the powered prosthesis successfully. This validated the mechanical design for walking over level ground and demonstrated that the LMPHJ is ready for next phase evaluation with hip disarticulation amputee participants.

Table of Contents

Table of Figures

List of Tables

Definitions

Abduction	The movement of a limb or other part away from the midline of the body
Adduction	The movement of a limb or other part toward the midline of the body
Amputee	A person who has had a limb amputated
Ambulation	The action of moving about or walking
Anterior	To the front of the body
Centre of mass	Point representing a body's mean position of mass
Distal	Away from the rest of the body
External moment	Moment applied from outside the body
Gait cycle	Interval between any repetitive events of walking
Frontal plane	Divides the body into front and back (aka, coronal plane)
Ground reaction force	Reaction force from the ground applied to the foot
Hemipelvectomy	Amputation of the lower limb that involves removal of part of the pelvis
Hip Disarticulation	Amputation of the lower limb through the hip joint
Internal moment	Moment generated by muscles and/or ligaments
Internal rotation	Rotation about long axis, with anterior surface moving medially
Kinematics	Joint or body segment movements
Kinetics	Forces and moments that produce movement
Lamination	A laminated structure of carbon fibre fabrics
Lateral	Away from the midline of the body
Medial	Towards the midline of the body
Posterior	To the back of the body
Prosthetic	An artificial body part
Proximal	Towards the rest of the body
Power	Rate at which work is done or energy is expended
Sagittal plane	Divides the body intro right and left
Stance	Gait cycle phase when foot contacts the support surface
Step	Foot strike of one extremity to foot strike of opposite extremity
Stride	Foot strike of one extremity to next foot strike of same extremity
Swing	Gait cycle phase without foot contact on the support surface
Transverse plane	Divides the body into upper and lower
Unilateral	Affecting only one side of the body

Nomenclature

2D	Two-Dimensional
3D	Three-Dimensional
A_s	Shear area
A_t	Tensile stress area of screw
CAD	Computer Aided Design
COM	Centre of Mass
FDM	Fused Deposition Modeling
FEA	Finite Element Analysis
GC	Gait Cycle
GRF	Ground Reaction Force
HD	Hip Disarticulation
HDA	Hip Disarticulation Amputee
HDP	Hip Disarticulation Prosthesis
HKAF	Hip-Knee-Ankle-Foot P
HP	Hemipelvectomy
HPA	Hemipelvectomy Amputee
I	Moment of Inertia
ISO	International Organization for Standardization
J	Polar moment of inertia
k_a	Surface condition modification factor
k_b	Size modification factor
k_c	Load modification factor
k_d	Temperature modification factor
k_e	Reliability factor
k_f	Miscellaneous-effects modification factor
K_f	Stress concentration factor in bending
K_t	Stress concentration factor in torsion
L_e	Thread engagement length
LMPHJ	Laterally Mounted Powered Hip Joint
M	Moment
n	Factor of Safety
r	Radius

RCM	Remote Centre of Motion
ROM	Range of Motion
S_e	Endurance limit
S_e’	Endurance limit at critical location
S_{ut}	Ultimate tensile strength
S_y	Yield strength
T	Torque
TF	Transfemoral
q	Notch sensitivity
ω	Angular velocity
α_v	Multiplying factor based on thread class
$\sqrt{a}$	Neuber constant
γ_{M2}	Partial safety factor
σ	Normal Stress
σ_{sy}	Shear strength
σ’	von Mises Stress
τ	Shear stress

Acknowledgments

First, I would like to thank my two supervisors, Dr. Edward Lemaire and Dr. Natalie Baddour, for their guidance, support, and encouragement throughout my research. Secondly, thank you to all the staff at Össur who supported this project. A special thank you to David Langlois, who has provided continuous feedback, support, and industry expertise. Additionally, to Gudni Ingimarsson and Aron Ingi Ingvason for their assistance during the review, assembly, and testing processes. Thank you to Prof. Patrick Dumond from the University of Ottawa for his mechanical expertise and assistance throughout the design process. Finally, thank you to Prof. Julie Nantel from the University of Ottawa for access to the Movement Performance Laboratory. Without the help of these knowledgeable individuals, I could not have achieved the outcome of this thesis.

I would like to say a big thank you to the entire Power Hip Research Team at the University of Ottawa. To Kelly Brannen for her knowledge sharing of previous research conducted, continuous teamwork, and for being a willing weekend adventure partner during our time in Iceland. Thank you, Hossein Gholizadeh, for his guidance through many conceptual designs and commitment to the project. Thank you to Farshad Golshan for his dedication and hard work on the control system. To Yousef Bader for his assistance with assembly and Michael Botros for his positivity and collaboration throughout the project.

Lastly, I would like to thank my family and friends. Mom and Dad, thank you for your continuous support and encouragement throughout all my academic pursuits. To my friends near and far, your visits, calls, and moral support kept me sane throughout these two years. Finally, thank you to my amazing partner Scott Goyetche who has been incredibly selfless, supportive, and patient as I completed this chapter of my academic career.

Chapter 1: Introduction

In the absence of native anatomy, prosthetic devices are often used to maintain mobility, independence, and quality of life for a person with a lower limb amputation. Prosthetic device design is challenging since the device becomes more complex as the amputation level increases. Hip disarticulation amputation (HDA), amputation through the hip joint, and hemipelvectomy amputation (HPA), amputation of part of the pelvic bone, are the highest levels of lower limb amputation, requiring prosthetic hip, knee, and ankle joints [1], [2]. Amputation level is significantly correlated with reduced motor function and increased metabolic cost during ambulation [3]–[5], resulting in severe mobility issues for these high-level amputees.

Hip-level amputees are met with large physical demands when using a prosthetic device. For this reason, HDA and HPA often opt for wheelchairs or arm crutches for ambulation. Those who use a prosthesis rely on lumbar spine movement for propulsion, accompanied by a heavier device than lower amputation levels, which imposes increased energy expenditure when walking [5]. Gait patterns are highly asymmetrical, walking speed is reduced, and range of motion (ROM) is limited when walking with a prosthetic limb [6].

Currently, most prosthetic hip joints on the market are mounted to the front of the prosthetic socket, positioned away from the anatomical joint centre. Commonly used devices include single-axis passive joints (ex. Ottobock 7E7) and the more advanced Ottobock Helix^{3D}, a polycentric joint that uses hydraulic stance control and flexion assist springs to improve amputee gait [7], [8]. Powered solutions are commercially available for knee and ankle joints, enabling walking mechanics closer to natural gait, thereby improving mobility and quality of life for prosthesis users [9]–[11]. Opportunities exist to explore hip-level powered prosthesis designs that locate the joint centre of rotation closer to the anatomical hip centre.

In this thesis, the mechanical design, fabrication, and validation of a laterally mounted powered prosthetic hip joint (LMPHJ) were completed to align the joint center to its anatomical position and provide powered assistance to augment user gait. Preliminary engineering calculations and finite element analysis (FEA) simulations were conducted with ISO 15032:2000 safety and structural requirements. Mechanical testing of a fabricated prototype was completed to ensure the device was appropriate for human use. Functionality was assessed through a 3D-printed prototype and a final design prototype using a hip prosthesis simulator with able-bodied participants.

1.1 Rationale

Powered prosthetics are advancing towards a future where an artificial limb will mimic the biomechanical function it is replacing. However, prosthetic hip joints have not kept pace with these developments [12], [13]. Currently available prostheses consist of passive devices that do not meet the needs of people with HDA or HPA. Walking with these prostheses can be difficult, leading to approximately 43% of amputees abandoning their prostheses shortly after being fitted [5], [13].

Improved mechanical functionality has been implemented into hip-level prosthetics by introducing the Helix^{3D} (Ottobock®) combined with microprocessor-controlled knee joints. This polycentric joint with a hydraulic unit improved amputee gait over previous devices [14]; however, the Helix^{3D} is a passive joint that maintains a mounting orientation to the front of the prosthetic socket. Without augmentation, amputees must generate hip movement through pelvic and back muscles, which can lead to long-term injuries [7].

Powered assistance and a laterally mounted orientation will provide hip-level amputees with a prosthetic system that enables more natural hip movement during gait. Powered prostheses, including knee and ankle joints, have demonstrated safe and efficient mobility for amputees [9], [15]. These active joints increase gait symmetry, minimize the risk of back injury, and improve the viability of safe, long-term prosthetic use [15]. The LMPHJ should promote more symmetrical loading across the hip joints and reduce the person’s energy expenditure. Accompanied by a customized control system, the amputee should feel confident and comfortable using the device.

Mobility, independence, and quality of life for people with HDA and HPA should improve with more advanced biomimetic prosthetic designs. A more functional device can provide amputees with improved, safer mobility, and this technology can enable users to participate more effectively in their daily lives.

1.2 Objectives

The objectives of this thesis are:

1. Design a laterally mounted powered hip joint
2. Manufacture a prototype device
3. Verify joint structural integrity
4. Assess joint functionality and usability
5. Validate the design through hip prosthesis simulator testing

1.3 Thesis contributions

Throughout this thesis, an innovative powered hip joint was developed, providing novel contributions to prosthetic design and wearable robotics. These contributions include:

- A novel laterally mounted powered hip joint prosthesis was developed to provide the hip moments required for more natural gait patterns. The lateral mounting orientation improved symmetrical loading across limbs compared to traditional front-mounted joints. Positive power generation enables safe and controlled movement compared to strictly mechanical systems.
- A pulley system drivetrain was created to position the electrical components in the usable space beneath the prosthetic socket (i.e., thigh segment), resulting in a more aesthetically pleasing design. The LMPHJ configuration better represents the anatomical structure of a lower limb and fits comfortably beneath clothing.
- ISO standard testing requirements were adapted to evaluate the laterally mounted system under maximum loading conditions. The testing protocol can be replicated in other labs.
- The LMPHJ demonstrated a wider ROM than front-mounted systems, enabling improved mobility across various terrains, sitting, reaching, etc.
- A new customized simulator that enables able-bodied people to walk with a hip-knee-ankle-foot (HKAF) prosthesis was developed for this project. The LMPHJ demonstrated the simulator's utility in testing hip prosthesis innovations.
- Mechanical and functional testing with a HKAF prosthesis using the new simulator validated the LMPHJ's ability to improve walking patterns. It confirmed that the design is ready for the next steps to test with hip amputee participants.

1.4 Thesis outline

This thesis consists of seven chapters. Chapter 2 presents the reviewed literature, which forms foundational knowledge of relevant anatomy, biomechanical parameters, hip-level amputations, and available prostheses. Chapter 3 outlines the system's functional and non-functional requirements for evaluating the design. Chapter 4 reviews the engineering design process followed, including several candidate designs, engineering analysis, details of the final configuration, and prototyping. Chapter 5 discusses the mechanical testing methods, along with a discussion of the results. Chapter 6 covers the functional testing completed highlighting the methodology, results, and discussion. Chapter 7 concludes this thesis and makes recommendations for the future of this research.

Chapter 2: Literature Review

This review was completed to gain an understanding of hip-level amputations, lower limb biomechanics during daily activities, and available prosthetic systems on the market.

2.1 Anatomical References

In research and clinical practice, anatomical terminology describes the orientation, direction, movement, location, or physical part of the human body. Foundational knowledge of this terminology enables clear communication of ideas.

2.1.1 Anatomical Planes

A two-dimensional section of a 3-dimensional object can be referred to as a plane. Three anatomical planes are commonly used to describe the human body: frontal plane, sagittal plane, and transverse plane (Figure 2-1). The frontal and sagittal planes are perpendicular to one another along the body's long axis. The transverse plane is orientated 90 degrees from the long axis [16]. Concerning the frontal plane, the anterior direction is towards the front of the body and posterior towards the back. Towards the center of the body is the medial direction, and away from the sagittal plane is lateral. The transverse plane divides the superior and inferior portions of the body [17]. The proximal direction is toward the body's center, and the distal is away from the body's center.

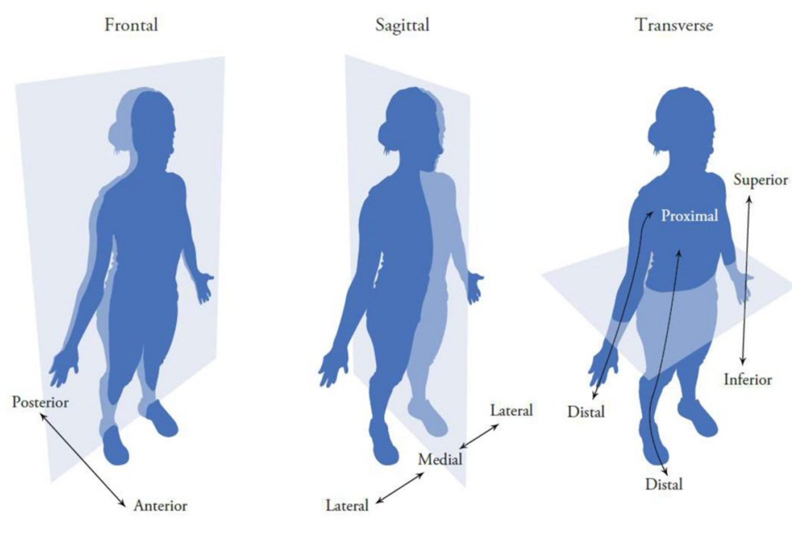

Figure 2-1: Anatomical directions in reference to respective anatomical planes (Adapted from [17])

2.1.2 General Motion

For body movements (Figure 2-2), flexion and extension describe the angle between two body parts, with flexion decreasing the angle between segments and extension increasing the angle. Abduction and adduction occur in the frontal plane, with abduction moving away from the body's midline and adduction moving towards the midline. Rotations around the body's long axis are internal rotation toward the center of the body and external rotation away from the body centre [17].

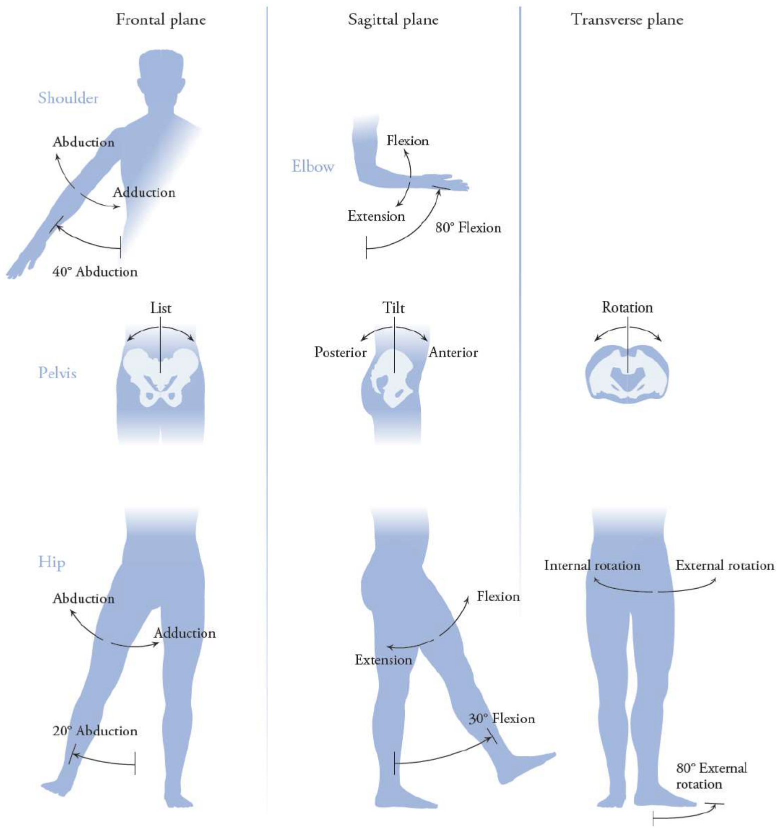

Figure 2-2 Anatomical movements (Adapted from [17])

2.1.3 Hip Anatomy

The pelvis provides structural support, load-bearing capabilities, and stability during daily activities [18]. The bony pelvis (Figure 2-3) has an anterior portion comprised of the sacrum and coccyx and a posterior portion with two hip bones. Each hip bone forms part of the pelvis and consists of an ilium, pubis, and ischium. The pelvis connects the spine to the lower limbs [18].

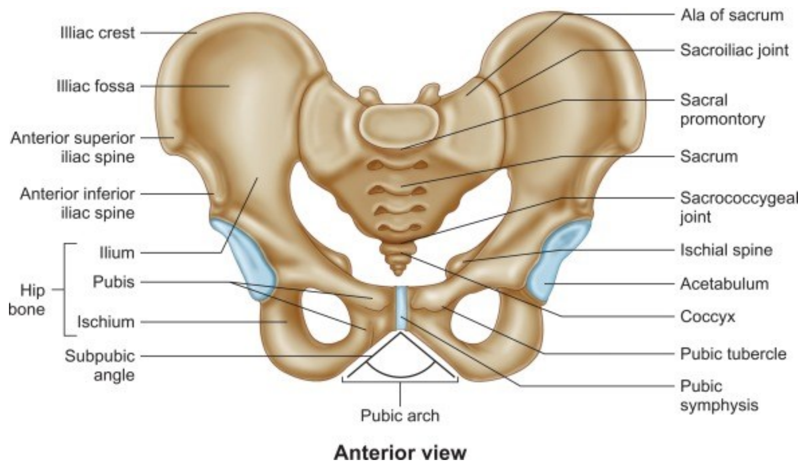

Figure 2-3: Bony pelvis anatomical features (Adapted from [19])

The hip joint is a ball and socket joint where the femoral head articulates with the acetabulum [20]. It is one of the most dynamic joints in the body, with an extensive ROM secondary to the shoulder joint [21]. The hip plays a vital role in routine activities such as standing, walking, and sitting. While considered basic movements, large bony structures and muscular support are required to maintain stability and meet the ROM requirements for ambulation.

2.2 Hip Disarticulation and Hemipelvectomy Amputees

Lower limb amputation involves removing part of the leg, often due to trauma, disease, or cancer. Limb loss is also a result of congenital limb deficiencies [8]. The absence of native anatomy affects a person's motor function and increases the metabolic cost for ambulation [3]–[5]. Amputation level dramatically affects the ability to walk using a prosthesis after a lower-limb amputation [1].

HDA and HPA are the highest levels of lower limb amputation. Balance and control throughout gait become challenging, in addition to the physical burden of carrying the device weight [1], [5]. These factors contribute to increased energy when performing daily activities, slower walking speeds, and asymmetric gait patterns. Hip-level amputees walk 40-50% slower and have 80%-125% increased energy expenditure compared to able-bodied individuals [3].

Hip-level amputations account for only 0.5% of lower-limb amputations; hence, less research is available on hip disarticulation (HD) and hemipelvectomy (HP) prostheses and rehabilitation [22]. According to a recent review by Gholizadeh et al. [23], since 1950, only 53 articles have evaluated HD and HP prostheses.

2.3 Walking Gait Cycle

Walking is a repetitive motion humans use to move about. The gait cycle (GC) is composed of two main phases: swing and stance. Stance phase accounts for approximately 60% of the GC and is the period when the foot is in contact with the ground. Single support is when only one foot is contacting the ground. Double support is when both feet are on the ground [17]. Swing phase is when the foot is off the ground.

A complete gait cycle (Figure 2-4) is the time between two consecutive instances of a recurring event, typically beginning and ending with foot strike of the same foot. Each event or functional phase is often referred to as a percentage of the total GC. A complete GC is as follows [24]:

- **Initial contact** (0% - 2%): GC initiation when the foot first contacts the ground and weight acceptance on this leg begins. This is also the start of stance phase and double-support.
- **Loading response** (2% - 12%): More of the foot contacts the ground, and weight acceptance continues.
- **Midstance** (12% - 31%): The start of single-support. During midstance, the ankle and hip joint centers are aligned. The body center of gravity reaches its highest point as the base of support is greatly reduced, and stability becomes more challenging.
- **Terminal stance** (31% - 50%): The second part of single-support.
- **Pre-swing** (50% - 60%): The second double-support phase and second loading period. The heel begins to lift off the ground.
- **Initial swing** (60% - 73%): The initial part of swing phase where the foot lifts off the ground and flexion begins to ensure toe clearance.
- **Midswing** (74% - 87%): Second part of the swing phase. Stability is more challenging because the contralateral leg is in single support.
- **Terminal swing** (87%- 100%): Flexion continues, swinging the leg forward to prepare for foot contact.

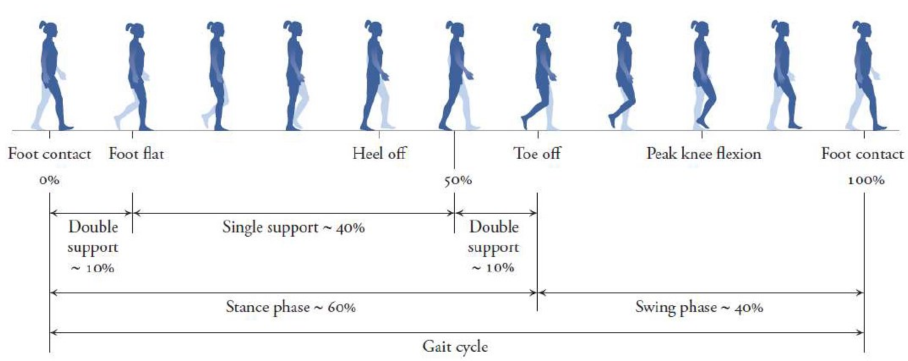

Figure 2-4: A complete gait cycle (Adapted from [17])

2.3.1 Ground Reaction Forces

Newton's third law states, "for every action, there is an equal and opposite reaction." During walking, our body's forces on the ground are reciprocated and referred to as ground reaction forces (GRF). In biomechanics, measuring these forces provides valuable data to characterize body movement. The GRF vertical component rises rapidly after initial contact and continues to rise throughout the loading response, above one times bodyweight [17]. GRF drops below bodyweight during midstance before rising again during terminal stance, where the foot pushes off the ground (Figure 2-5).

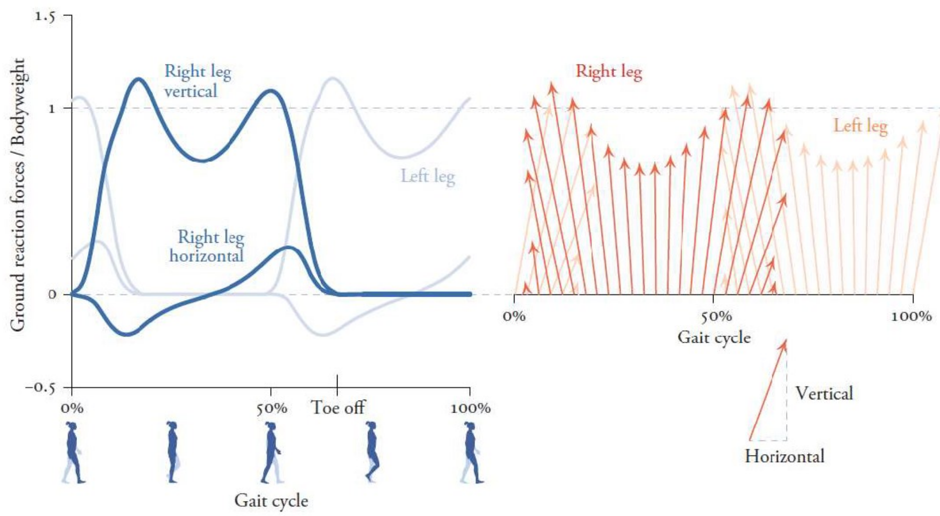

Figure 2-5: Ground reaction forces throughout one gait cycle (Adapted from [17])

2.4 Biomechanics

During gait, able-bodied people generate muscular activity to provide the power and moments required to ambulate. HD and HP amputees cannot entirely compensate for these kinetic requirements without these leg anatomical features. This presents the challenge of prosthetic design to produce a system capable of generating biomimetic behaviours through structural and functional aspects. To address an amputee's needs, an understanding of amputee gait biomechanics will help form design requirements. Since amputees have many biomechanical deviations in their gait patterns compared to able-bodied individuals, determining why specific compensation strategies are used can assist in designing a more suitable prosthetic system.

2.4.1 Range of Motion

When completing daily activities, prosthetic limb range of motion (ROM) is typically less than the contralateral side, contributing to asymmetrical gait patterns. For able-bodied individuals, hip ROM is approximately 50°. For a hip-level amputee, Schnall et al. [25] reported 20.7° mean flexion and 12.2° mean extension for a 32.9° ROM. This is compared to 58.4° mean ROM on the participant's sound side. Showing a similar trend for hemipelvectomy amputees, Karimi et al., [6] reported 27.3° mean ROM for the prosthetic side and 40.7° ROM for the sound side (Figure 2-6). This study attributed the reduced prosthetic side ROM to the hip's anterior mounting orientation. These results were measured during walking; however, other daily activities require an increased ROM, such as sitting, stair ascent, or bending down to tie a pair of shoes. For this reason, the more advanced Helix^{3D} has 130° maximum flexion [26].

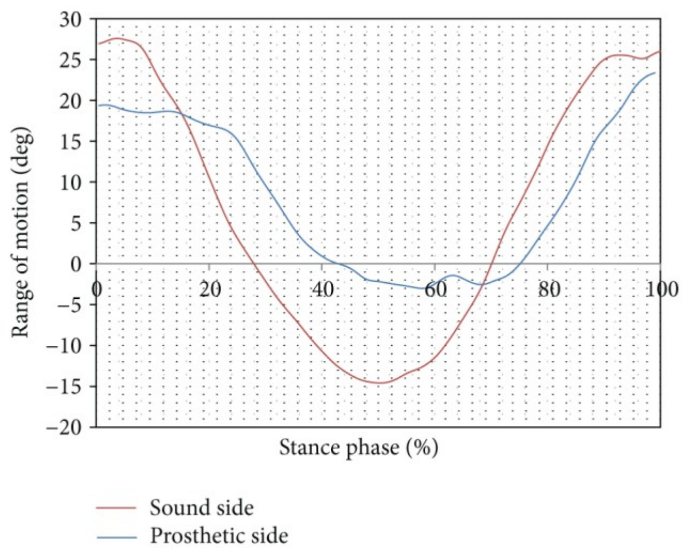

Figure 2-6: Hip range of motion during stance phase (Adapted from [6])

Increased pelvic tilt during gait can lead to back issues [7]. Amputees use this compensation strategy to advance the limb forward into the swing phase [27]. Figure 2-7 demonstrates this pattern compared to a control group of able-bodied individuals. It is hopeful that pelvic tilt will decrease with powered assistance.

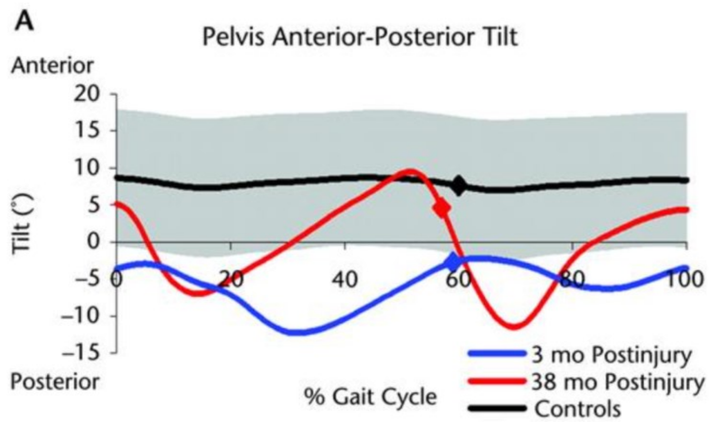

Figure 2-7: Pelvic tilt of HDA during level ground walking (Adapted from [25])

2.4.2 Temporal-spatial Parameters

Amputee walking speed is linked to increased energy expenditure. Self-selected walking speed for hip-level amputees is about 40%-60% slower than able-bodied individuals, imposing challenges to ambulate efficiently [5], [25]. A young soldier following a hip disarticulation had a 0.86 m/s walking speed over level ground [25]. People using an Otto Bock 7E7 and Helix^{3D} averaged 1.06 m/s walking speed [28], compared to approximately 1.4m/s for able-bodied individuals.

Slower walking speeds accompany shorter and inconsistent step lengths between the intact and prosthetic limbs. For the prosthetic side, the step length is typically in the range of 0.6 m - 0.7 m, compared to slightly greater lengths for their contralateral limb [5], [7], [25].

2.4.3 Kinetic Parameters

The high degree of asymmetry demonstrated in amputee gait patterns leads to asymmetrical loading across the sound and prosthetic limbs. Commonly, the intact limb supports bodyweight for more extended periods and under higher forces [25], [29]. The maximum vertical GRF at the prosthetic side is approximately bodyweight when walking (Figure 2-8) [25].

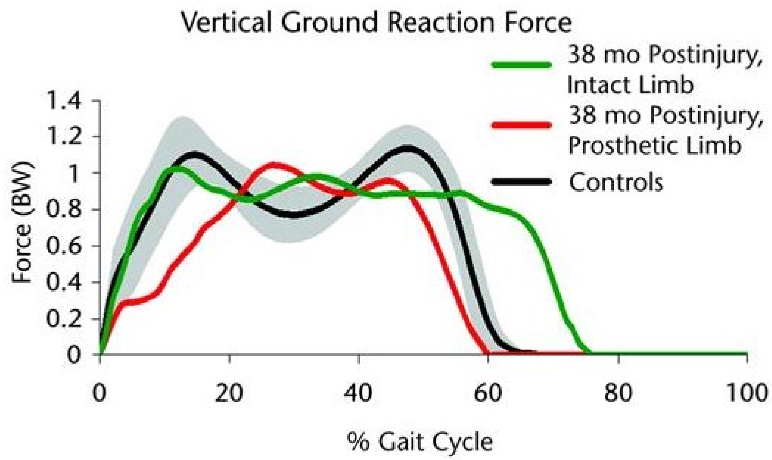

Figure 2-8: Vertical GRF for an HDA 38 months post-surgery during level walking (Adapted from [25])

Force asymmetry can increase during activities such as sit-to-stand, stand-to-sit, or stairs. In a study involving transfemoral (TF) amputees, GRF asymmetry was approximately 69% between limbs during the transition of sit-to-stand (Figure 2-9) [30]. During stair ambulation, asymmetry was approximately 45% [31]. With improved prosthetic systems, normalized ambulation should decrease these differences; therefore, the forces experienced by the prosthesis should be closer to the intact limb.

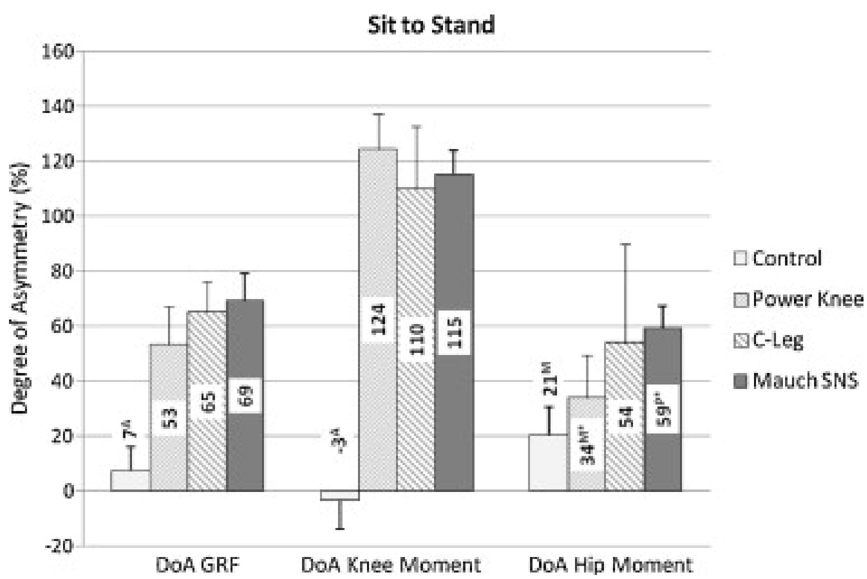

Figure 2-9: Degree of asymmetry measured during sit-to-stand task using various prosthetic knee joints (Adapted from [30])

Hip flexion moments are generated by muscular activity in able-bodied people. Amputees must rely on their prosthetic system for this functional element [7]. Demands vary across daily activities such as walking, inclined/declined walking, and stair ascent/descent. When comparing a microprocessor-controlled (C Leg®) and mechanical (Mauch SNS®) knee joint over level-ground walking, kinematic data showed peak hip moments of approximately 1.2Nm/kg for the C Leg® and 1.4Nm/kg for the Mauch SNS® (Figure 2-10) [29]. Hip moments are generally large during sit-to-stand tasks; however, amputees load their sound limb almost entirely until the task is near complete [10]. In a study involving TF amputees using a powered knee joint, hip moments on the prosthetic side were 0.46 +/- 0.19 Nm/kg [30]. In instances where amputees must rely on their prosthetic limb to overcome high moments, such as during inclined walking, hip moments are typically greater.

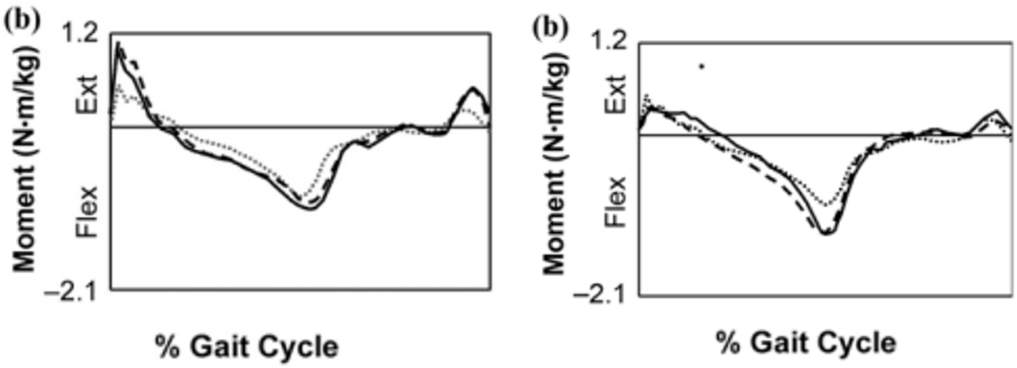

Figure 2-10: Hip moment on the intact limb (left) and prosthetic limb (right) when walking over level ground for people wearing C-Leg® (solid line), Manch SNS® (dashed line), and an able-bodied control group (dotted line) (Adapted from [29])

The hip is the most energy-intensive joint during gait [32]. Joint power is the product of the joint moment and angular velocity [29]. Hip-level amputees cannot generate power through hip muscle activity; therefore, it must be provided by other means. The hip power output of TF amputees can be considered to determine the power requirements of a powered hip joint. Segal et al. [29] reported hip power across eight participants, comparing two prosthetic knee joints over level-ground (Figure 2-11). A maximum peak sagittal-plane hip power of 0.83W/kg was measured, exceeding the intact side power output. This increased power was thought to compensate for the lack of power generated by the prosthetic ankle joint. In another study, looking at biomechanical factors in TF amputees when ascending and descending stairs and ramps, a maximum peak hip power generation of 2.4W/kg +/- 1.2W/kg was measured when climbing stairs with the Power Knee [33].

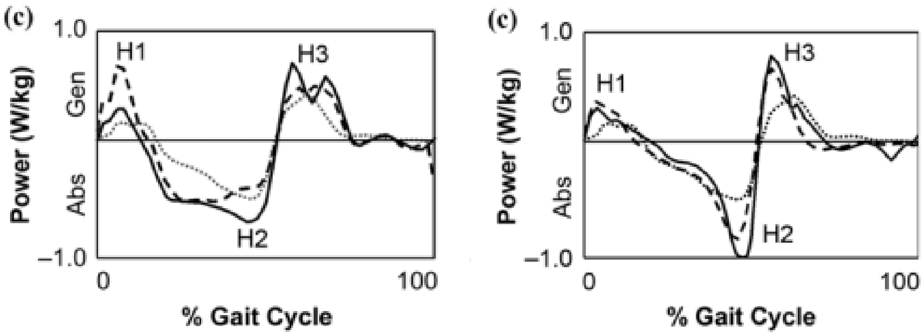

Figure 2-11: Hip power on intact limb (left) and prosthetic limb (right) when walking over level ground for people wearing C-Leg® (solid line), Mauch SNS® (dashed line), and able-bodied control group (dotted line). Gen = power generated, Abs = power absorbed, H1 = peak sagittal plane hip power in early stance (+), H2 = peak sagittal-plane hip power in mid-stance (–), H3 = peak sagittal-plane hip power in late stance (+). Positive (+) indicates power produced; negative (–) indicates power absorbed (Adapted from [29])

2.5 Hip Prosthesis Testing and Standards

Various tests must be executed to validate a prosthetic joint design to ensure the device meets the requirements, functions as intended, and complies with the appropriate international standards.

2.5.1 Structural Testing (ISO Standard)

Lower-limb prostheses experience large loads when in use and, therefore, must be designed to be sufficiently strong during daily activities. Structural testing is required to ensure safety and reliability. Prosthetic hip joint structural testing is governed by ISO 15032:2000 *Prostheses – Structural testing of hip joints* [34]. The standard includes static and cyclic loading, applied in two planes. The static tests represent worst-case scenario forces applied to the joint. Cyclic tests simulate the repetitive loading experienced during walking. Each test has multiple levels, with the highest including test loads for a 100kg user with adequate factors of safety [34].

2.5.2 CAD Simulations

Experimental structural testing is necessary to validate a designed prosthetic device; however, producing prototypes and conducting these tests can be costly and time-consuming. Determining mechanical behaviour is critical in the design process, and finite element analysis (FEA) is the most widely used numerical analysis to complete these evaluations through computational simulation tools [35]. The concept of FEA divides any complex object into a mesh of many small shapes, known as finite elements, that together accurately model the original part [36].

Using a 3D computer-aided design (CAD) model, structural testing can be simulated using FEA to identify failure points or optimize the part's weight and geometry before manufacturing. This tool is used for engineering applications and is frequently used in prosthetic development. In a study conducted by Phanphet et al. [37], the structural and fatigue testing outlined in ISO 10328 for knee prostheses was simulated prior to fabrication and testing, where the results confirmed the FEA predictions. Another study used FEA to determine the stress-strain behaviour of a prosthetic foot and associated components, with agreement found between FEA results and experimental testing [35].

2.5.3 Functional Testing

Hip prosthesis functional testing is often completed through quantitative and qualitative assessment of HDA or HPA participants. Traditional evaluation methods include quantitative measures of gait biomechanics [14], [1], [7] or energy cost [4], [5], and qualitative questionnaires [38].

2.5.3.1 Robotic Testing

Prosthetic evaluation through recruiting HDA or HPA participants is challenging when developing prosthetic devices. Common limitations include time-consuming evaluations, low repeatability, qualitative assessment reliability, participant recruitment due to the limited population, and risks associated with testing human participants [39]. To eliminate many of these barriers, Xinwei et al. [39] developed a Gait Simulation and Evaluation (GSE) system for hip prostheses evaluation (Figure 2-12). This robotic simulator replicated pelvic motions during a gait cycle and demonstrated the feasibility of using robotic testing to evaluate hip prostheses without participants. Robotic testing can offer advantages over traditional methods, including conducting tests in controlled conditions and repeated evaluation while eliminating the liability and risks associated with prostheses tests [39].

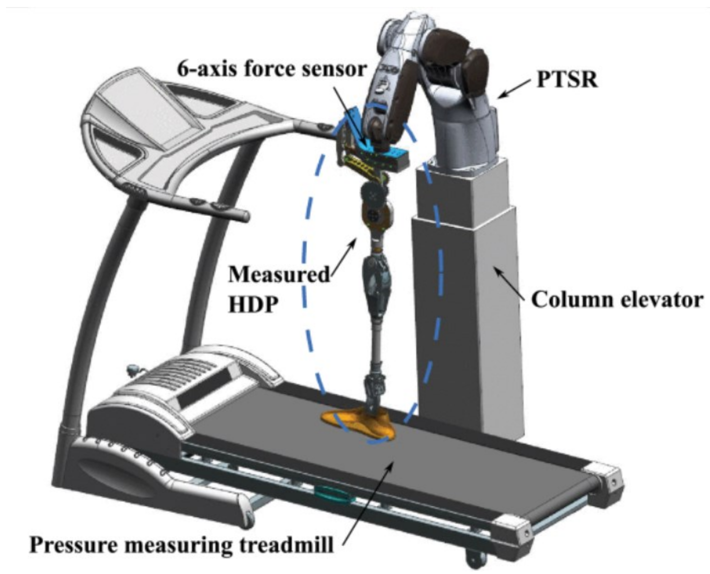

Figure 2-12: Gait Simulation and Evaluation System for hip prostheses (Adapted from [39])

2.6 Conventional Prostheses

Hip prostheses have evolved slowly, likely due to the low incidence of this level of amputation and the short life expectancy post-amputation in the past. Before the 1950s, traditional prosthetic devices for unilateral HDA or HPA were simple, single-axis or otherwise known as monocentric joints attached to the side of the pelvic socket, some with semi-automatic locks [40]. These were referred to as locked prostheses because the hip joint was locked during gait. A manual lever could be pressed to release the lock for sitting. The locked prostheses caused instability during walking and increased fall risk. In cases with no locks, prostheses were more challenging to control, and stability became a concern [40].

Traditional prostheses required large pelvis thrust, generated by spinal muscles, to propel the leg forward [41]. Hip flexion was achieved through this pelvic rotation of the prosthetic socket. Gait was described as awkward, jerky, and tiring [40]. The two main types of locked prostheses were saucer-type and tilting table prostheses.

As the name suggests, the saucer-type socket involves a saucer-shaped socket. The system comprised a single-axis joint, a pelvic strap, and often straps over the shoulders (Figure 2-13). Hip joint positioning was to the side of the socket but anteriorly to the acetabulum to provide a level of stability. This type was most suitable for amputees without a total hip disarticulation, meaning some residual bone was left that assists with stability [40].

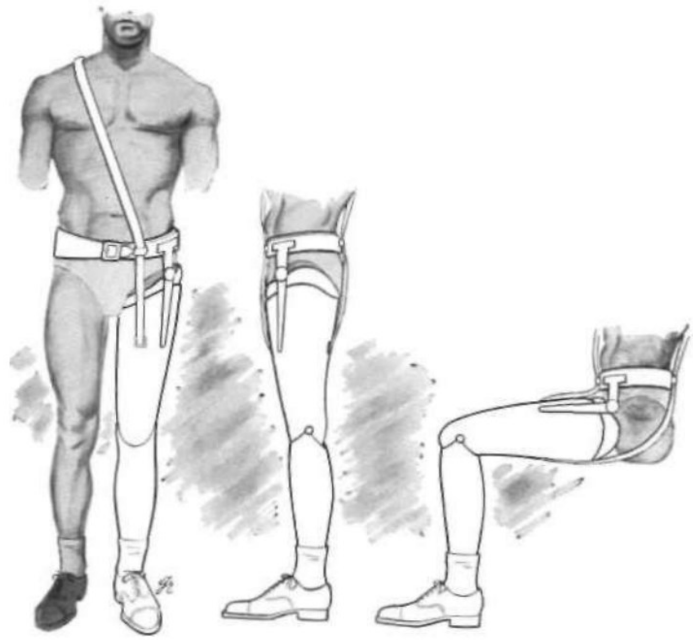

Figure 2-13: Saucer-type hip joint prosthesis (Adapted from [40])

Of the traditional prostheses, the tilting table (Figure 2-14) was more commonly used due to its additional support, offering increased stability for users. The socket was typically made of leather that wrapped around the stump and was secured with a belt and sometimes shoulder straps. A metal, single-axis joint was positioned at the anatomical hip joint center of rotation. Many variations of the tilting table prostheses were experimented with to assist in weight-bearing, including roller support, a latch mechanism, and positioning the hip joint beneath the socket [40].

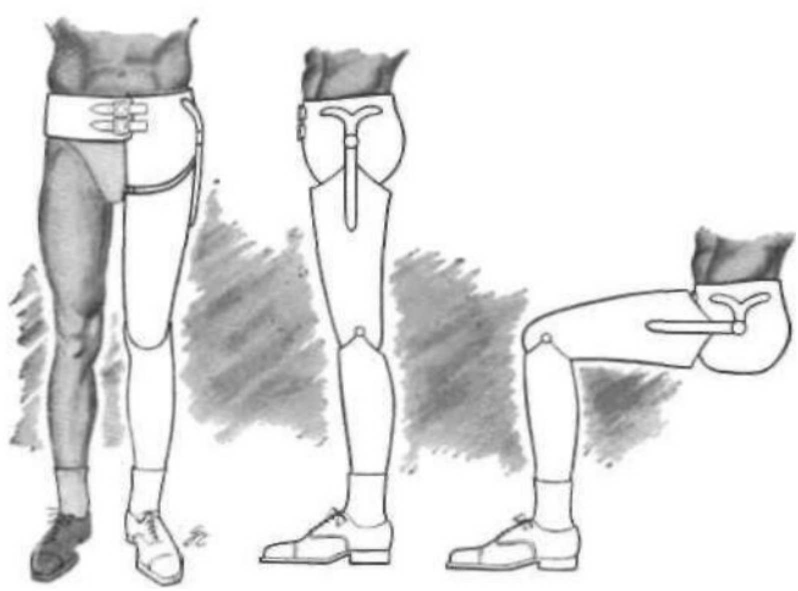

Figure 2-14: Tilting table hip joint prosthesis (Adapted from [40])

2.6.1 Single axis: Canadian Prosthesis

A Canadian rehabilitation engineer aimed to improve conventional hip prosthesis functionality. In 1954, what is now known as the Canadian-type hip disarticulation prostheses (Figure 2-15) was developed to avoid the stress concentrations in the locks and simplify the releasing mechanism [17]. The final design included two major changes, joint positioning and a new socket design.

The joint was mounted to the front of the prosthetic socket, anterior and distal to the acetabulum. Sagittal plane rotation was free but fixed in the medial/lateral direction to provide lateral support. This positioning results in the load line passing in front of the knee joint, preventing buckling and considerably increasing stability [42]. To eliminate the need for a hip-lock, a mechanical bumper was implemented to ensure hyperextension did not occur, and a hip-flexion limiter was incorporated only to allow enough flexion for walking [43].

A cast surrounding the residual limb was taken to to ensure an accurate fit. This formed the socket shape and was the start of a more user-specific approach to prosthetic fittings. An adjustable waistband was made from heavy elastic to ensure a secure but comfortable fit [43]. Together, this socket design increased user comfort and restricted residual limb movement within the socket.

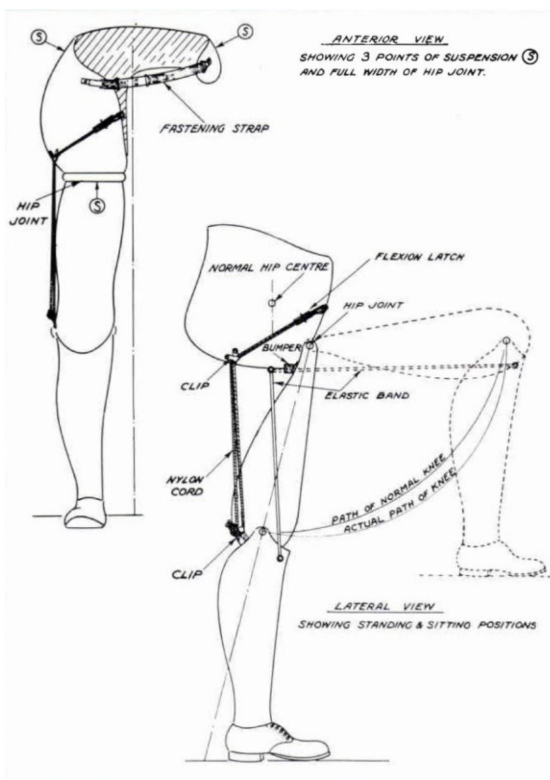

Figure 2-15: Canadian hip disarticulation prothesis (Adapted from [43])

Since the advent of the Canadian prosthesis, most hip prostheses are mounted to the front of the prosthetic socket, and previous concepts have become non-existent in the market [44]. Major modifications have been made to increase hip prosthesis usability and functionality; however, the basic concepts of these systems stem from McLaurin's design.

2.6.2 Hip Flexion Bias

One notable disadvantage of the Canadian prosthesis is that the leg length must be shorter than the intact leg to ensure foot clearance during swing phase. To address this, the Hip Flexion Bias system (Figure 2-16) was designed [45]. This design involved a spring in the joint's thigh segment that compressed during stance, storing potential energy. Kinetic energy would be released during swing, propelling the leg forward. The spring mechanism allowed for variable leg length, sufficient toe clearance, and stability at foot strike, contributing to improved gait patterns [45].

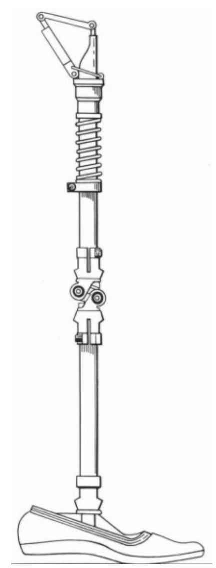

Figure 2-16: Hip Flexion Bias System (Adapted from [45])

2.6.3 Reversed Polycentric Knee Disarticulation Joint (Ottobock 3R21) as a Hip Joint

Another hip joint design variation to address the leg length problem involved using a polycentric knee disarticulation joint mounted in reverse (Figure 2-17). The four-bar linkage system (Ottobock 3R21) shortens throughout the gait cycle, increasing toe clearance during midswing and stability when the step is initiated [45].

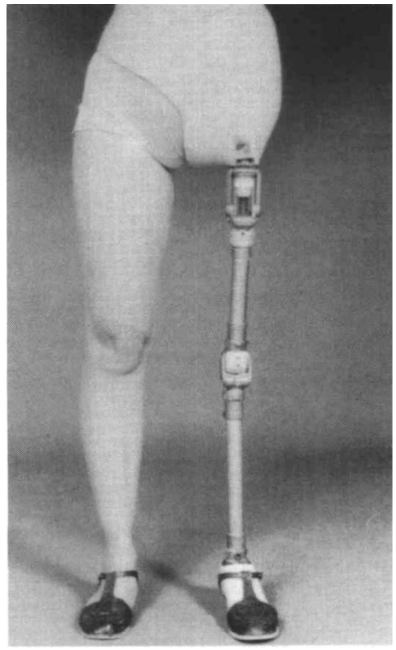

Figure 2-17: Reverse Polycentric Knee Joint (Adapted from [45])

2.6.4 Polycentric Hip Joint (Helix3D 7E10)

Today's most advanced prosthetic hip joint in the market is the Ottobock Helix^{3D} system (7E10). This polycentric joint has a hydraulic unit to control both swing and stance phase, and is mounted to the front of the prosthetic socket [14], [46]. Helix^{3D} (Figure 2-18) introduces more degrees of freedom, externally rotating during swing, and polyurethane springs to facilitate swing phase initiation [14]. Studies comparing functional outcomes to single-axis joints showed significantly improved gait patterns with Helix^{3D} [7], [28], including improved hip extension during stance, more controlled flexion during swing, improved knee function, and reduced pelvic tilt [7].

Figure 2-18: Ottobock Helix^{3D} Prosthetic Hip Joint (Adapted from [26])

2.7 Powered Lower-Limb Prostheses

Despite technological advances in prosthesis design and evidence indicating improved ambulation with the use of powered prostheses [9], most prosthetic devices are passive. Hip-level amputees require prosthetic hip, knee, and ankle joints to ambulate; therefore, each component should contribute the required functionality and power requirements to enable near-normative joint mechanics. Robotic prosthesis technology is still in the early stages of replicating the function of a missing limb; however, further powered prosthesis developments will assist in this becoming a reality.

2.7.1 Powered Ankle-Foot Prosthesis

While walking, the human ankle delivers high mechanical power and net-positive work to help propel the leg forward [9]. Commercially available robotic prostheses can meet these demands and deliver human-like ankle responses [9], [47]. For transtibial amputees that use a powered ankle, equivalent metabolic cost and step-step transitions compared to able-bodied individuals over level ground walking can be achieved [48]. These ankles generate power through a battery, thus lessening the energy expenditure required by users [49]. Adapting to different walking velocities and ambulating across different terrains and inclines is where the kinematic and kinetic function does not yet represent identical biological dynamics. However, a powered prosthesis can perform significantly better than commonly used passive alternatives [48], [50], [51].

2.7.2 Powered Knee Prosthesis

Transfemoral prostheses contain a knee joint that can be mechanical passive, microprocessor-controlled passive, or active. Powered knee prostheses provide positive power at the knee to improve biomimetic performance and restore mobility. In studies comparing a powered knee joint to a passive microprocessor knee during the sit-to-stand task, inclined/declined walking, and stair ambulation, the power knee improved function and reduced intact limb loads across these movements [10], [33]. Individuals requiring knee prostheses additionally require a prosthetic ankle joint/foot that can contribute to the effectiveness and functionality of a powered knee. In one study, researchers believed that a lack of gait symmetry achieved with a powered knee prosthesis was partially attributed to the prosthesis's limitations without a powered ankle [11]. This emphasized the importance of considering the prosthetic limb as a system that must function together.

While robotic technology in prosthetic knee joints is evolving, microprocessor-controlled knees are more commonly used. Microprocessor-controlled joints offer metabolic efficiencies compared to traditional mechanically passive devices [51], and ambulation can be achieved with few differences compared to powered systems [10]. However, passive devices have limited potential compared to powered devices to reduce metabolic costs and enable more natural gait patterns across various daily activities. These limitations are driving current and future research toward optimized robotic prostheses.

2.7.3 Powered Hip Prothesis

To date, no powered hip prostheses are commercially available to HDA and HPA. Two researchers have explored integrating robotics into hip-level prostheses. Hata et al. [52] proposed a powered hip disarticulation prosthesis that actuated the hip and knee joints with two electric motors. Limited evaluation of this prototype was completed, and no follow-up studies were performed; therefore, there was little contribution to determining the effects of a powered hip joint prosthesis on the person. More recently, Ueyama et al. [13] developed a robotic hip disarticulation prosthesis (Figure 2-19) to determine whether hip-level robotics improve HDA mobility. Biomechanical data were collected with the use of the robotic prosthesis, as well as a non-powered prosthesis, for comparison. Results indicated that improved gait patterns were achieved with the powered prosthesis. However, the experiments were conducted with a non-amputee, therefore, these findings cannot be directly translated to the target population [13].

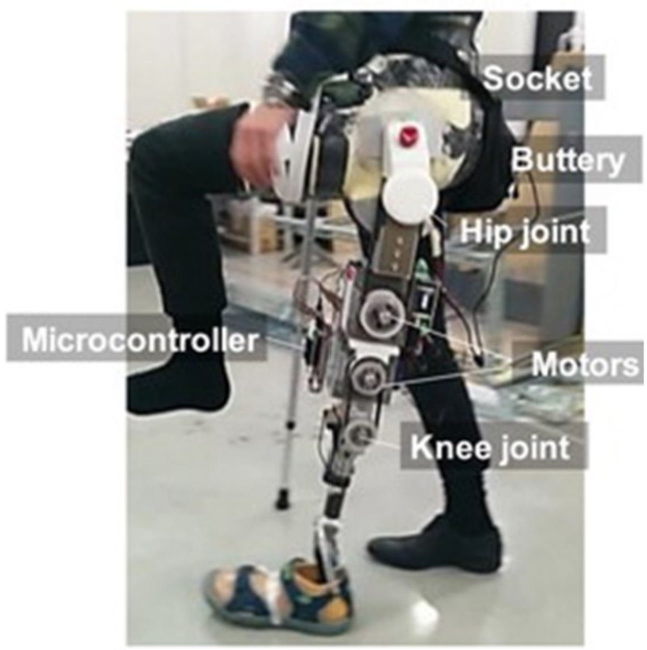

Figure 2-19: Powered hip prostheses tested by a non-amputee participant (Adapted from [13])

Although not explicitly designed for HDA, a study by Ishmael et al. [53] demonstrated reduced metabolic costs for TF amputees when walking with a powered hip exoskeleton (Figure 2-20). The metabolic cost savings were converted to a 12 kg relief from the user [53]. These findings suggested that providing hip assistance could improve walking economy for higher-level amputees. The exoskeleton's lateral alignment coincides with the similar orientation proposed in this thesis.

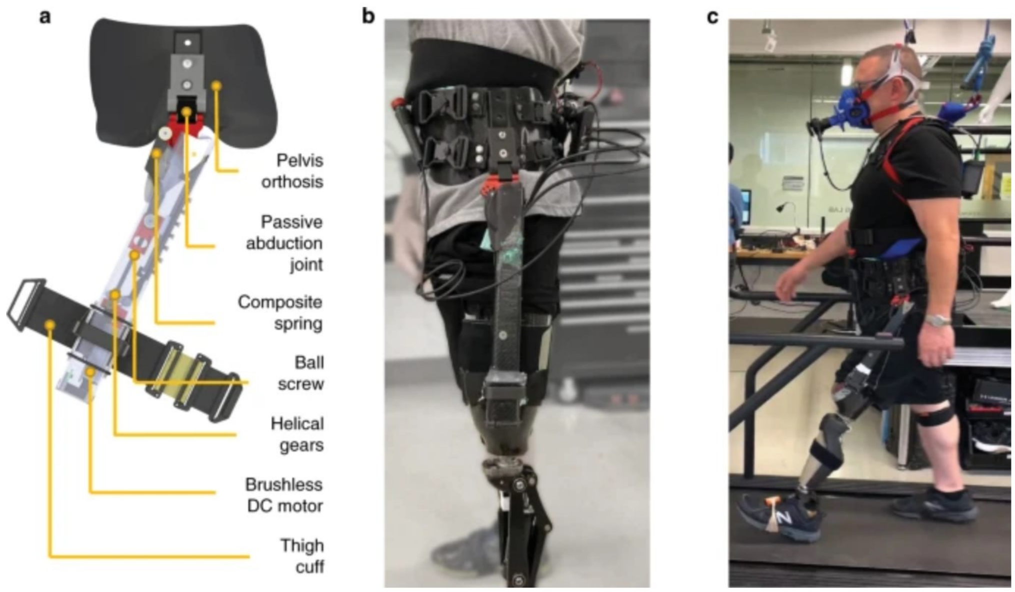

Figure 2-20: Powered hip exoskeleton to provide hip assistance for transfemoral amputee (Adapted from [53])

2.8 Prothesis Hip Joint Alignment

As discussed, most hip joint prostheses are mounted to the front of the pelvic socket, following the advent of the Canadian Prosthesis. This alignment permitted a stronger connection between the joint and socket, enabled hip joint motion, and improved stability over its locked joint predecessors. The unique orientation, located away from the joint center, ensures that when a load is transmitted between the foot and hip joint, the load line always passes in front of the knee joint (Figure 2-21). This provides knee security against buckling and remains stable unless it contacts the extension bumper. At the point of contact, as the hip progresses forward, the moment generated at the hip disturbs the stability of the knee joint, causing the hip to flex to begin swing phase [42]. While this mounting orientation has been successful for over half a century, the contrasting axis of rotation between the prosthetic and sound limb is limiting for a more symmetrical gait pattern.

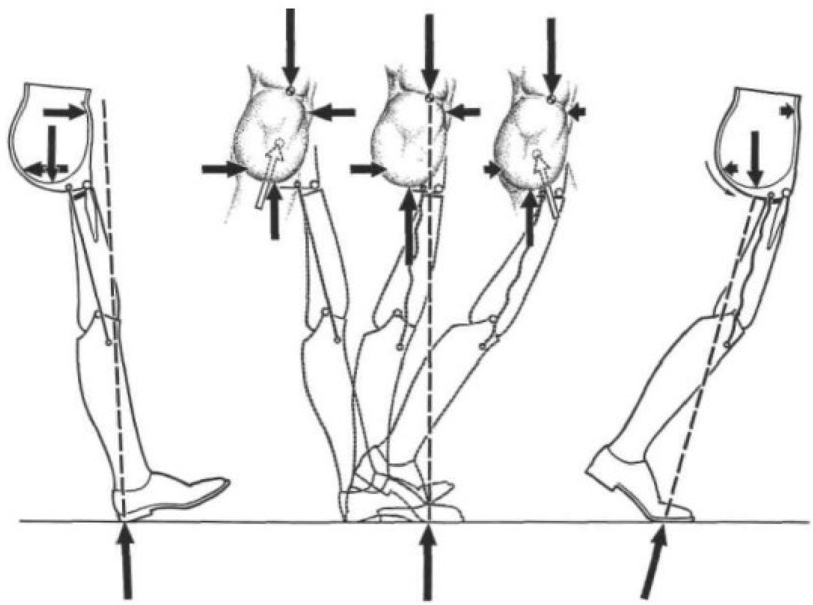

Figure 2-21: Load line of front-mounted hip prosthesis in the sagittal plane (Adapted from [42])

2.8.1 Laterally Mounted Hip Joints

As discussed in Section 2.6.1.2, the tilting table prosthesis metal joint was positioned laterally to the acetabulum. While joint alignment coincided with the anatomical joint center, there were common problems with weight-bearing, stability, and functionality [40]. These concerns are not thought to translate directly to the concept of this thesis because structural, safety, and functionality will be achieved through compliance with international standards, powered assistance, and control, as well the learnings from the downsides of traditional designs.

The idea of a laterally mounted joint was revisited in 2010 when Dr. Hasahi Naito presented a laterally mounted hip disarticulation prosthesis (Figure 2-22) at the 13th ISPO World Congress. However, limited literature is available on this design. The prosthesis had a passive, single-axis joint with a rail and roller configuration supported load bearing. Neutral alignment of the hip and knee joint compared to the sound side resulted in decreased pelvic tilt and improved gait patterns compared to a Canadian type [54].

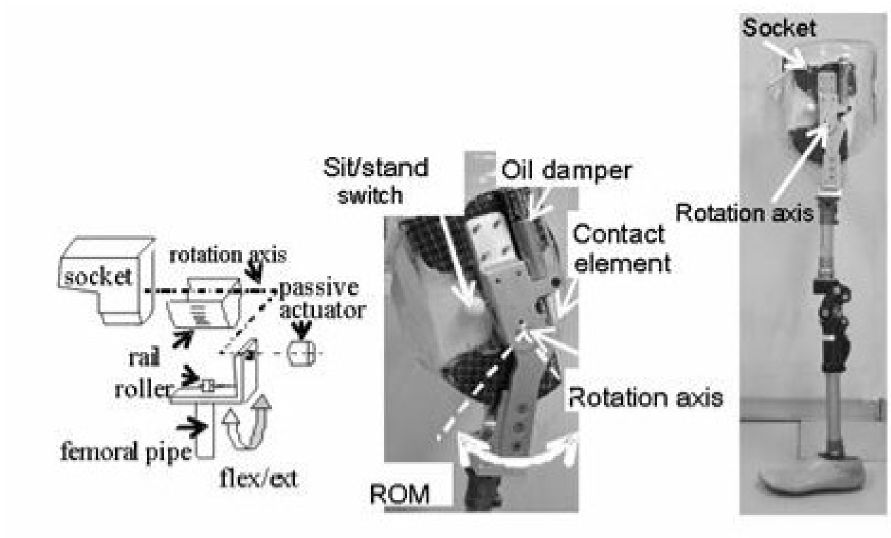

Figure 2-22: Laterally mounted passive hip joint (Adapted from [54])

2.8.2 Remote Center of Motion

A Remote Center of Motion (RCM) mechanism was proposed to position the hip joint axis of rotation to its anatomically correct position (Figure 2-23) [55]. A double parallelogram design created a virtual hinge that represented the hip joint rotating about the acetabulum [55]. While this joint was mounted to the front of the socket, repositioning the center of rotation pertains to this thesis.

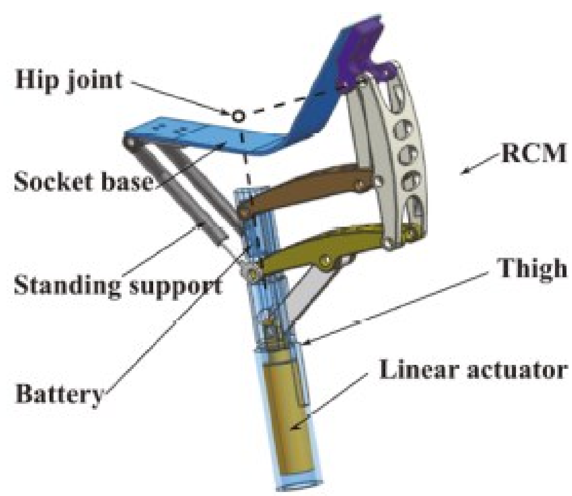

Figure 2-23: Remote Center of Motion prosthetic hip joint model (Adapted from [55])

The joint was tested by an amputee and compared to a single-axis joint and the participant's intact limb. The RCM mechanism reduced leg length discrepancy, enabled walking patterns closer to the intact limb, and reduced pelvic tilt (Figure 2-24) [55]. While these results encouraged center of rotation relocation to the acetabulum, preliminary results based on one participant cannot be generalized for all HDA and HPA. Further research needs to be conducted on this concept.

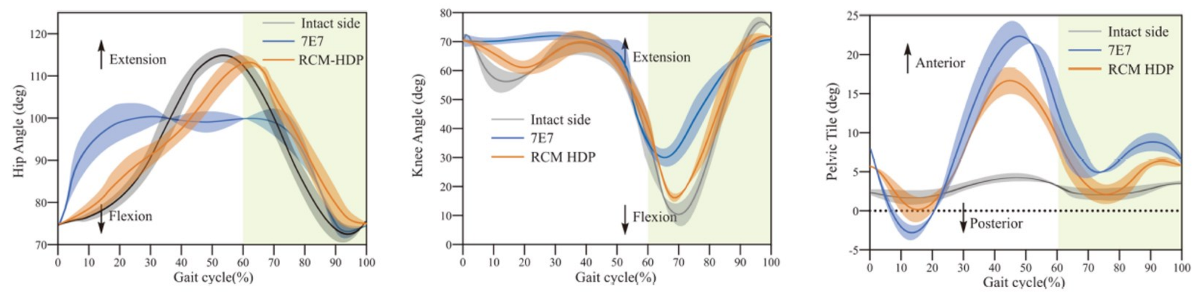

Figure 2-24: Gait characteristics measured using RCM mechanism (Adapted from [55])

2.9 Summary

Hip joint prosthesis development has occurred slowly, with currently available devices still not meeting the needs of HDA and HPA. The existing gap in technology is suggested by asymmetrical gait patterns [6], [25], [30], high energy expenditure during ambulation [3]–[5], and ultimately, prosthetic abandonment by this population [5], [13]. HDA and HPA account for the lowest percentage of lower limb amputees [23] but endure the most difficulty when walking with prosthetics [5]. Increased metabolic costs, lack of control, and balance issues while walking with prostheses are among some of these individuals' daily challenges.

Most hip prostheses have passive joints mounted to the front of the prosthetic socket. Today, the leading prosthetic hip joint is the Helix^{3D}, which maintains the front-mounted orientation but offers advantages of a polycentric design accompanied by a hydraulic unit for control. Improved gait patterns have been achieved using the Helix^{3D}, although the passive nature and front mount present limitations in advancing prosthetic technology [7], [28].

Though currently, available hip prostheses include only passive devices, the reviewed literature suggests that powered prostheses should improve HDA and HPA gait [9]–[11]. The biomechanical requirements of gait show that the hip is an energy-intensive joint [32] and must generate large moments to perform daily activities such as inclined walking, stairs, and sitting. A prosthetic hip joint design should help meet these demands; therefore, an active element is required. Further, a lateral mounting orientation should enable more symmetrical gait patterns. While this concept has only been revisited in a passive device since conventional prostheses, such as the tilting table prosthesis, improved gait patterns were achieved compared to front-mounted systems [54].

An improved, powered prosthetic hip joint is required to improve the safety and quality of life for HDA and HPA.

Chapter 3: Design Criteria

The laterally mounted powered hip joint (LMPHJ) design and development followed an engineering design process. The project iteratively advanced throughout the design process to ensure the LMPHJ's design included the requirements to meet end-user needs. The success of this thesis involved thoughtful design and comprehensive evaluation of the novel prosthetic device based on available literature and well-accepted international standards. Throughout this chapter, the design criteria required to address the rationale and objectives of the project outlined in Chapter 1 are discussed. Section 3.1 emphasizes the need for providing hip-level amputees with adequate prosthetic devices. Sections 3.2 and 3.3 outline the functional and non-functional requirements for the system. Section 3.3 summarizes these requirements into the overall design criteria for the LMPHJ.

This thesis focuses on the mechanical aspects of the powered prosthesis. A customized control system is required but is beyond the scope of the thesis. The design will interface with an aluminum chassis containing all electrical components. Consideration for electrical connections is included in the scope, but the chassis design was completed in parallel.

3.1 Identification of Need

Many HDA and HPA abandon their prosthesis because of the challenges associated with ambulation using currently available devices. In design terms, this abandonment is indicative that existing technology does not meet the needs of hip-level amputees. Since the advent of the Canadian prosthesis, most hip joints have followed the front-mounted configuration. Alignment at the natural center of rotation should be explored to progress toward a prosthetic solution that enables movement closer to that of able-bodied individuals.

3.2 Functional Requirements

The design must encompass functionalities to support users throughout daily activities such as walking, sitting, and stair ascent/descent. The available literature can help to assign quantitative measures for the intended LMPHJ design. Because this joint will be integrated into existing HD prosthetic systems (i.e., hip, knee, and ankle joints), TF gait is an ideal comparator for functionality. TF gait provides a reasonable target compared to lower-level amputations since both populations require a prosthetic knee and ankle joint for ambulation. Therefore, it is reasonable to use available data collected for TF amputees to help formulate the functional requirements.

The LMPHJ should enable the user to walk over level-ground. Hence, sufficient ROM, walking speed, and power/torque requirements must be defined. The ROM should be at least that of the Helix 3D (130° flexion, 15° extension) and match its weight rating of 100 kg [46]. Additionally, the maximum loading level ISO standard 15032:2000 corresponds to a 100 kg person, which will be used during structural testing. A maximum test force of 3360N is required at this level [34]. Section 2.4.2 reported a walking speed of 1.06 m/s for HDA over level-ground walking. However, to account for the anticipated increase in performance with this design, data for TF amputees was considered. In a recent study involving TF amputees, walking speeds up to 1.5 m/s were measured [56], while the self-selected walking speed for this population is typically between 1.0 m/s-1.3 m/s [29], [57]. At a speed of 1.1m/s, the maximum angular velocity at the hip in TF amputees was 130°/s [58]. To accommodate variations in gait and faster walking speeds, a requirement of 150.0 °/s was specified.

Walking on uneven terrain and inclined surfaces affects gait biomechanics, introducing balance and energy expenditure challenges for amputees [59], [60]. As the walking surface gradient increases, the peak sagittal-plane hip joint moment increases [61]. In accordance with Canada Mortgage and Housing Corporation (CMHC), accessible ramps require a slope no steeper than a 1:12 ratio, or roughly an 8% incline [62]. For this inclination, peak hip moment in early stance is approximately 1.21 Nm/kg [61], corresponding to 121.0 Nm for a 100kg person. The maximum hip moment measured for TF amputees using a microprocessor-controlled knee [29] in Section 2.4.3 was nearly the same; therefore, a torque requirement of 125.0 Nm was specified.

The powered element of this design is of high importance. Section 2.4.3 indicates peak hip power over level ground to be 0.83 W/kg. To ascend ramps or stairs, the maximum hip power on the prosthetic limb was 2.7 W/kg for ramps and 3.6 W/kg for stairs [33]. Accompanied by the weight rating, this equates to a maximum power requirement of 360.0 W.

3.3 Non-functional Requirements

In addition to functional requirements, non-functional requirements must be satisfied for the overall success of the design. Most notable is user safety. Minimizing risk to the amputee will be prioritized, ensuring no sharp edges are exposed and providing stability through mechanical and control system efforts. Additionally, factors of safety based on international standards and industry expert advice will be included in all designed components.

The key element of this novel prosthetic device is the mounting orientation. The LMPHJ must be mounted to the side of the prosthetic socket with the axis of rotation positioned at the acetabulum. The joint must not contact the socket throughout the ROM; therefore, a radial clearance of approximately 130.0 mm from the hip centre of rotation will be required based on dimensions from pelvic radiographs [63] and socket geometry. In addition, the joint must fit beneath regular clothing so as not to protrude in any direction beyond average anthropometric measurements. Considering females in the 50th percentile, thigh clearance is 12.9 cm [64]. Therefore, an anterior or posterior protrusion from the axis of rotation must not exceed 6.5 cm. Laterally, the joint should not protrude more than the anatomical width at the hips. This requirement was defined by measurements taken by clinicians of HDA and HPA. Laterally, the distance between the acetabulum and the outermost part of the limb is approximately 10.0-11.0 cm. For hip-level amputees, soft tissue and the prosthetic socket occupies roughly 5.0 cm of this space, leaving approximately 5.5 cm for the LMPHJ design.

Common engineering considerations in design are cost, weight, and ease of manufacturing. Reducing costs can be achieved by using off-the-shelf components where possible, and designed parts should be easily machinable. A limit of 20 machined parts was set to reduce the amount of machining required. While the actuator should assist the amputee with the prosthesis weight burden, component weight should be minimized without sacrificing strength and functionality. The Össur Power Knee weighs 2.7kg [65]. While similar electronic components will be included in the LMPHJ, the device will be overall larger and more complex than the Power Knee. Additionally, considering it is a prototype, a 30% weight increase will be considered acceptable, equating to a maximum weight of approximately 3.5kg.

3.4 Design Criteria Summary

Table 3-1 and Table 3-2 summarize the LMPHJ design criteria.

Table 3-1: LMPHJ functional design criteria

Requirement	Criteria
Range of motion	130.0° flexion, 15.0° extension
Hip angular velocity	150.0 °/second
User weight capacity	Max 100.0 kg
Hip torque	Peak moment: 125.0 Nm
Hip power	Peak power generation: 360.0 W

Table 3-2: LMPHJ non-functional design criteria

Requirement	Criteria
Minimize weight	≤3.5 kg
No sharp edges	Fillet exposed edges
Laterally mounted	Lamination plate secured on lateral side of prosthetic socket
Ease of manufacturing	Less than 20 machined components
Must fit under clothing	Lateral protrusion ≤ 5.5 cm
Does not interfere with sitting	Posterior protrusion from axis of rotation ≤ 6.5 cm
Does not interfere with prosthetic socket	Motor positioned 130.0 mm distal to the axis of rotation

Chapter 4: Design and Development

A novel design was developed to best address the requirements outlined in Chapter 3. The LMPHJ design (Figure 4-1) will be discussed in detail throughout this chapter.

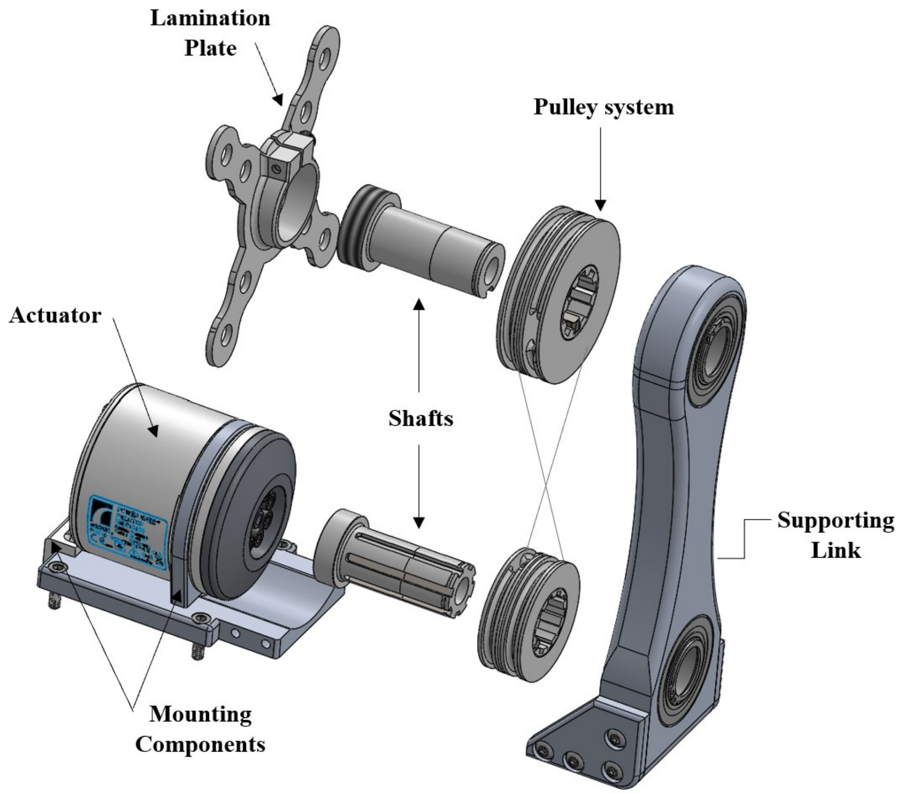

Figure 4-1: Main components of the final laterally mounted powered hip joint design

The design evolution is presented, beginning with initial candidate designs. Then, the final design is outlined, along with analyses completed and design decisions that led to this configuration. The FEA analyses conducted are discussed to ensure the design's structural integrity prior to fabrication and mechanical testing. Lastly, a 3D-printed and final full-scale prototype is presented, showcasing the design.

The LMPHJ shown in Figure 4-1 is a mechanical system that actuates the prosthetic limb during the gait cycle to improve user mobility. The system includes the following main components:

- Pulley system: Drivetrain composed of two sets of pulleys in a crossed configuration to enable safe hip flexion and extension.
- Shafts: Structural components to support weight-bearing and actuation. The distal shaft interfaces with the motor and transmits the motion. The proximal shaft interfaces with the lamination plate, providing the axis of rotation.
- Supporting link: Structural element connecting the proximal and distal shafts.

- Lamination plate: Connecting component between the system and prosthetic socket.
- Actuator: An Össur Power Knee™ microprocessor-controlled motor modified for the LMPHJ design, providing sufficient torque and power to the system.
- Mounting components: Designed components for mounting the actuator and integrating the LMPHJ to the distal portion of the prosthetic limb.

4.1 Candidate Designs

Various solutions were explored throughout the design process. During the conceptual design phase, many aspects of the LMPHJ were deliberated and proposed, often multiple times. Candidate designs were reviewed by faculty members, fellow students, and industry professionals from Össur. Incrementally, the design evolved to reach a solution that best met the requirements and offered an innovative solution to the problem.

4.1.1 Joint Type

There are two types of prosthetic hip joints: single-axis and polycentric joints. Single-axis, or otherwise referred to as monocentric, joints are simple, compact mechanisms requiring fewer components, lessening the manufacturing and assembly time. However, while using these joints, users often experience a lack of control, limited stability, and increased pelvic tilt required for walking, ultimately leading to unnatural gait patterns, safety concerns, and secondary injuries [7]. Polycentric joints, such as the Helix^{3D}, have improved functionality over single-axis joints, evidenced by improved gait patterns [7], [28]. To achieve these improvements, polycentric joints are typically larger, heavier, and more complex, with many components. The advantages over single-axis joints hold true for passive systems; however, when selecting a joint type for the LMPHJ, consideration of the powered aspect was critical.

No powered hip prosthesis is available, so active knee joints were considered to assess the effects of positive power generation on joint function. The Össur Power Knee™ is a single-axis joint and, in contrast to traditional monocentric joints, the Power Knee™ enables safe and efficient walking [10]. Therefore, the disadvantages of existing single-axis hip joints could be met with the design's mechanical functionalities, microprocessor controls, and powered assistance throughout gait. Additionally, powered assistance should reduce the number of compensatory movements, such as pelvic tilt [10], and, combined with the lateral mounting orientation, a more natural gait pattern should be achieved. For these reasons, the decision was made to develop a single-axis joint, to create a simple yet effective prosthetic hip joint. The single-axis design was essential to reduce the system's size and complexity, meet geometric constraints for lateral protrusion, and reduce manufacturing time.

4.1.2 Actuator Selection

The hip is an energy-intensive joint; therefore, an actuator that could meet the power and torque requirements was necessary. This project was done in collaboration with Össur; therefore, the first candidate was the Power Knee™ motor (Figure 4-2). The motor is a successful prosthetic component, and in-house resources for developing controls are available. However, considering the lateral protrusion constraint, an actuator with a smaller profile was explored.

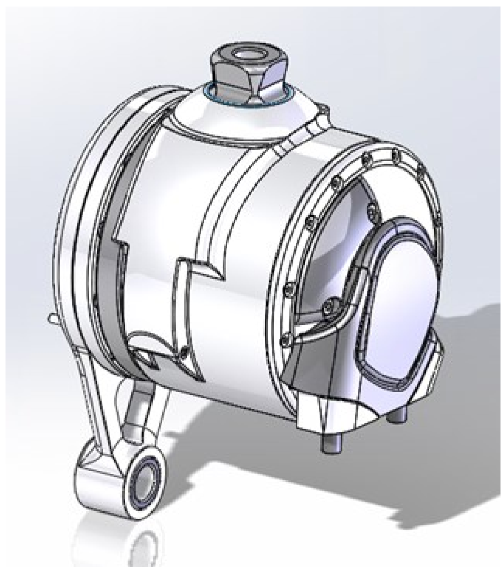

Figure 4-2: Össur Power Knee™ actuator

The Maxon Exoskeleton Drive GEN.1 (Figure 4-3) consists of a pancake brushless DC motor for joint actuation and is used in hip and knee exoskeletons. The motor provides a small amount of space savings with a width of approximately 57 mm [66], compared to the 70 mm Össur actuator. However, the unit only delivers 54 Nm [66] of continuous torque, nearly half the Össur motor's 96 Nm. Based on the high torque ratio of approximately 5:2 that would be required to meet the system's 125 Nm torque requirement, the Maxon actuator was not selected for the LMPHJ system. The Össur Power Knee™ actuator was chosen for its torque-generating capability, easier implementation of controls, and proven use in lower limb prosthetics. Also, Össur was a project partner, so the development team had access to essential Power Knee design and control information.

Figure 4-3: Maxon Exoskeleton Drive GEN.1 (Adapted from [66])

4.1.3 Actuator Location

The purpose of the lateral mounting orientation was to position the axis of rotation at the anatomically correct location. Several ways were considered to achieve this centre of rotation. The most straightforward approach was to mount the actuator at hip level. This motor orientation would emulate common powered hip exoskeletons where the actuators are mounted laterally (Figure 4-4 (left)) [53], [67], [68]. The second option was introducing a drivetrain and positioning the motor beneath the prosthetic socket (Figure 4-4 (right)). This would reduce lateral protrusion at the hip but introduce complexity to the design.

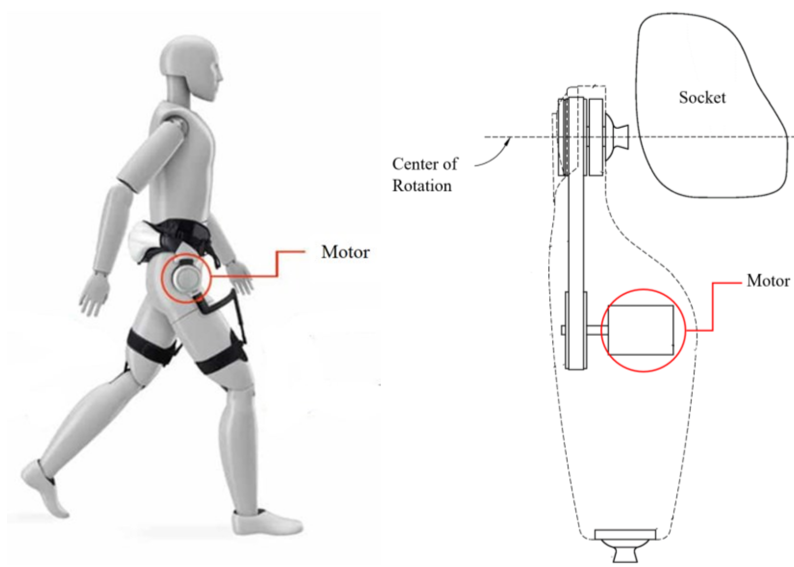

Figure 4-4: Honda's Walk Assist showing the powered exoskeleton's motor positioning at hip level (Adapted from [68]) (left). Conceptual design of powered prosthetic hip joint with motor mounted beneath the socket (Adapted from [69]) (right)

The available lateral space when mounting the actuator at the hip was a variable factor to consider. This geometric constraint varies from person to person, depending on the level of amputation, the amount of soft tissue at the amputation site, and socket design. Figure 4-5 represents approximate measurements from known clinicians in Iran. For HPA, up to 12.0 cm is available for the joint; however, this space can be reduced to 5.0 – 6.0 cm laterally for HDA. Another factor to consider was the torque requirement. When mounting the Power Knee™ motor at the hip, the joint would be a harmonic drive system with 96 Nm maximum torque output.

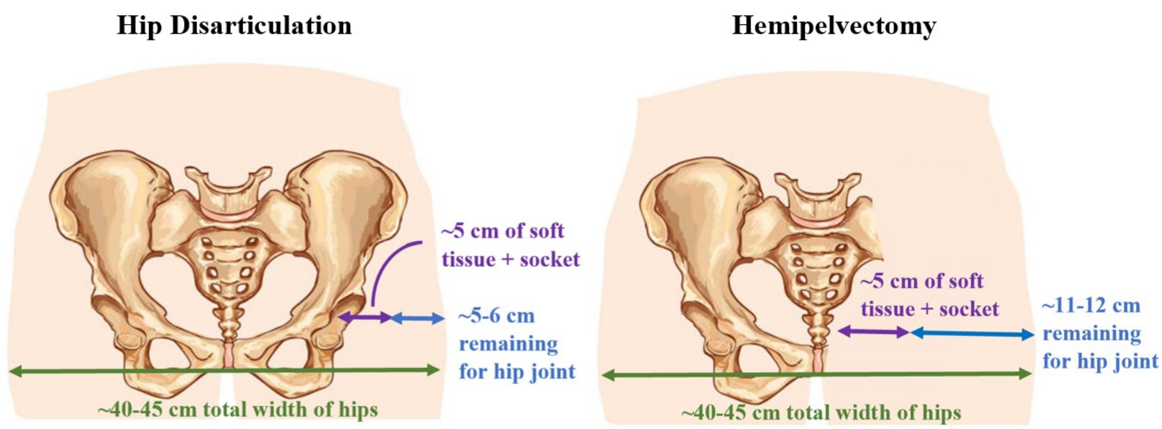

Figure 4-5: Available space for prosthetic hip joints for HDA (left) and HPA (right)

While this motor positioning represents a more straightforward system, the concept was not feasible considering the maximum 5.5 cm lateral protrusion and 125.0 Nm torque requirements. The motor dimensions combined with mounting components would be approximately 9.0 cm, making the joint too bulky to fit beneath a pair of pants in most cases for HDA. The direct drive system also did not meet the system torque requirements. Therefore, the decision was made to position the actuator in the usable space beneath the prosthetic socket and implement a drivetrain with an adequate torque ratio and new interfacing requirements.

4.1.4 Socket Interface

Initially, it was desired to have a highly adjustable mounting system to ensure the joint could be positioned accurately at the center of rotation and the leg angled correctly. Various adapters (Figure 4-6) were developed to allow different angular positions and flexibility in the mounting location on the lamination plate. Hinges or wedges were used to adjust the prosthetic leg's angular orientation in the frontal plane. A gear-like connection was trialed to change the joint's sagittal plane mounting orientation, and a standard pyramid adapter connection could provide limited adjustability in multiple directions. A series of slots allowed joint positioning along the lamination plate.

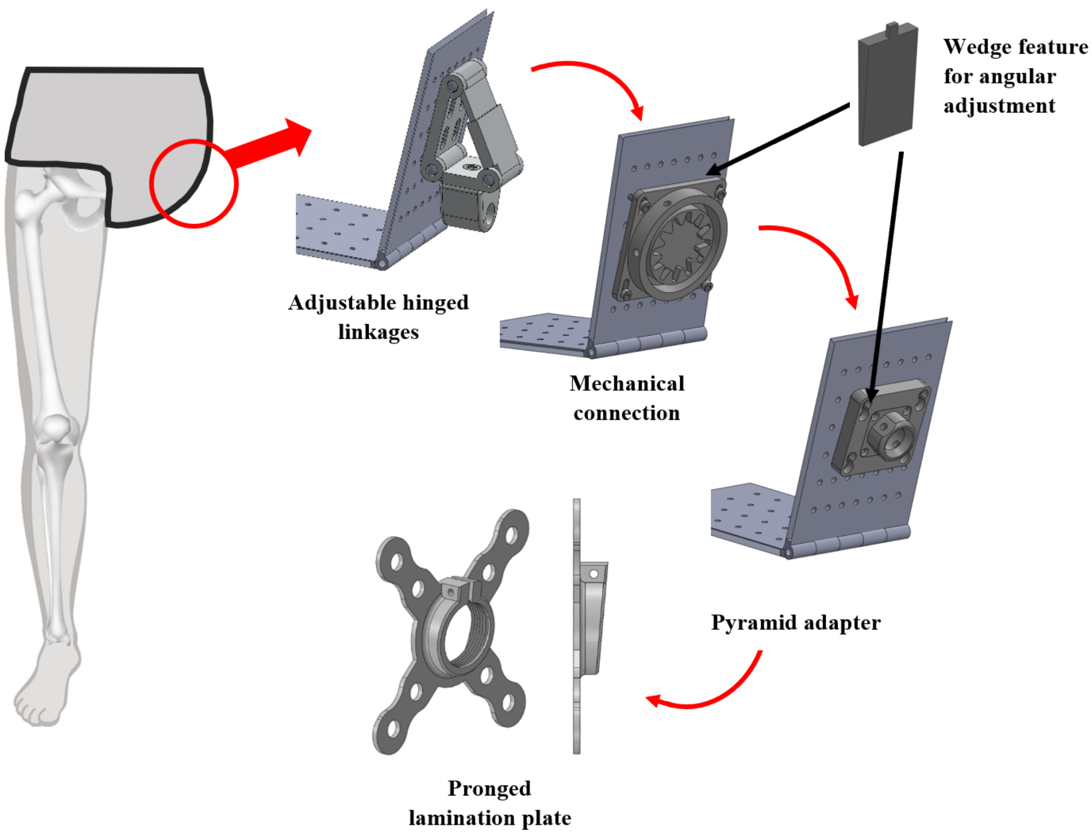

Figure 4-6: Socket interface candidate designs

Ultimately, a high level of adjustability was “nice-to-have” but not necessary. The reality is that prosthetics are often highly customized to the user. In the final design, a pronged lamination plate will be positioned at the anatomical joint centre and bent to form the socket by the prosthetist before lamination. A standard angular feature is built into the lamination plate with further angular adjustments accommodated in the lamination process.

4.1.5 Drivetrain selection

Different drivetrains were discussed to transmit the power from the motor to the hip axis of rotation. The Powered Hip research team conducted preliminary research on drivetrain systems that eliminated a gear train due to geometrical and weight requirements. A belt drive system using timing belts and a chain drive system using chains and sprockets were also considered. However, based on the large tensile loads required to actuate the joint, the size of belt or chain required to withstand the forces was too large to meet the space requirements. Therefore, timing belts and chains were not selected based on strength limitations and geometric constraints.

Of the drivetrain options explored to transfer power from the motor to the hip axis of rotation, a pulley system using ropes was the most viable option. This concept included many iterations (Figure 4-7) to ensure proper functionality, strength, and safety. Modeling and physical prototypes determined the final pulley system design.

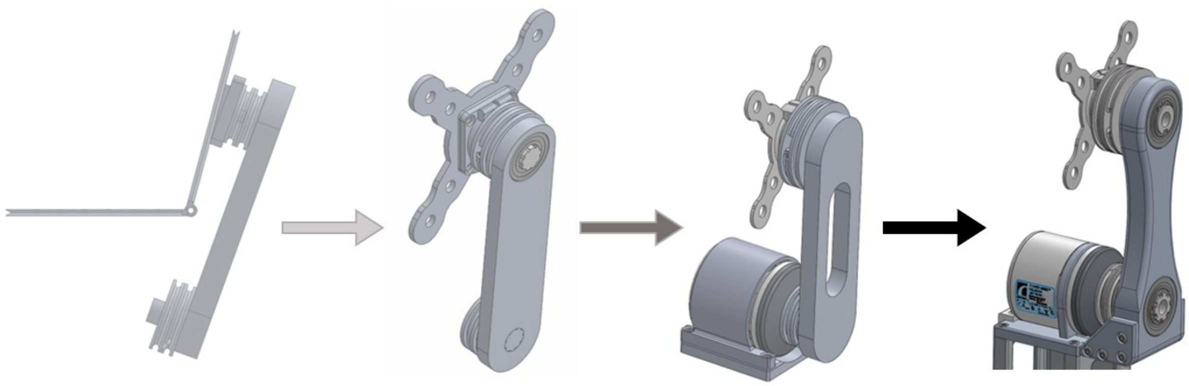

Figure 4-7: Pulley system design evolution

4.1.6 Material Selection

Materials with a high strength-to-weight ratio are favorable in the prosthetic industry. Össur recommended Aluminum 2024-T4 or 17-4PH Stainless Steel (Table 4-1) for any machined structural elements, depending on the strength requirements for the part. Therefore, unless otherwise indicated, most of the final prototype was manufactured from these materials.

Table 4-1: Mechanical properties of Aluminum 2024-T4 [70] and 17-4PH Stainless Steel (H900) [71]

Material	Utlimate Tensile Strength (MPa)	Tensile Yield Strength (MPa)	Shear Strength (MPa)	Density (kg/m^3)
Aluminium 2024-T4	469	324	283	2780
17-4PH Stainless Steel (H900)	1210	1090	830	7700

Based on calculations, simulations, and expert experience, modifications to the geometry and material of selected components were implemented prior to production. Additionally, adjustments were made to reduce tolerance chains, which are the accumulated variation throughout processing steps, thereby simplifying manufacturing. The final design, outlined in the following sections, results from a thorough design process.

4.2 Pulley System

Pulleys are used for the LMPHJ mechanical drive system. To achieve the intended functionality, the system includes two sets of custom-designed pulleys with two ropes in a crossed configuration. The pulleys are rigidly connected to the shafts using keys, and the shafts are attached through a supporting link. The top pulleys are fixed, while the motor actuates the bottom pulleys. This configuration does not allow for free rotation with respect to the prosthetic socket, which is essential for safety and control. Uncontrolled movement of the joint can result in instability and fall risks.

Movement of the leg in flexion or extension can only be achieved through motor actuation. The motor drives the bottom pulley, which causes the supporting link to rotate around the top pulley's axis of rotation through tension in the ropes. Dual pulleys were required to achieve this motion, with one rope driving flexion and the other driving extension (Figure 4-8 (left)), emulating the function of flexor and extensor muscles. On a smaller scale, this concept has been used in other biomimetic applications, such as the design of a robotic finger where two groups of wires, acting as tendons, are used in a crossed configuration to transmit flexion and extension between joints [72].

If only one set of pulleys or an open configuration were used (Figure 4-8 (right)), rotation of the top pulley or rope movement along the pulley would be required to achieve motion around the axis of rotation. This introduced safety and control issues in both cases because the leg could move about the socket without motor actuation. Since the top pulley must be fixed relative to the socket, and the ropes must be fixed relative to the pulleys, the crossed rope configuration is required to generate movement. The torque applied to the distal pulleys results in a reaction moment at the proximal pulley in the same direction, thus, generating movement. In the case of the open system, the reaction moment at the axis of rotation is opposite to the applied motor torque; therefore, the system cannot move as intended.

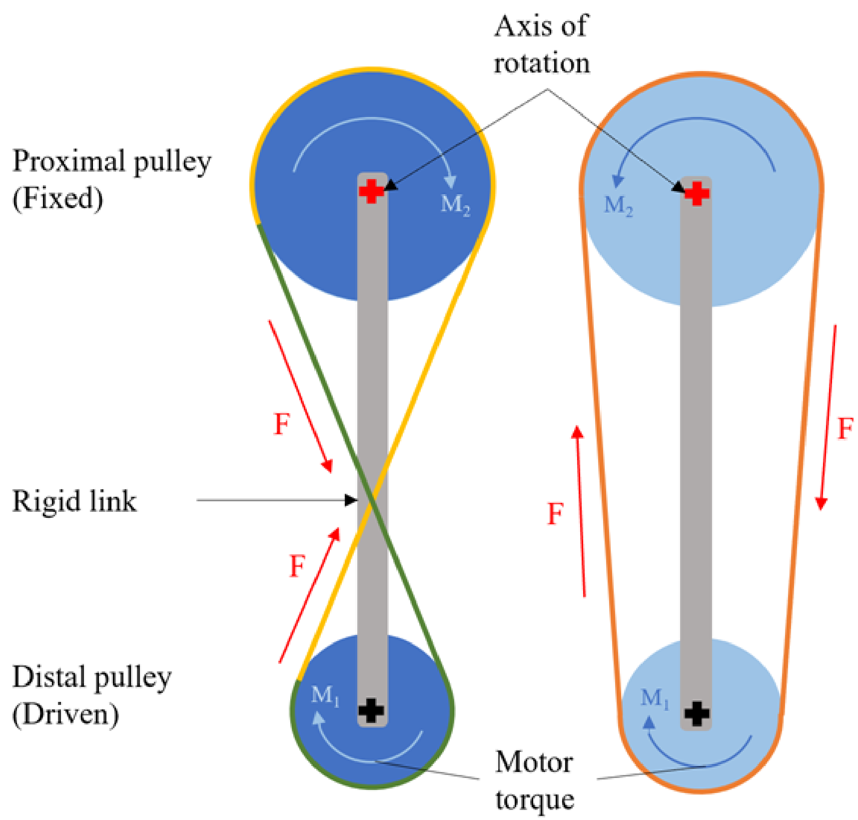

Figure 4-8: Pulley systems where F is the tension in the ropes, M_1 is the motor torque, and M_2 is the reaction moment at the axis of rotation. Crossed rope concept for LMPHJ actuation, with dual rope system represented in green and yellow (left). Open pulley system with one continuous rope represented in orange (right).

4.2.1 Pulley Size Optimization

Pulley size optimization was achieved by balancing the inverse relationship between torque and angular velocity. A minimum size ratio between the proximal and distal pulleys was needed; however, this ratio could not be so large as to sacrifice angular velocity beyond the requirements. The maximum hip moment required was 125.0 Nm, and the maximum angular velocity was 150 °/s. The Össur actuator specifications indicated that the maximum motor torque is 96.0 Nm with a maximum speed of 300.0 °/s. Equation 4-1 defines the relationship between angular velocity and pulley diameter:

$$d_1\omega_1 = d_2\omega_2 \tag{4-1}$$

where d is the diameter of the pulleys and ω is the angular velocity.

Equation 4-2 represents the relationship between torque and pulley diameter:

$$\frac{d_1}{d_2} = \frac{\tau_1}{\tau_2} \tag{4-2}$$

where d is the diameter of the pulleys and τ is the torque.

Considering these relationships and the Össur actuator specifications, a size ratio between 0.50 and 0.77 satisfied both moment and speed requirements. In addition to shaft diameter geometrical constraints and sufficient space for the rope to be secured inside the pulleys, the final design includes a 55.0 mm outer diameter distal pulley and a 75.0 mm outer diameter proximal pulley. Considering the groove in the pulleys where the ropes will apply compressive forces, a diameter of 47.0 mm and 65.0 mm was used when determining loads in the ropes.

4.2.2 Rope

Due to the high tensile strength and lightweight properties, a rope was selected for the pulley system over chains or belts. The pulley ropes are spliced at both ends, secured around the pulley's inner diameter, and wrapped around the exterior (Figure 4-9). These ropes experience high loads and must remain in constant tension. Vectran® is a high-performance fiber that was selected due to its high strength, low-stretch, and creep-resistant nature [73]. When the motor operates at peak torque (96.0 Nm), the rope tension is upwards of 4085 N (Equation 4-3).

$$F = \frac{\tau}{r} \tag{4-3}$$

where F is the tensile force in the ropes, τ is the torque applied, and r is the radius of the pulleys.

Marlow Excel V12 with a 3 mm diameter was chosen, with an average break load of 993 kg (9741 N), beyond the LMPHJ loads [74]. The rope's low stretch and no creep properties are critical because if slack is introduced into the system throughout its use, the motion could become jerky and unsafe for the user.

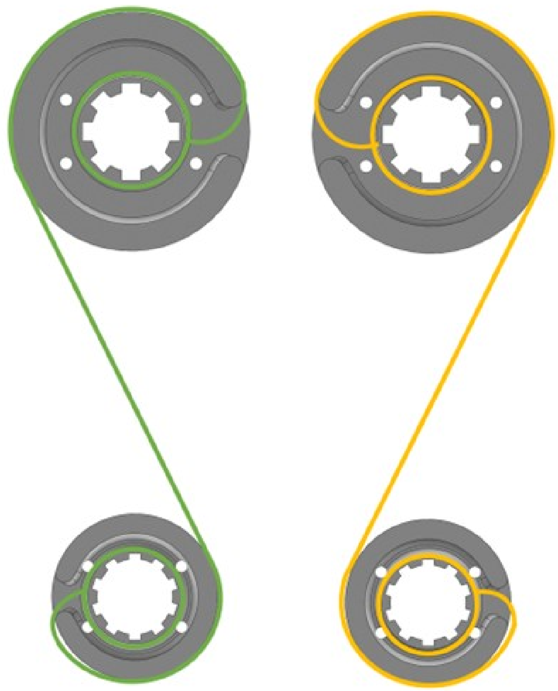

Figure 4-9: Rope configuration for both pulleys demonstrating the crossed configuration using two spliced ropes. The ropes are secured around the inner diameter of the pulleys, exit the opening, and wrap around the exterior groove

Considering its attractive mechanical properties, Vectran® is used in other biomedical applications, such as textile-based artificial anterior cruciate ligaments [75]. In one study, Vectran® rope improved stiffness and reduced breaking strain under cyclic loading [75]. Therefore, the designed pulley system is expected to successfully drive the system under high, cyclic tensile loads while adding minimal weight.

4.2.3 Tensioning Solution

Determining how to tension the pulley system was challenging because a simple assembly method that would not require additional lateral components on the shaft was desired. Additionally, the pulleys had to be tensioned separately due to the dual-pulley, crossed-rope configuration. A keyway solution was decided because it allows the pulley to rotate around the shaft until appropriate rope tension is achieved and the key is inserted to maintain this tension. An odd number of keyways on the shaft and an even number on the pulleys were implemented to offer more angular positions, improving the tensioning solution. As demonstrated in Figure 4-10, a keyway was available every 9 degrees (1.9 mm of rope) for 56 possible combinations. Because the system does not require a large pre-load, the pulleys can be tensioned using an angle grinder-type wrench.

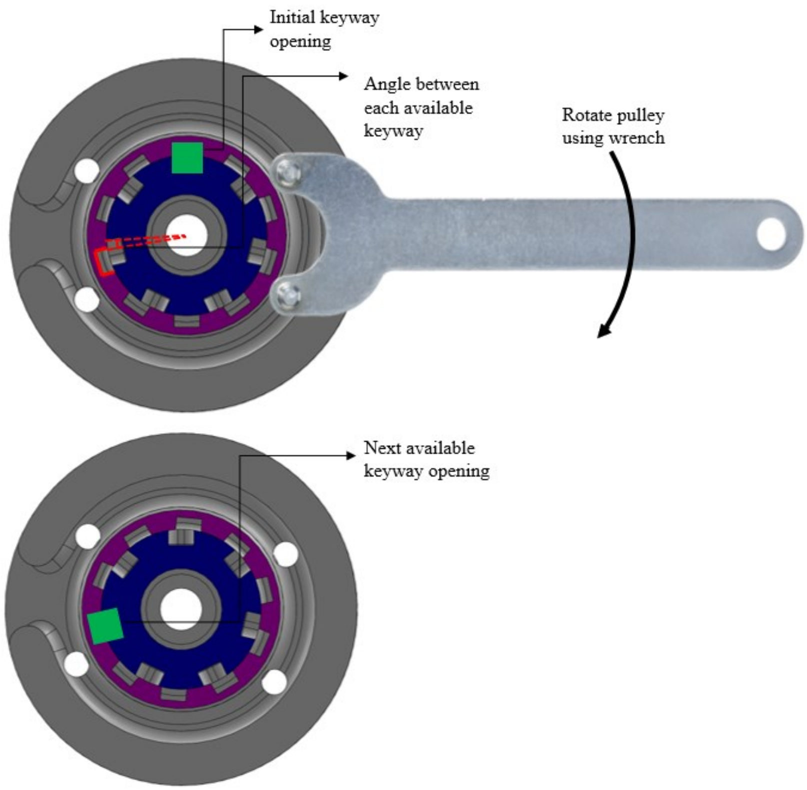

Figure 4-10: Keyway tensioning solution between the shafts (blue) and pulleys (purple) using an angle grinder wrench. The highlighted green key demonstrates the various possibilities for positioning the pulley to achieve tension in the ropes

4.2.4 Pulley Design

Customized pulleys (Figure 4-11) were required to accommodate the outlined configuration of the LMPHJ pulley system. The shaft diameters governed the inner diameter, and the outer diameters were based on the torque requirements of the system. The width was dependent on the key length required. Keyways and holes for an angle grinder wrench were implemented to achieve tensioning and fix the pulleys to their respective shafts. An opening and groove around the outer circumference were required so the spliced rope could exit the pulley and wrap around the exterior. Pulley plates capped each pulley to secure the rope inside and resist some compressive loads. The pulleys and pulley plates were machined from 17-PH H900 steel.

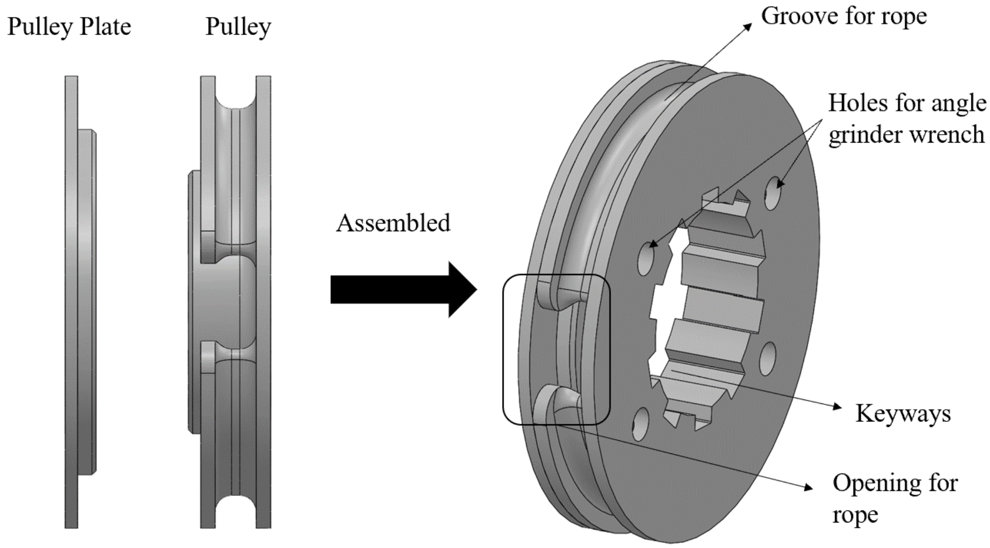

Figure 4-11: Pulley design

4.3 Shaft Design

Proximal and distal shafts were included in the LMPHJ design. The proximal shaft is located at the hip axis of rotation and interfaces with the lamination plate. The distal shaft is integrated into the motor and positioned at its axis of rotation. These shafts will be subjected to high forces and fatigue loading; therefore, design decisions ensured that the shafts were strong enough, remained as lightweight as possible, possessed a strategic shaft layout, and reduced stress concentrations.

4.3.1 Distal Shaft

The distal shaft transmits power and motion from the actuator to drive the LMPHJ system. The interface on the lateral side of the Össur Power Knee actuator was modified compared to the Power Knee connection to accommodate the LMPHJ drivetrain. The shaft uses the existing socket screws as dowels for a centering feature, and securement is achieved using the screw in the center (Figure 4-12).

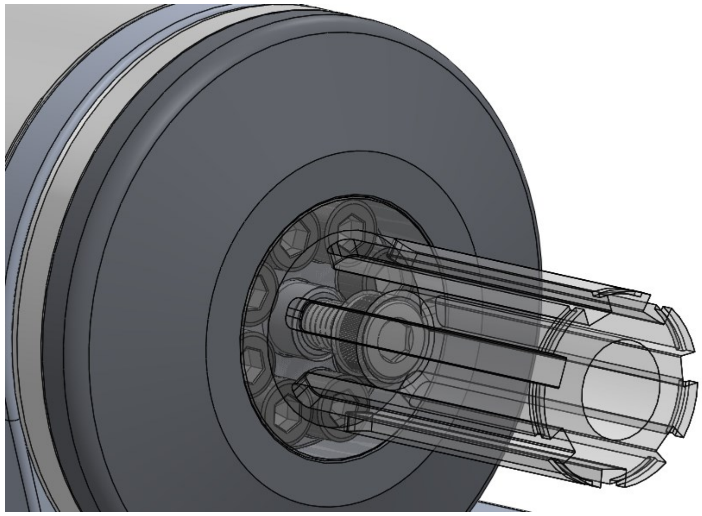

Figure 4-12: Distal shaft interface to the lateral side of the motor using existing hardware

The total shaft length is 64 mm; however, only 54 mm is usable (Figure 4-13). The remaining length is the insert for the motor interface, in which the existing motor cap dictates the diameter. Seven 4 mm keyways are around the circumference to accommodate the tensioning solution, outlined in Section 4.2.3. A retaining ring groove is located towards the end of the shaft to constrain all components.

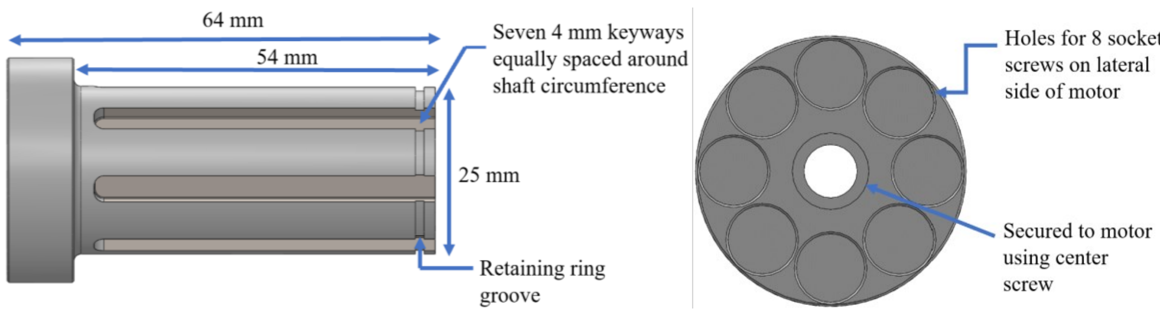

Figure 4-13: Side view (left) and back view (right) of the distal shaft

The shaft diameter was based on a fatigue analysis discussed in Section 4.3.4. To simplify the analysis, the diameter at the base of the keyways for the distal shaft was assumed. That is, the analysis was conducted considering a hollow shaft with an outer diameter of 21 mm and an inner diameter of 12.75 mm. The effects of a single keyway on the shaft fatigue analysis are available in the literature [76], [77]; however, it was unclear how to assess the multiple stress concentrations introduced by the abundance of keyways. Assuming the smaller diameter simplified the analysis and produced conservative results.

4.3.2 Proximal Shaft

The proximal shaft (Figure 4-14) is similar to the distal shaft, with a few exceptions. The lamination plate interface was based on a standard M36 threaded connection used in industry with a pinch screw to prevent rotation [78]. Only one keyway was required to fix the proximal pulleys because tensioning is achieved at the distal location. A 6 mm key was needed since the proximal shaft will be subjected to higher torque based on the torque ratio between pulleys.

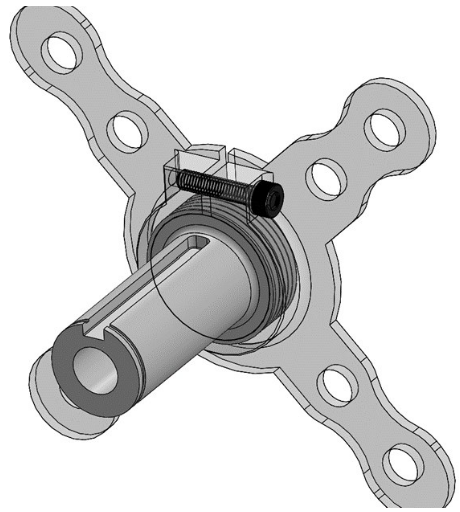

Figure 4-14: Proximal shaft design with threaded connection and a single keyway

4.3.3 Axial Layout

The axial layout of both shafts was based on minimizing the shaft bending moment and providing a viable sequence for assembly and disassembly. Figure 4-15 outlines the shaft layout.

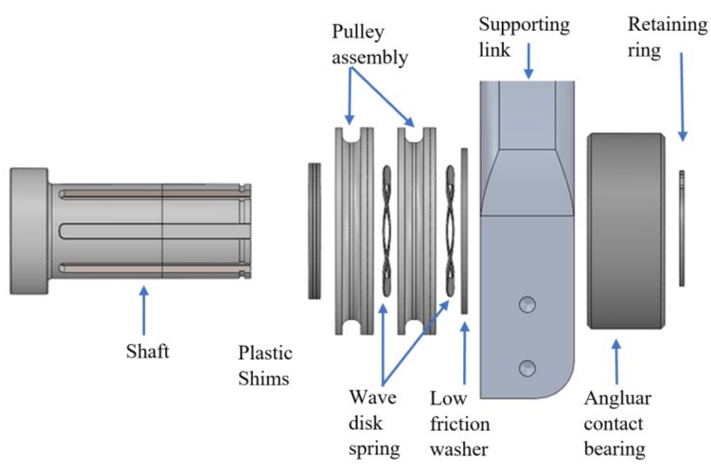

Figure 4-15: Shaft axial layout

4.3.4 Fatigue Analysis

Fatigue failure occurs when members are subjected to variable, repeated, alternating, or fluctuating stresses [77]. The LMPHJ will be used for repetitive gait cycles and subjected to repeated, fluctuating stresses since the user loads and unloads the prosthesis during each step. The actuation system will experience variable stresses along the shafts. While cyclic testing in ISO 15032:2000 is outside the scope of this thesis, a fatigue analysis was conducted for the shafts to determine an appropriate diameter, verify material selections, and design against fatigue failure for future iterations.

A separate analysis was conducted for each shaft; however, the process followed was identical. The assumptions made for the analyses are as follows:

- Maximum loads specified in ISO 15032:2000 (3360N) [34]
- Maximum Q-angle for females of 22 degrees [79]
- Axial stresses are negligible
- Maximum bending stresses will occur during midstance
- Maximum torsional stresses will occur during the maximum torque output of the motor
- Room temperature (20°C)
- Shafts have a uniform cross-section
- For distal shaft analysis, use the diameter at the base of the keyways

When conducting shaft analyses, the first step is creating a free body diagram (Figure 4-16) and calculating the associated forces and moments. Critical locations along the shaft where stresses will be highest inform the design. Critical locations typically occur where bending moments are high, torque is present, and stress concentrations exist [77]. These are identified through the bending moment and shear force diagrams shown in Figure 4-17. The critical location for both shafts occurs at the outermost pulley's midpoint.

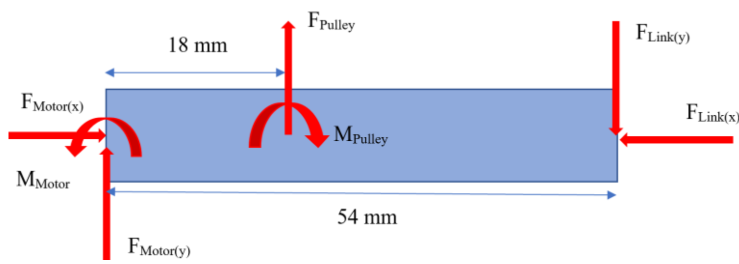

Figure 4-16: Shaft free body diagram where $F_{motor(x)}$, $F_{motor(y)}$, and M_{motor} are the reaction forces and moments at the motor interface. F_{Pulley} is the tension in the rope and M_{pulley} is the reaction moment at the pulley. $F_{Link(x)}$ and $F_{motor(y)}$ are the reaction forces at the bearings within the supporting link

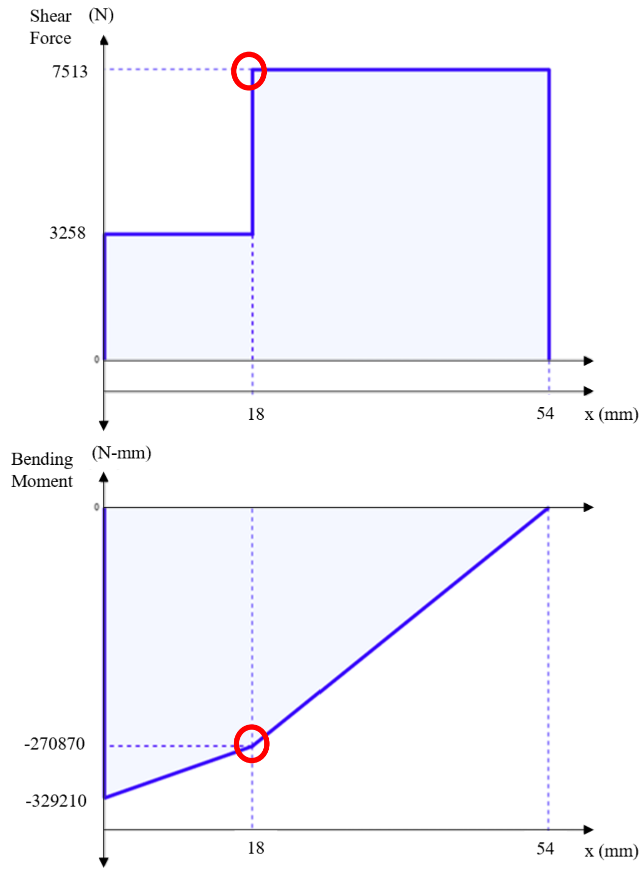

Figure 4-17: Shear force and bending moment diagrams for distal shaft analysis

Bending, torsional, and axial stresses may be present at critical locations; however, axial loads are typically negligible [77]. These stresses exist in midrange and alternating components. For many applications, there is a midrange torsional component and an alternating bending component; however, based on this design, these are reversed. The motor torque can alternate between -96.0 N and +96.0 N, depending on the direction of rotation. However, the bending moment is always in the same direction. These are given by:

$$\sigma_m = K_f \frac{M_m c}{I} \qquad \tau_a = K_{fs} \frac{T_a c}{J} \tag{4-4}$$

where σ_m is the midrange stress due to bending, τ_a is the alternating stress due to torsion, M_m is the midrange bending moment, T_a is the alternating torque, K_f is the stress concentration factor in bending, K_{fs} is the stress concentration factor in torsion, I is the moment of inertia, J is the polar moment of inertia, and c is the radius.

In combination with the distortion energy theory, the von Mises stresses for a round shaft with a circular cross-section can be written as:

$$\sigma_a' = (\sigma_a - 3\tau_a{}^2)^{1/2} = \left[\left(\frac{32K_f M_a}{\pi d^3}\right)^2 + 3\left(\frac{16K_{fs} T_a}{\pi d^3}\right)^2\right]^{1/2} \tag{4-5}$$

$$\sigma_m' = (\sigma_m - 3\tau_m{}^2)^{1/2} = \left[\left(\frac{32K_f M_m}{\pi d^3}\right)^2 + 3\left(\frac{16K_{fs} T_m}{\pi d^3}\right)^2\right]^{1/2} \tag{4-6}$$

where σ'_a is the alternating von Mises stress, σ'_m is the midrange von Mises stress. σ_a is the alternating stress due to bending, τ_m is the midrange stress due to torsion; however, these are not present in this analysis, so these components are zero.

These equations can be substituted into various failure criteria to determine important design parameters, such as the factor of safety or minimum shaft diameter. The DE Goodman criteria [77] was used as a conservative measure to determine the required shaft diameter for this application. This criterion is expressed as:

$$\frac{\sigma_a}{S_e} + \frac{\sigma_m}{S_{ut}} = \frac{1}{n} \tag{4-7}$$

where S_e is the endurance limit, S_{ut} is the ultimate strength, and n is the factor of safety.

Substituting the von Mises stresses into this equation and rearranging for shaft diameter, Equation 4-7 was used to compute the distal and proximal shaft diameters, considering a 1.3 factor of safety:

$$d = \left(\frac{16}{\pi d^3}\left\{\frac{1}{S_e}\left[4\left(K_f M_a\right)^2 + 3\left(K_{fs} T_a\right)^2\right]^{1/2} + \frac{1}{S_{ut}}\left[4\left(K_f M_m\right)^2 + 3\left(K_{fs} T_m\right)^2\right]^{1/2}\right\}\right)^{1/3} \tag{4-8}$$

Slight modifications were made to these equations to account for the hollow cross-section, using the moment of inertia (I) and polar moment of inertia (J) defined in Figure 4-18. Using these relationships, an appropriate inner diameter was determined.

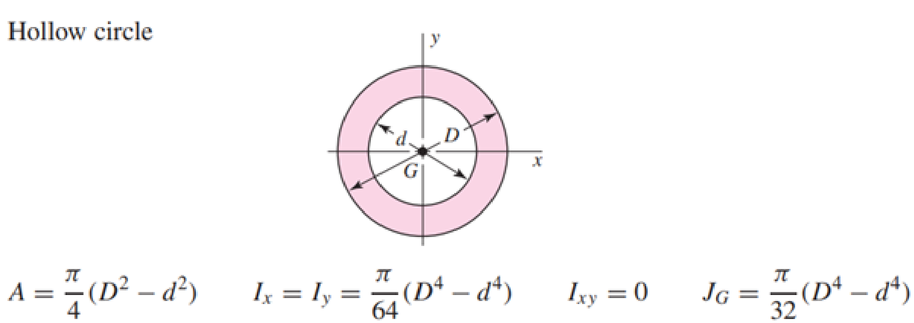

Figure 4-18: Geometric properties for hollow circle cross-section. Where A is the cross-sectional area, D is the outer diameter, d is the inner diameter, I is the moment of inertia, and J is the polar moment of inertia

Many factors should be considered before evaluating the above equations. Estimating the endurance limit is needed since the shafts will be subject to cyclic loading. The endurance limit of a material is determined experimentally and is defined as the stress value at which an infinite amount of loading cycles can be applied without failure [80]. Many factors influence this limit. Marin identified six factors relating to the part's material, manufacturing, environment, and design, represented in Equation 4-8, and used to calculate the endurance limit [77].

$$S_e = k_a k_b k_c k_d k_e k_f S_e' \tag{4-9}$$

where, S_e is the rotary-beam test specimen endurance limit, S_e' is the endurance limit at the critical location along the specimen, k_a is the surface condition factor, k_b is the size modification factor, k_c is the load modification factor, k_d is the temperature modification factor, k_e is the reliability factor, and k_f is the miscellaneous factor.

An important shaft design consideration is stress concentrations. Fatigue stress analysis results highly depend on the stress concentration factors [77]. Stress concentrations occur in areas of geometric irregularities that alter the flow of stress in a part. Examples of where these might exist are shoulders, keyways, pinholes, or grooves. Efforts were made to reduce stress concentrations; however, in the final shaft designs (Figure 4-13 and Figure 4-14), keyways and a groove for a retaining ring at the end of the shaft were required. A keyway will produce a stress concentration near a critical point at the load-transmitting component [77]. This occurs at the critical points highlighted above at the midpoint of the outermost pulley. Considering an endmill keyseat, the stress concentration will be a function of the radius at the base of the keyway. A typical ratio of r/d=0.02 was used, corresponding to stress concentration factors of 2.14 for bending and 3.0 for torsion [77].

Retaining ring grooves impose stress concentrations. The theoretical stress concentration factors can be determined using charts (Figure 4-19). For typical grooves, the ratio r/t is about 1/10, corresponding to stress concentration factors of 5.0 for bending and 3.0 for torsion [77]. The retaining ring groove for both shafts is not at a critical location; therefore, the stress concentrations associated with these were not included in the analysis.

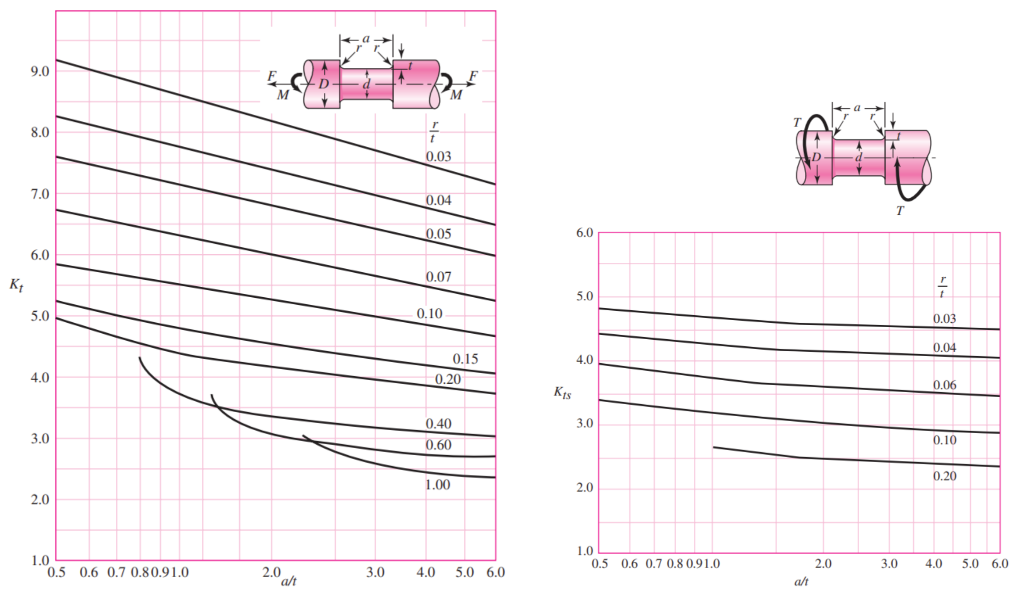

Figure 4-19: Theoretical stress concentration factors for flat bottom groove in a shaft (Adapted from [77])

Another parameter is the notch sensitivity, q, which measures the sensitivity of a material to geometric discontinuities [81]. Stresses are locally high where notches occur, and fracture may occur if the material cannot accommodate the high-stress levels. This factor is influenced by the stress concentration factors shown in the equation below:

$$q = \frac{K_f - 1}{K_t - 1} \tag{4-10}$$

True notch sensitivities are determined through experimental testing; however, published experimental values for many materials can provide reasonable estimates. The notch sensitivity can be selected using charts such as Figure 4-20 using the material's ultimate stress and notch radius.

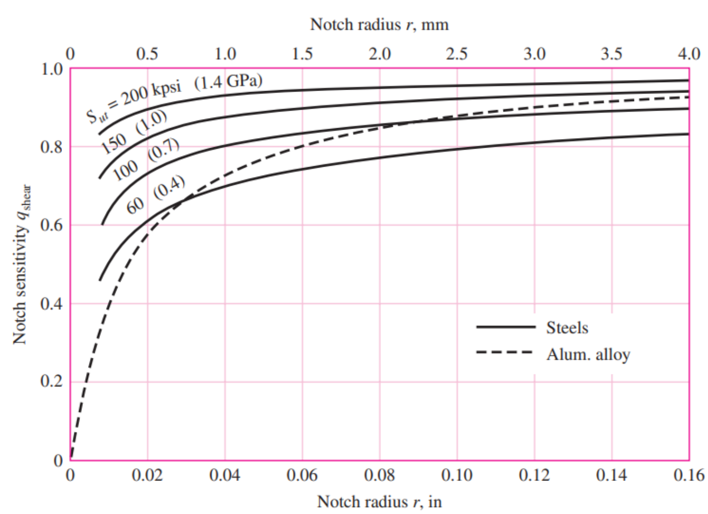

Figure 4-20: Notch sensitivity chart for steels and aluminum alloys (Adapted from [77])

Alternatively, Figure 4-20 is derived from the Neuber Equation [77], which can be used to calculate the notch sensitivity more accurately. Rearranging the equation to the form below was used where, $\sqrt{a}$ is the Neuber constant (i.e., material constant that is a function of the ultimate strength):

$$q = \frac{1}{1 + \frac{\sqrt{a}}{\sqrt{r}}} \tag{4-11}$$

A similar design across both shafts was desired. Since the distal shaft required a through-hole, a hole was introduced at the proximal shaft. The hole also reduced the overall weight of these parts since it was determined they would need to be machined from steel. The maximum inner diameter was determined through iterations, varying the inner diameter while maintaining a safety factor of at least 1.25. The safety factor may seem low; however, in the prosthetic industry, where weight and size are critical to the success of a design, safety factors of this magnitude are common.

4.3.5 Shaft Analysis Results

The analysis outlined in Section 4.3.4 was employed to verify the material selection and proximal and distal shaft geometries. Proximal and distal shafts were designed to be the same size; therefore, a final outer diameter of 25.0 mm and an inner diameter of 12.75 mm were used. This maintained a safety factor of 1.7 for the distal shaft and 1.3 for the proximal shaft. High-strength steel 17-PH H900 is used to resist the high torsional and bending stresses during operation. Stress concentrations were minimized by eliminating a pin connection, and weight was reduced by implementing the transverse hole in each shaft.

4.4 Key Design

The motor torque is transmitted to the pulley system using keyed connections. The keys prevent the rotation of the pulleys with respect to the shafts and enable safe and controlled movement. These critical elements were designed to fail to protect the more expensive components if acceptable operating limits were exceeded. High-strength 8630 alloy steel key stock was selected to eliminate the need to machine keys, and a 1.15 factor of safety was specified.

Direct shear and crushing are two failure modes to be considered when selecting appropriate keys. However, checking for failure due to crushing is sufficient for square keys since the failure will be less critical for shear stress according to the distortion energy failure theory [77]. Considering the free body diagram of the key (Figure 4-21), the force can be determined:

$$F = \frac{T}{r} \tag{4-12}$$

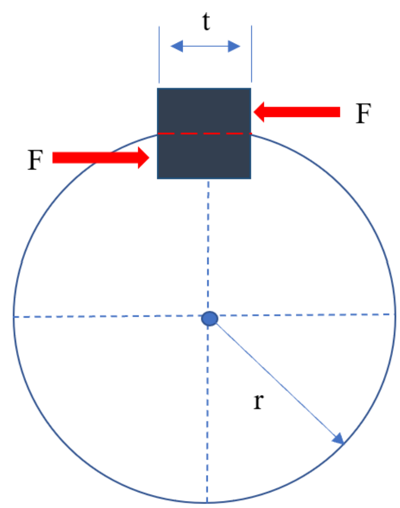

Figure 4-21: Free body diagram for a key. *F* is the force, *t* is the key thickness, and *r* is the shaft radius

The required key length to resist crushing was determined using Equation 4-12. The area for half the key face was used per Figure 4-21:

$$n = \frac{S_y}{\sigma} = \frac{S_y}{F \big/ \frac{tl}{2}} \qquad (4\text{-}13)$$

$$l = \frac{2Fn}{tS_y}$$

where l is the length of the key, F is the force, n is the factor of safety, and S_y is the key's material yield strength.

The final key specifications are outlined in Table 4-2. Each key was to be the same length, given the pulley system's geometrical constraints, and the length was minimized to limit joint lateral protrusion. A final length of 10.0 mm was selected to satisfy these requirements. A 4 mm x 4 mm square key was suitable for the distal shaft; however, a 6 mm x 6 mm key was required for the proximal shaft due to high torques induced by the pulley size ratio.

Table 4-2: Key design parameters

Key Location	**Size (mm)**	**Minimum Length (mm)**	**Final Length (mm)**	**Material**
Distal shaft	4x4	10.03	10.00	8630 Alloy Steel
Proximal shaft	6x6	9.06	10.00	8630 Alloy Steel

4.5 Supporting Link

A supporting link between the proximal and distal shafts was required to facilitate rotation, provide structural support, and ensure adequate clearance between the motor and prosthetic socket through the full ROM (Figure 4-22). Each socket is unique to the user; however, the furthest distances from the center of rotation occur at the base or front of the socket. These distances governed the supporting link length.

In a study that included pelvic radiographs of 50 men and 50 women, the distance between the base of the ischium and hip center of rotation was 71 mm (±6.35) for men and 65 mm (±6.72) for women [63]. Additional space was accounted for soft tissue and the prosthetic socket (5 cm). The actuator geometry was considered, allowing future iterations to include an outer casing that encloses the joint. The radial clearance was 130 mm, with a total distance between shafts of 167.5 mm.

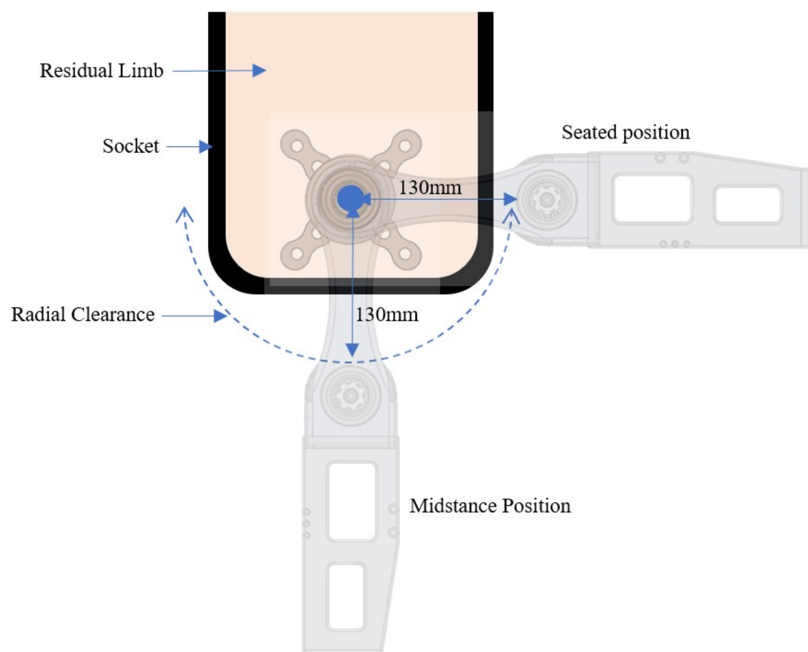

Figure 4-22: Radial clearance required to ensure no interference between the LMPHJ and prosthetic socket throughout the ROM

The link was machined from 2024-T4 aluminum because it is lighter than steel alternatives and has relatively high strength. Rotation about each shaft was required to enable hip flexion and extension. Bearings were an appropriate choice to allow this rotation; however, due to the Q-angle feature of this design, angular contact bearings were required to accommodate the axial and radial loads. The bearings' size depended on the shaft geometry; therefore, an inner diameter of 25 mm was required. Sealed Angular Contact Double Row Ball Bearings were selected for their ability to handle a combined load capacity equivalent to 2200 kg dynamic load and 1450 kg static load. This load capacity is beyond the loads experienced at the bearing locations. Assuming the maximum weight capacity and forces induced by the actuation system, the theoretical maximum forces possible at the bearing locations will be approximately 8200 N (835 kg).

4.5.1 Topology optimization

The supporting link is a critical weight-bearing component that will endure extensive loading during use. The part's geometry was partially optimized through Solidworks Topology Optimization Tool. This feature takes input for design constraints and goals to optimize part geometry through an iterative algorithm. In accordance with the design criteria defined in Section 3.4 and ISO 15032:2000, the study's goal was to minimize the part's weight, and a constraint was added to ensure the vertical displacement did not exceed 15.0 mm.

The Solidworks optimization tool considers the part's original geometry and assesses how the part deforms under the specified loads. Using the "subtraction method," the software iteratively compares this deformation to the maximum deflection identified and recommends a near-optimized solution considering the constraints [82]. The result is a version of the original part indicating material that can be removed and critical areas that cannot be removed through a spectrum (Figure 4-23).

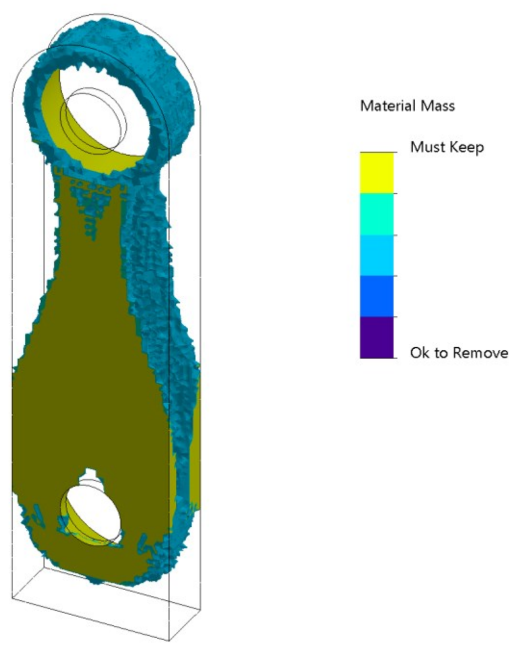

Figure 4-23: Solidworks Topology Optimization results. The gradient key (right) indicates what material must be kept for structural integrity and what material can be removed to achieve the study's goals

Through topology optimization, considerations for ease of manufacturing, and interfacing components, the final supporting link design is shown in Figure 4-24. The width of the selected bearings dictated link thickness.

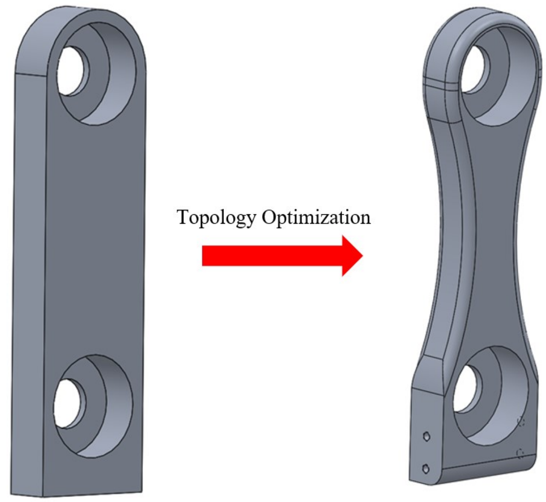

Figure 4-24: Finalized supporting link designed influenced by topology optimization

4.6 Lamination Plate

The lamination plate (Figure 4-25) connects the LMPHJ to the prosthetic socket. The lamination plate design was adopted from existing pronged lamination plate designs [78]. Since sockets vary between users, the prongs can be bent to the socket shape prior to lamination. The prong shape and holes allow lamination resin to penetrate and create a stronger hold. The standard M36 threaded connection for prosthetic applications was implemented to connect to the proximal shaft.

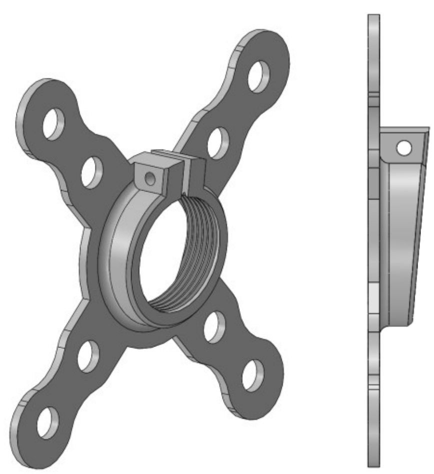

Figure 4-25: Pronged lamination plate design

A unique element of this design is the Q-angular feature. Naturally, the human femur is angled medially, allowing the leg to rotate about the acetabulum without colliding with the pelvic bone. This is referred to as the quadricep angle, or "Q-angle" (Figure 4-26), and has normative values of 17.0 degrees for women and 12.0 degrees for men [79]. Aiding the initiative to improve symmetry across limbs, a 5.0-degree angle in the frontal plane was implemented to orient the prosthetic thigh segment medially. The angular feature was only applied to 5.0 degrees since some users can have a smaller natural quadricep angle, additionally, socket design can account for some of this angle. Further adjustments for each user will be accommodated in the lamination process.

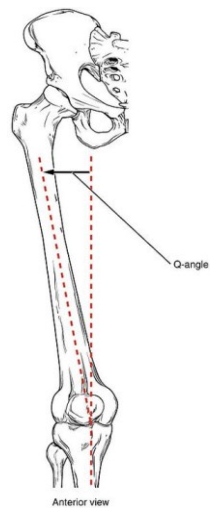

Figure 4-26: Quadricep angle of the human leg (Adapted from [72])

4.7 Low-friction washers

The supporting link rotates around the proximal and distal shafts while the pulleys driving the motion remain fixed. A small gap between moving parts was required to eliminate any rubbing between metal components. Low-friction washers were introduced to limit the wear of contacting components and provide this spacing. Polytetrafluoroethylene (PTFE) washers offer exceptional anti-friction properties, allowing low-friction contact between rotating components [83]. The selected washers are also very low profile and lightweight, therefore, are negligible contributions to the overall system weight and lateral protrusion.

4.8 Wave Disk Springs

Disk springs are positioned along the shaft to compensate for any dimensional variation and reduce the sensitivity of tolerance stacking of the shaft assemblies. Eliminating play along the shaft lengths ensures that the parts remain in place and that the pulley system self-aligns. The disk spring space-saving nature is desired, with a compressed height at a working load of 0.3 mm.

4.9 Modified Actuator Components

The Össur Power Knee actuator was used for this thesis. In contrast to Power Knee actuation, rotation only occurs on the lateral side for the LMPHJ, with the remainder of the motor fixed relative to the electronics chassis. Several components were modified to integrate the actuator into the system for mounting purposes.

A motor mounting ring (Figure 4-27) was introduced to restrict motor movement within the device and ensure an appropriate axis of rotation alignment. This component replaces a bearing in the original Power Knee actuator that is not required in the LMPHJ design. Ten screws positioned radially along the circumference secure the ring to the motor casing. Two screws secure the bottom on the part to the top plate of the aluminum chassis.

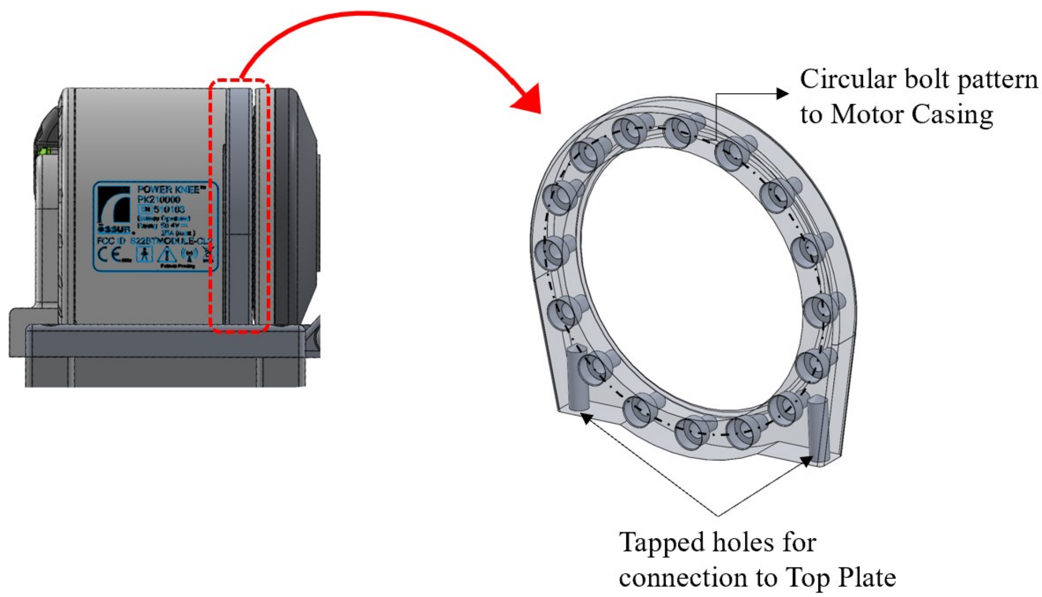

Figure 4-27: Motor mounting ring design

The medial mounting part (Figure 4-28) was designed to be easily inserted into a usable cavity on the medial side of the motor. A rubber O-ring was implemented to ensure a snug fit and reduce the level of tolerancing required for machining. Together with the motor mounting ring, lateral movement of the motor is restricted.

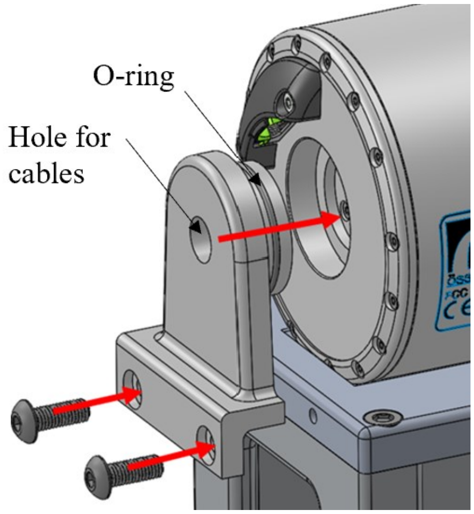

Figure 4-28: Medial mounting part design

In the Power Knee, the lateral motor cap (Figure 4-29) had a lever arm required for actuation; however, this was removed since it interfered with the LMPHJ design. The distal shaft connects to this component using the existing socket screws as dowels and the center screw for securement. This connection was implemented to connect to the existing actuator design easily.

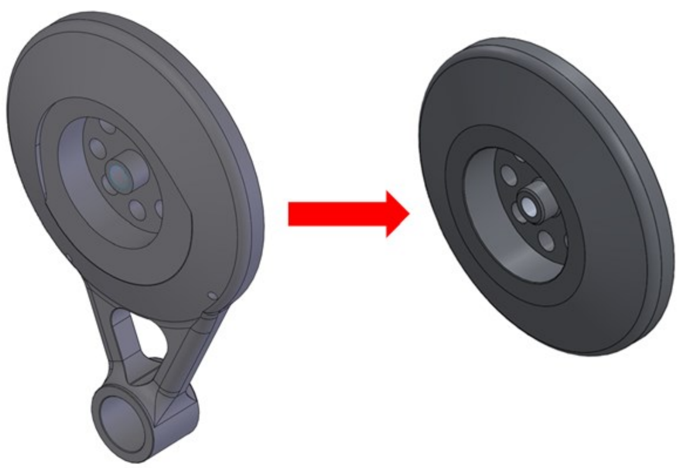

Figure 4-29: Lateral motor cap design (right). Modified from existing motor component (left)

4.10 Top Plate

While the aluminum chassis that houses the electronics falls outside the scope of this thesis, the top plate of this design (Figure 4-30) required modification for the LMPHJ. A 29.0 mm extension was added to connect the supporting link and the cage. A rigid connection between these parts was required to enable rotation; otherwise, the distal shaft would rotate within the bearing connection without generating the desired motion. Grooves were added to accommodate the circular nature of the actuator. One groove is deeper than the other to provide clearance for the rotating portions of the motor, avoiding contact between moving metal components. Two holes were added on the bottom of the plate to secure the motor mounting ring, and tapped holes were added to the side for the medial mounting part. The overall plate thickness was increased from 8.0 mm to 10.0 mm because the modified part was initially not strong enough, according to the FEA simulations outlined in Section 4.12.

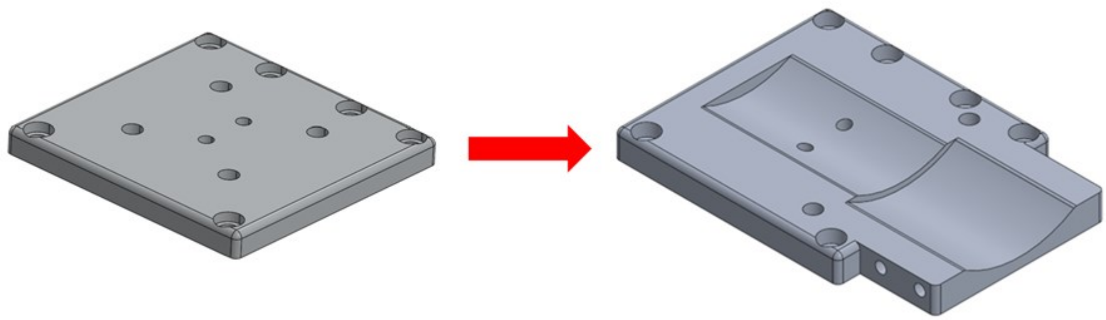

Figure 4-30: Top plate design for interfacing to the distal portion of the prosthetic limb. Original design (left) and modified design (right)

4.11 Braces

Two braces (Figure 4-31) are used anteriorly and posteriorly to connect the supporting link to the top plate. The friction between these elements creates sufficient hold during weight-bearing and actuation. Four M5 screws are used to secure each side, two vertically and two horizontally, to prevent rotation about the screws. A tolerance chain was broken by positioning the supporting link outside of the top plate. In previous candidate designs, the link contacted the top of the plate, which introduced a tolerance chain and could have affected distal shaft alignment.

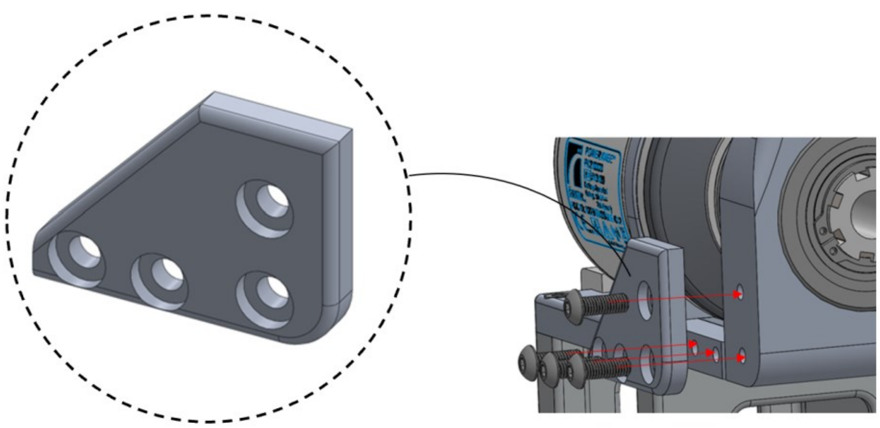

Figure 4-31: Brace design used to secure the supporting link to the top plate of the electronics chassis

4.12 FEA Simulations

Finite element analysis (FEA) was used to determine the stress-strain behavior of LMPHJ components. These behaviors would then be used to verify material selection and part geometries. SolidWorks simulations were performed to determine if the designed components were strong enough and identify areas for optimization. FEA can reduce the number of physical prototypes required and establish areas of concern or over-design before manufacturing. The simulation results aided design decisions and reasonably indicated how the system should perform during mechanical testing. Following any design modification, the simulations were re-run, and the results were re-evaluated to verify the design.

Assembly-level simulations were completed to better understand the part's behavior when subjected to loads. Simulating the assembly provides a holistic understanding of the system and improves results over part-level simulations because component interactions are considered. The objective of the Solidworks studies was to simulate the required tests outlined in ISO 15032:2000.

Appropriate connectors and contacts were applied to the parts to represent the assembly within the study. Simplifications were made to the model to reduce the simulation's computational costs while maintaining an accurate model representation. This included suppressing features that did not contribute to LMPHJ structural behavior but could introduce challenges when meshing the assembly.

The pulley system and shaft components, such as disk springs and washers, were excluded because they do not provide structural support. Therefore, this simplification was deemed to have minimal effects on simulation accuracy. A mock motor was modeled in place of the Össur actuator because the motor's complexity and the parts' interaction are not accurately represented in simulation. Additionally, the abundance of small components created problems for meshing. All screws and bearings were replaced with the appropriate connectors modeled in the simulation study. Due to meshing errors, a rigid connection was added between the motor mounting ring and the mock motor's inner face, which was deemed suitable since the ten radial screws connecting these parts will produce a rigid-like connection.

The assembly simulations were set up to represent the ISO 15032:2000 testing conditions. However, adaptations were required to accommodate the laterally mounted system because this standard is based on front-mounted hip joints. Test rigs were based on the dimensions provided in the standard. The rigs accounted for the LMPHJ Q-angular feature, so the load is applied in the appropriate planes, as per Figure 4-32. Materials were specified as Aluminum 2024 T4 for the rigs to ensure adequate strength. Under section 7.2.2 of the standard, the proof test of end attachments should withstand at least 5476 N at the A100 level, which the modeled rigs satisfy when simulated independently.

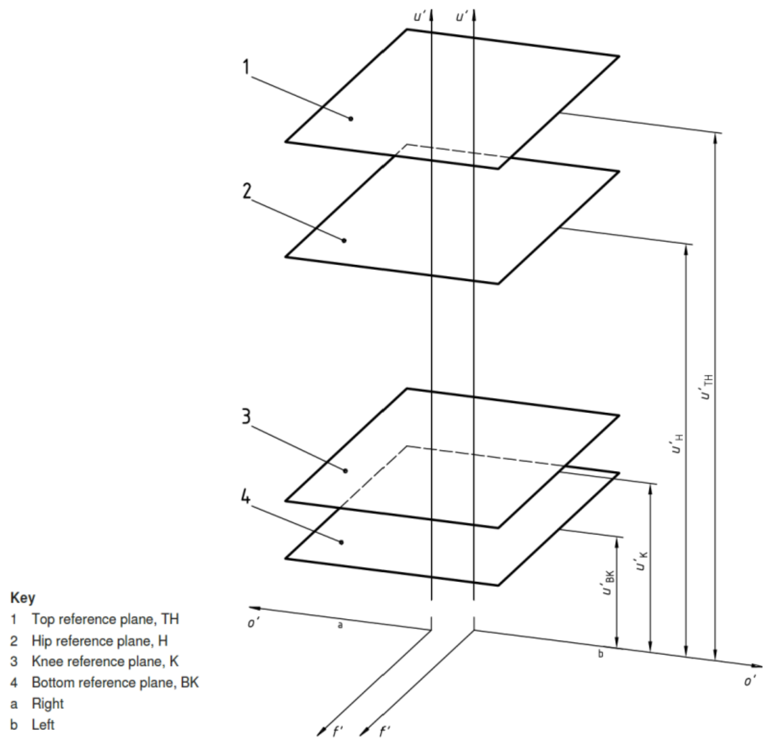

Figure 4-32: Reference planes and axes used to define loading conditions for ISO structural testing. The top and bottom reference planes (TH, BK) correspond to vertical offsets of the load application points. The hip and knee reference planes (H, K) correspond to the vertical offsets of the hip and knee center of rotation (Adapted from [34])

Only the required tests were conducted in simulation. Further, only the static failure tests were conducted because the testing conditions were the same for both the proof and ultimate tests. Only the ultimate test required higher loads. The A100 level loads were applied for each test because these represent the highest loads across all tests. This narrowing of the simulations reduced computational time, and if the joint was sufficiently strong under the highest loading condition, it should also pass any tests with the same set-up at lower forces. The ductile failure load was applied for each test because this would be the predominant reason for failure in the LMPHJ metal alloys [84]. The tests are outlined in Table 4-2, and the loading conditions are presented in Figure 4-33.

Table 4-3: Simulations conducted using ISO standard parameters

Type of Test	Loading Condition	Test Loading Level
Static Failure	A-P extension test	A100 = 3360 N
Static Failure	M-L test	A100 = 3360 N
Static Torsion	Torsional test	50 Nm

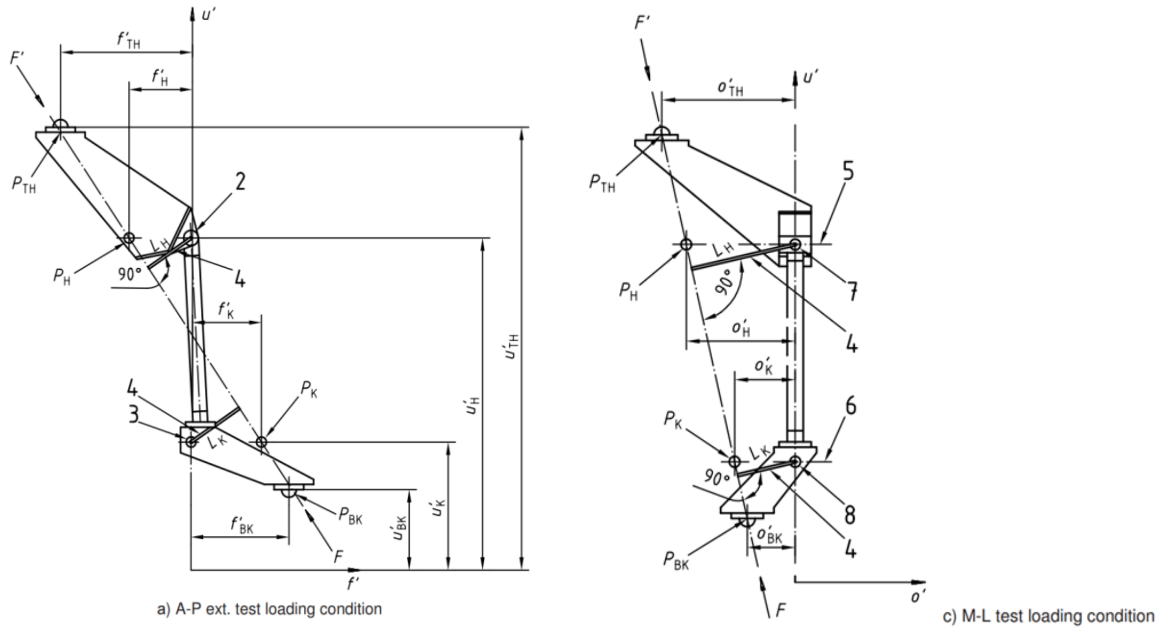

Figure 4-33: Loading conditions defined in the ISO standard for the A-P ext. test (left) and M-L test (right) (Adapted from [34])

4.12.1 Failure Criteria

Following each simulation, the results were examined and compared against the part's mechanical properties in addition to the failure criteria defined in the ISO standard [34]:

- 6.4.3.7: The test sample shall satisfy the requirements of the static A-P or M-L failure test if it sustains the ultimate test force for brittle failure $F_{su,brittle}$, or if ductile failure occurs at a load exceeding the ultimate test force for ductile failure $F_{su,ductile}$.
- 6.4.2.10: If permanent deformation exceeding 15 mm occurs, the test sample does not satisfy the requirements of the static A-P or M-L proof test of this International Standard.
- 6.4.2.11: If any individual component of the test sample fails to function safely after this test, record that this component does not satisfy the requirements of the static A-P or M-L proof test of this International Standard in the combination of components in the test sample.
- 6.5.2.9: The test sample shall satisfy the requirements of the static torsional proof test of this International Standard if the relative angular movement between the ends of the test sample does not exceed 3°, and the hip unit continues to function safely

While Solidworks does not indicate whether a part may fail or suggest its functionality after simulation, this can be inferred from the resulting stresses and deformations. All designed components are machined from Aluminum 2024-T4 (324 MPa yield strength, 469 MPa ultimate tensile strength) or 17-4 PH Stainless Steel H900 (1379 MPa yield strength, 1448 MPa ultimate tensile strength).

If any of the listed conditions were not satisfied, or if the stresses exceeded the allowable stresses of the selected material, appropriate changes were made to part geometries or a material change was implemented, and the simulations were rerun.

4.12.2 Static A-P Extension Failure Test

The "A-P Extension Test" involves loading the LMPHJ in the u'-f '-plane, which corresponds to anterior-posterior. Using the dimensions defined in the ISO standard set-up, a test rig (Figure 4-34) was modeled to ensure that the test load would be applied at the correct location according to the loading condition defined in Figure 4-33 (left). An angular feature was required to account for the 5° angle at the lamination plate to orient the point of application in the correct plane. Only the failure test was conducted with an ultimate load of 3360 N, corresponding to the ductile failure load.

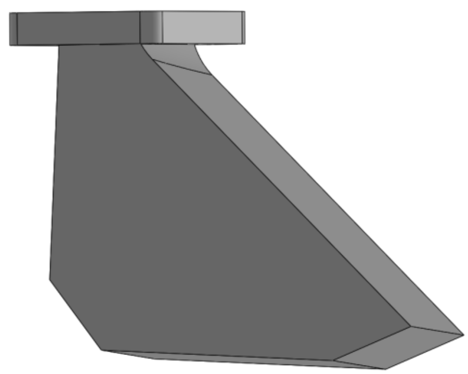

Figure 4-34: A-P ext. test rig design based on dimensions provided in the ISO standard

Figure 4-33 shows a force-couple applied near the hip and knee joint; however, this loading condition can be replicated by fixing one of these points in simulation or testing. The lamination plate was fixed at the top, and the load was applied off-axis of the knee. This was done because the same knee joint can be used for front-mounted and laterally-mounted hip joints.

The stress gradient shown in Figure 4-35(left) can be deceiving across various materials, each possessing different material properties. For this reason, high-stress area investigations were completed using the iso-clipping tool, where areas of specific stresses can be isolated. Solidworks default settings provide a gradient between the measured maximum and minimum von Mises stresses.

The displacement plot (Figure 4-35(right)) was also of interest to ensure the LMPHJ would satisfy the ISO standard. As evidenced by the gradient below, the maximum deflection measured was 11.72 mm. Based on the simulation results, the LMPHJ should not fail during the Static A-P Failure Test, and ISO Standard requirements regarding loading and displacement were satisfied.

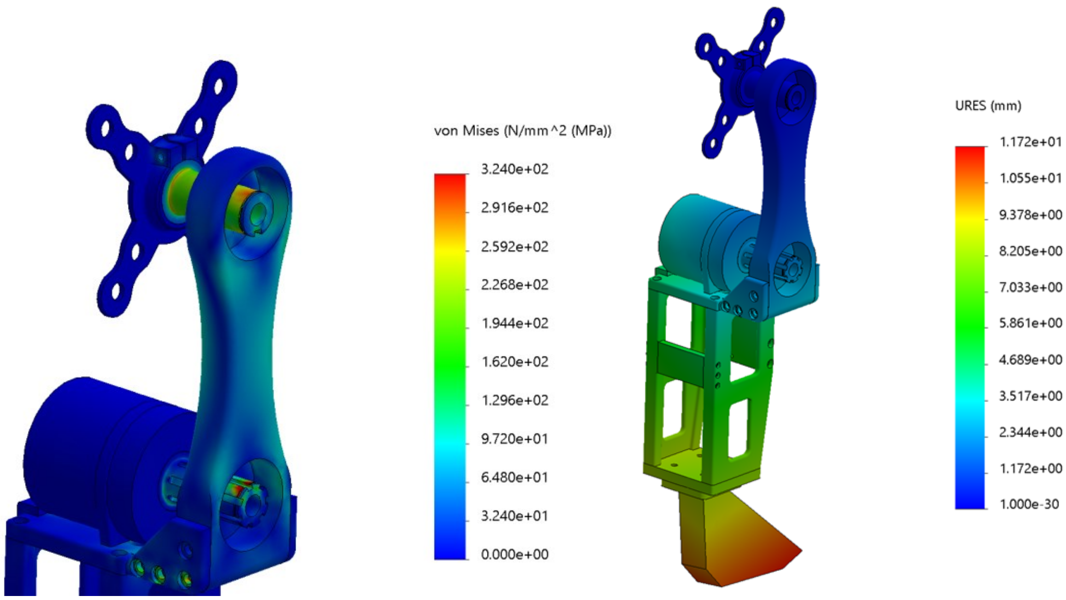

Figure 4-35: Stress gradient (left) and deflection plot (right) for A-P ext. simulation

4.12.3 ML Failure Test

The “ML Failure Test” was similar to the AP-Extension test. The difference was that the single load application was applied off-axis of the knee in the u’-o’-plane, corresponding to the medial-lateral direction. A test rig (Figure 4-36) was modeled to position the point of application in accordance with Figure 4-33. Using the 3360 N ductile failure ultimate load, the simulation was run by applying this load at the test rig while the lamination plate at the hip was fixed.

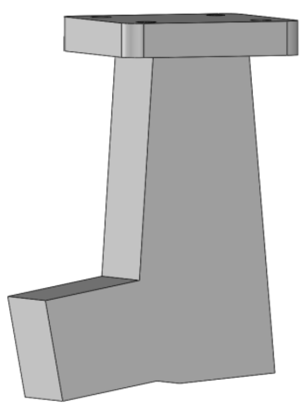
Figure 4-36: M-L ext. test rig design based on dimensions provided in the ISO standard

The high-stress areas (Figure 4-37 (left)) were examined to ensure failure would not occur by comparing these to the mechanical properties provided in Section 4.12.2. The maximum deflection was 14.27 mm (Figure 4-37 (right)). Based on these results, the LMPHJ should not fail during structural testing under the ML loading condition.

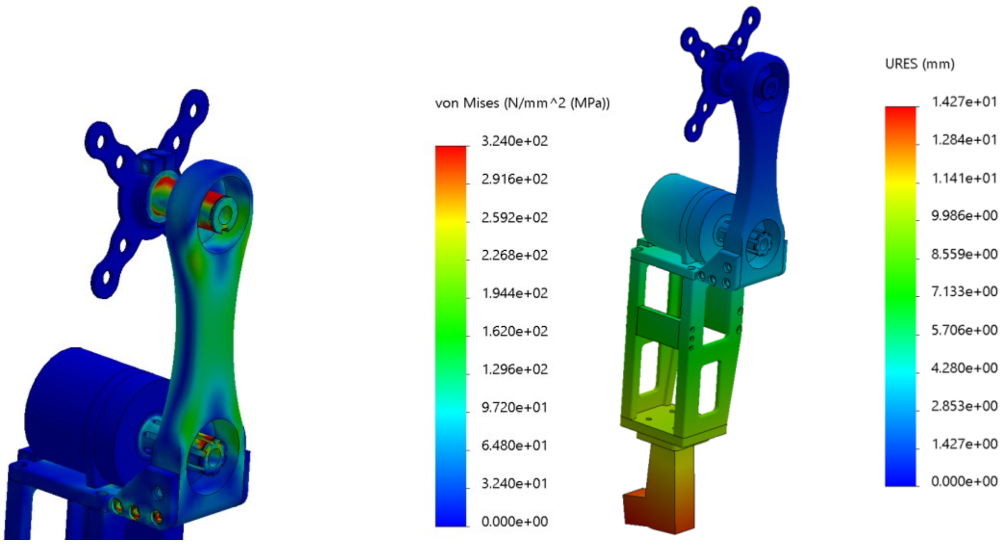

Figure 4-37: Stress gradient (left) and deflection plot (right) for ML simulation

The highest stresses and largest displacements were measured following the ML-Failure test. These results were expected due to the loading conditions and joint geometry. The supporting link is weaker against bending stresses in the ML direction. This also correlates to less resistance to deformation, resulting in the higher displacements measured.

4.12.4 Static Torsional Proof Test

The static torsional test was simulated to evaluate the design's structural integrity against the torsional loads specified in the ISO standard. The simulation was run in full extension with the hip and knee joint centers aligned. The lamination plate was fixed at the top of the LMPHJ, and the twisting moment was applied using a test rig (Figure 4-38) at the bottom of the chassis.

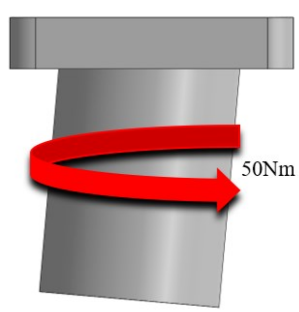

Figure 4-38: Torsion test rig

Solidworks does not compute the angular displacement to compare against the failure criteria defined in Section 4.12.2. However, the resulting stresses and displacements were very low when compared to the previous testing conditions (Figure 4-39); therefore, the LMPHJ was deemed to pass this test.

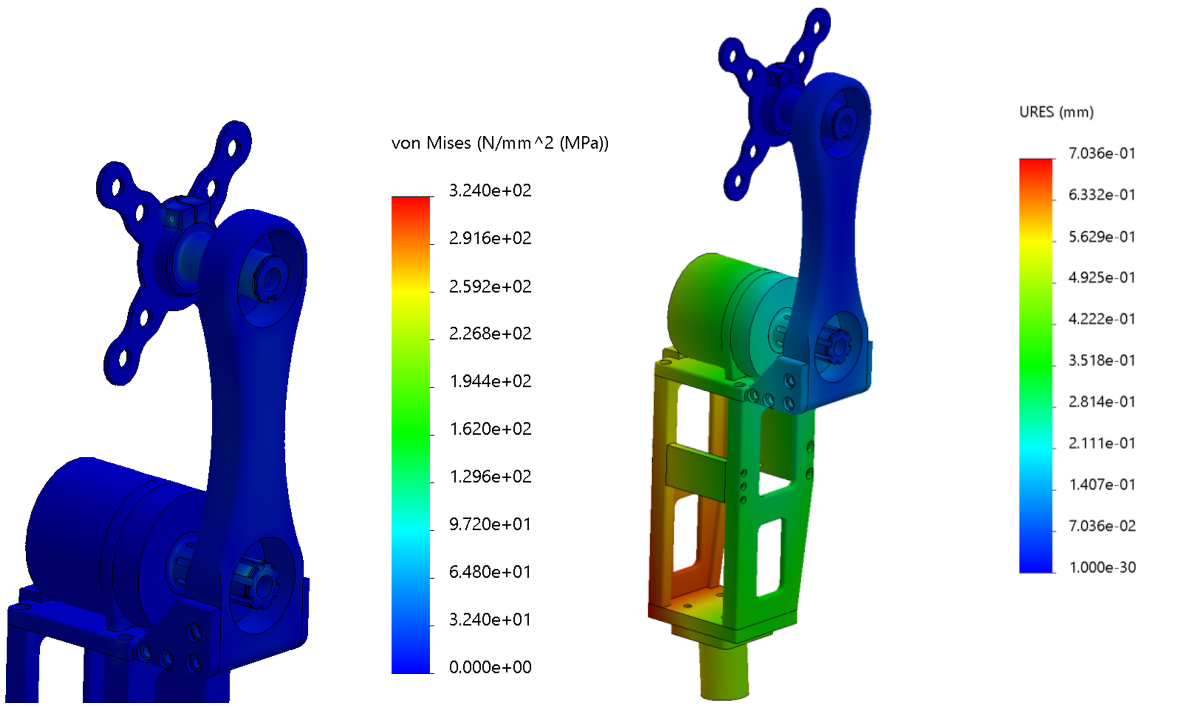

Figure 4-39: Stress gradient (left) and deflection plot (right) for torsional test simulation.

4.13 Fastener Selection

The LMPHJ assembly includes a variety of threaded fastener connections that must be strong enough to withstand operational loads. The forces that each fastener experiences during testing are returned through the assembly-level simulations. Solidworks provides an axial and shear force for each connector (Table 4-4). Using this information, accompanied by various international standards, calculations were completed to make appropriate selections on the size and grade of screws required for each location. These calculations are discussed in Sections 4.13.1-4.13.3 with the summary of results in Table 4-4. Based on these results, selections were made to use standard screws and minimize the variation of fasteners required to make procurement easier.

Table 4-4: Fastener selection summary. TP = Top Plate, PB = Posterior Brace, AB = Anterior Brace, MP = Medial Part, MR = Motor Ring, LP = Lamination Plate

Screw ID	**Screw Size**	**Maximum Tensile Load (N)**	**Maximum Shear Force (N)**	**Minimum Class Required**	**Selected Length (mm)**
TP_1	M5	861.64	447.88	4.6	14
TP_2	M5	1776.20	447.00	4.8	14
TP_3	M5	873.49	521.15	4.6	14
TP_4	M5	824.02	416.40	4.6	14
TP_5	M5	1657.60	312.27	5.6	14
TP_6	M5	1410.00	334.73	4.6	14
PB_1	M5	4044.00	4773.60	9.8	10
PB_2	M5	1082.10	5425.20	4.6	10
PB_3	M5	6246.20	4422.50	12.9	10
PB_4	M5	867.25	823.38	4.6	10
AB_1	M5	4380.20	4997.20	9.8	10
AB_2	M5	1959.10	5649.00	5.8	10
AB_3	M5	7091.10	5741.70	12.9	10
AB_4	M5	2515.50	1827.90	5.8	10
MP_1	M4	922.55	119.46	4.8	8
MP_2	M4	935.88	102.94	4.8	8
MR_1	M5	1973.40	215.00	5.8	12
MR_2	M5	1258.20	275.19	4.6	12
LP_1	M5	1190.50	N/A	4.6	18

Standard lengths and nominal diameters for metric fasteners were selected based on geometrical constraints and their location relative to high-stress areas. The purpose of the threaded fasteners is to hold two parts together, achieved by screwing the fastener into a tapped hole. Three common failure modes for threaded connections are external thread failure, shear failure, and internal thread failure [85]. According to the ISO 898-1 standard: *Mechanical properties of fasteners made of carbon steel and alloy steel – Part 1* [86], bolt shearing should be the intended failure mode under tensile loading. Fracture is typically more desirable than stripping the internal or external threads because it is economically better to replace the fastener than the machined components [87]. However, thread failure can occur if the connections are not designed appropriately; therefore, the following sections outline the calculations completed to verify the fastener selections.

4.13.1 External Thread Failure Check

Maximum tensile resultant forces across all simulations are shown in Table 4-4 for each connector. These values were compared to the proof loads outlined in ISO 898-1:2012 [86] for the screw size across the various property classes. Based on this comparison, the class indicated in Table 4-4 was provided as a minimum requirement.

4.13.2 Shear Failure Check

Utilizing the maximum axial resultant forces from the simulations, a check against shear failure was complete. The European Union Standard EN 1993-1-8:2005:2005 – *Design of joints* was used to determine the design resistance for individual fasteners subjected to shear and/or tension. The shear strength for each screw was computed using the following equation [88]:

$$F_{V,Rd} = \frac{\alpha_V f_{ub} A}{\gamma_{M2}} \tag{4-14}$$

where, α_V is a multiplying factor based on the class, f_{ub} is the ultimate tensile strength of the bolt, A is the tensile stress area of the bolt, and γ_{M2} is a partial safety factor for resistance of cross-sections in tension to fracture. Under Section 6.1 of EN 1993-1-1:2005 – *General rules and rules for building*, $\gamma_{M2} = 1.25$ [89]. The calculated shear strengths were then compared to the simulated axial loads in the screws. The calculated values were to be higher than the loads experienced; otherwise, the screw would fail in shear. If a failure mode was predicted to occur, a higher strength size or class was required, and the calculations and comparisons were repeated.

4.13.3 Internal Thread Failure Check

The internal threads throughout the assembly were commonly Aluminum Alloy-2024, therefore, checking for failure in this area was critical because it is a lesser-strength material than the steel bolts used. To ensure that this failure mode does not occur, adequate thread engagement length is required.

FED-STD-H28/2B – *Screw-Thread Standards for Federal Services* was used to calculate the required engagement length for each screw [87]. The following equation is provided in the standard to determine the shear area for internal threads,

$$A_s = \pi n L_e d_{min}[\frac{1}{2n} + 0.57735(d_{min} - D_{2max})] \tag{4-15}$$

where, A_s is the shear area, n is the number of threads per in, L_e is the length of thread engagement, d_{min} is the external thread's minimum major diameter, and D_{2max} is the internal thread's maximum pitch diameter. Using the maximum tensile loading of the screws outlined in Table 4-4, the shear area can be calculated:

$$A_s = \frac{F_b}{\sigma_{sy}} \tag{4-16}$$

where F_b is the screw's tensile load, and σ_{sy} is the thread material's shear strength. For Aluminum Alloy 2024, the shear strength is 283MPa. With A_s computed, the above equation was rearranged, and the minimum length of thread engagement was calculated. Using these results, the nearest standard screw size was selected. In areas where multiple screws join two components, the longest length was selected for all screws to maintain uniformity throughout the design and procurement process.

$$L_e = \frac{A_s}{\pi n d_{min}[\frac{1}{2n} + 0.57735(d_{min} - D_{2max})]} \tag{4-17}$$

4.14 Prototypes

Prototyping was completed at different stages throughout the design process to assess the functionality, usability, and LMPHJ's overall performance regarding the design criteria. Rapid prototyping using 3D printed components provided a tangible way to evaluate design elements before manufacturing the complete system. The final LMPHJ prototype is presented with the associated electronics and control system.

4.14.1 3D Printed Prototype

A 3D printed prototype (Figure 4-40) was initially developed to test the pulley system functionality. The objective was to provide a proof of concept for the tensioning method and ensure a complete ROM. No structural aspects were examined. Modifications were made to the design only to include parts required to accomplish this objective, and part geometry was reduced to decrease print times. A servo motor was used for actuation; therefore, connecting components for the motor were designed.

Figure 4-40: 3D Printed Prototype of LMPHJ

All 3D printing was completed at the University of Ottawa Richard L'Abbé Makerspace. The modified 3D CAD models were converted to STL file format for 3D printing. Cura slicing software was used to convert the parts into a usable format for the printers. Most parts were printed using the software's recommended settings; however, for some parts with intricate geometries, changes to the print settings were made in accordance with the laboratory technician's suggestions. Parameters that can be adjusted include orientation, infill density, support material, temperature, layer height, and line width, which can alter print quality and time. The Ultimaker S3 [90] Fused Deposition Modeling (FDM) printer was used to create all components. The prototype demonstrated the tensioning method's feasibility and sufficient ROM, with angles achieved beyond the requirements.

4.14.2 LMPHJ Prototype

The final design of the LMPHJ outlined in this Chapter was manufactured and assembled using a combination of machined and off-the-shelf components (Appendix A). This prototype (Figure 4-41) was used for mechanical testing and functional evaluation and assessed against the design criteria.

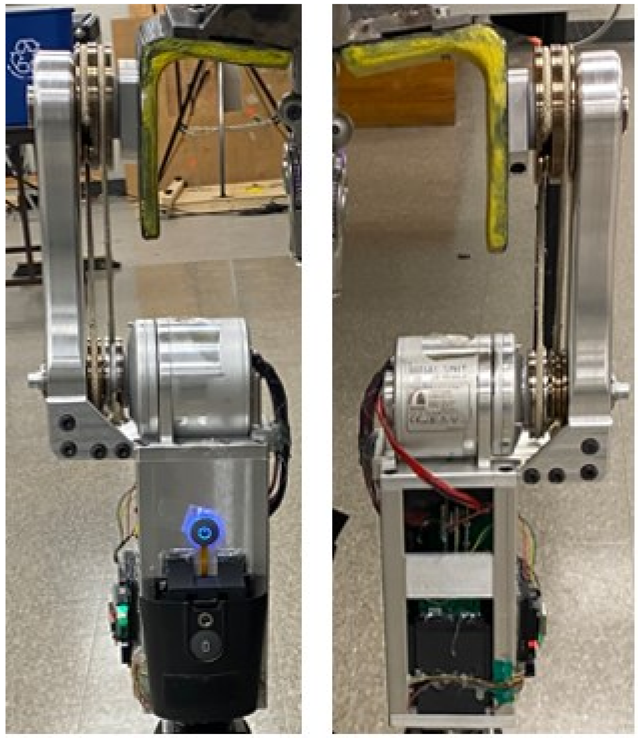

Figure 4-41: Final LMPHJ Prototype - front view (left), back view (right)

Engineering drawings for designed components (Appendix B) were created and outsourced for machining by Össur. To reduce manufacturing time and since the LMPHJ would not connect to a prosthetic socket for testing, a standard M36 adapter was used instead of the lamination plate. All other components were consistent with the design outlined in Chapter 4. A total of 16 parts required machining, meeting the design criteria for ease of manufacturing. Procurement of all off-the-shelf components was completed through McMaster Carr. The ropes were purchased and spliced at a local sailing shop, The Chandlery.

The LMPHJ final assembly was completed at the University of Ottawa and fit to each participant by the Power Hip Research Team for functional testing. The mechanical system, including the actuator, weighs 3.5 kg, meeting the design requirement. The electronics chassis weighs 2.2 kg for a total system weight of 5.7kg. The prototype validated the manufacturing methods and assembly procedure.

4.14.3 Control System

The LMPHJ required a control system to provide the correct amount of powered assistance at different points throughout the gait cycle. While the development and instrumentation of the control system was not included in the scope of this thesis, the controls played a critical part in the functionality of the LMPHJ. Collaboration between many Power Hip project team members was required to ensure the mechanical design and controls were correctly integrated to actuate the prosthesis as intended. The complete intelligent control system remains under development, therefore, for this iteration of the LMPHJ design, the control system followed a pre-determined gait profile.

At a high level, the control system takes input from the inertial measurement unit (IMU) and load cell sensors regarding the position of the joint and the user's applied motion and force to determine their intent for locomotion. Based on the anticipated intent and data from the sensors, an algorithm computes the required parameters to achieve the desired motion. Then, the error between the actual and desired hip joint position is calculated, resulting in an actuation command sent to the motor to drive the hip to generate movement. This framework can be broken down into three levels, outlined further in Figure 4-42.

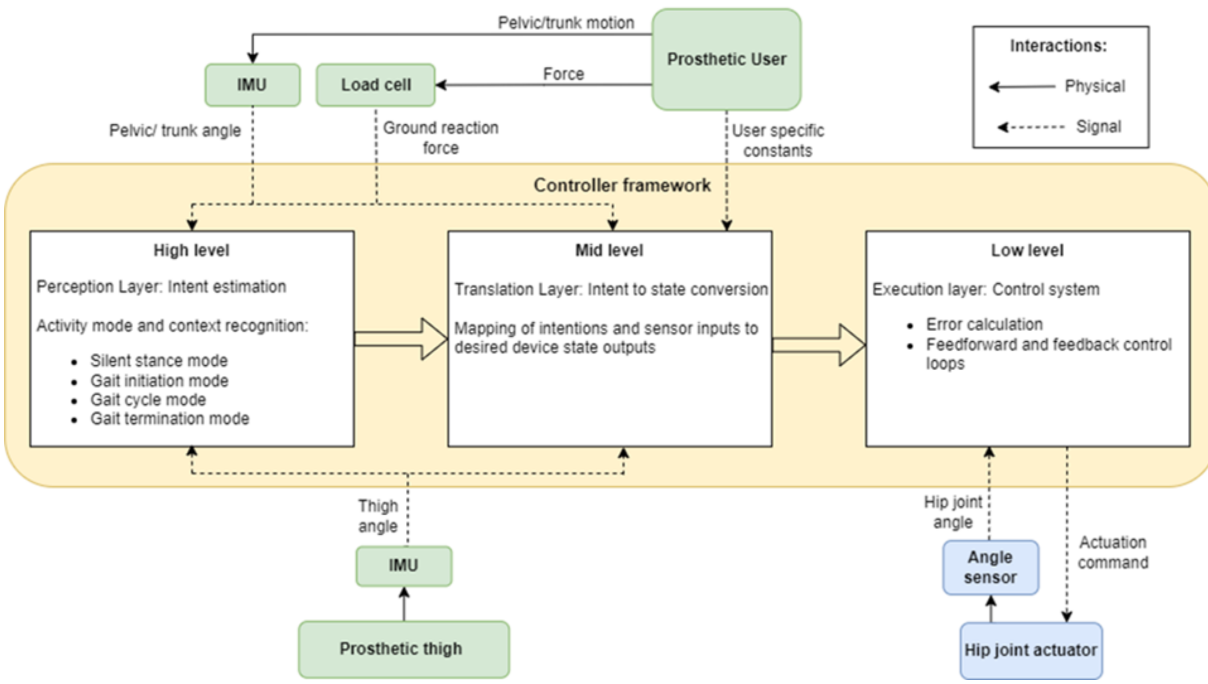

Figure 4-42: Control system framework (Created by Farshad Golshan)

Chapter 5: Mechanical Testing

Mechanical load testing was conducted to validate LMPHJ structural integrity. The joint was loaded based on the concepts represented in ISO Standard 15032. All structural testing was completed at Össur's facilities in Reykjavik, Iceland, with the help of Össur engineering staff.

5.1 Modified ISO Standard Loading Conditions

The loading conditions defined in ISO 15032 are based on the loads experienced by front-mounted prosthetic hip joints. The standard states, "For asymmetrical units, the position of the effective knee-joint centre and the effective hip joint centre shall be established from the manufacturer's/submitter's written alignment" [34]. Therefore, to accurately represent the loading conditions of the LMPHJ, the conditions for structural testing were modified. The modifications were based on how the loads are represented for the front-mounted joints assuming the foot contact point, GRF line of action, and reference to the center of mass.

The objective of the mechanical testing was to ensure LMPHJ structural integrity for walking with the simulator and validate that the joint can withstand the loading required by international standards. Provided the LMPHJ is a prototype, the joint was not considered ISO-compliant following testing. Instead, the standard provided a reference for the test protocols and loads.

5.1.1 Reference Planes and Axes

The reference planes and vertical offsets (Figure 4-32) remained the same because they reference the position of the knee, hip, and other points relative to the ground. The coordinate system was adjusted relative to the criteria provided in the standard:

- The coordinate system has an origin at ground level. The distance from the ground to the knee reference plane is 500 mm [91].
- The u'axis is a line extending from the origin and passing through the effective joint center defined by the middle of the proximal and distal shafts. Its positive direction is upwards (in the proximal direction).
- The o'-axis is perpendicular to the u'-axis and parallel to the hip joint centerline. The positive direction is outwards (in the lateral direction).
- The f'-axis is perpendicular to both the u' and o'-axis. The positive direction is towards the toe (in the anterior direction).

5.1.2 M-L Loading Condition

For the medial-lateral (M-L) test, the line of application lies in the u'-o' plane. Load line orientation was determined by assuming the COM is located at the center of the pelvis, and the foot contact point in the frontal plane would be in line with the anatomical hip joint center (Figure 5-1). The ground reaction force vector is directed from the foot contact point towards the body's COM to maintain balance [92].

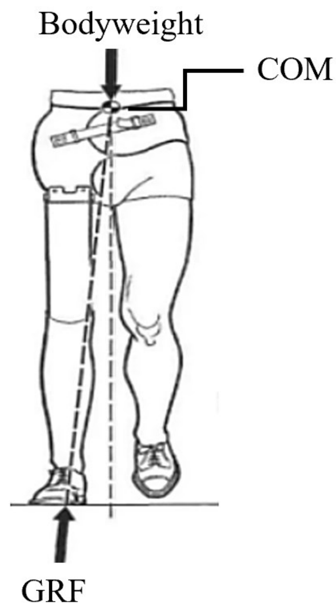

Figure 5-1: GRF line direction of action implemented in the development of the loading conditions for the ML test setup (Adapted from [42])

A SolidWorks model, including the reference planes and load line, was used to calculate the horizontal offsets required to generate this loading condition (Figure 5-2).

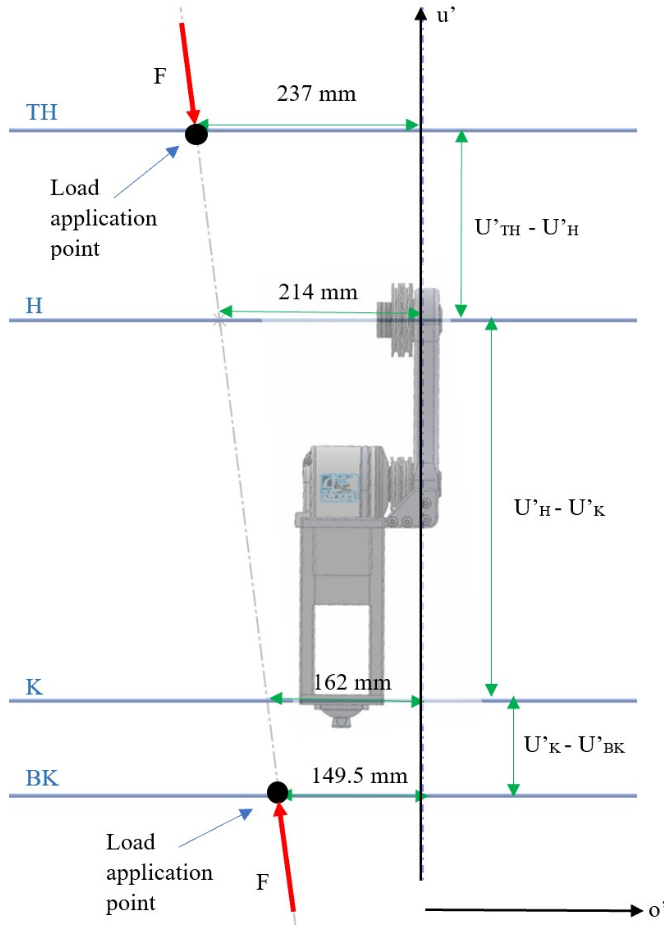

Figure 5-2: Loading conditions for ML static load tests

5.1.3 A-P Loading Condition

The anterior-posterior (A-P) test occurs in the u'-f' plane. For this condition, the load line orientation was maintained because the line of action would be the same as for a front-mounted joint, and in this plane, the force could be easily translated to a known reference point. The line of action was relocated to pass through the effective hip joint center due to its proximity to the centre of mass in this plane. Again, the u'axis horizontal offsets were determined using the Solidworks model.

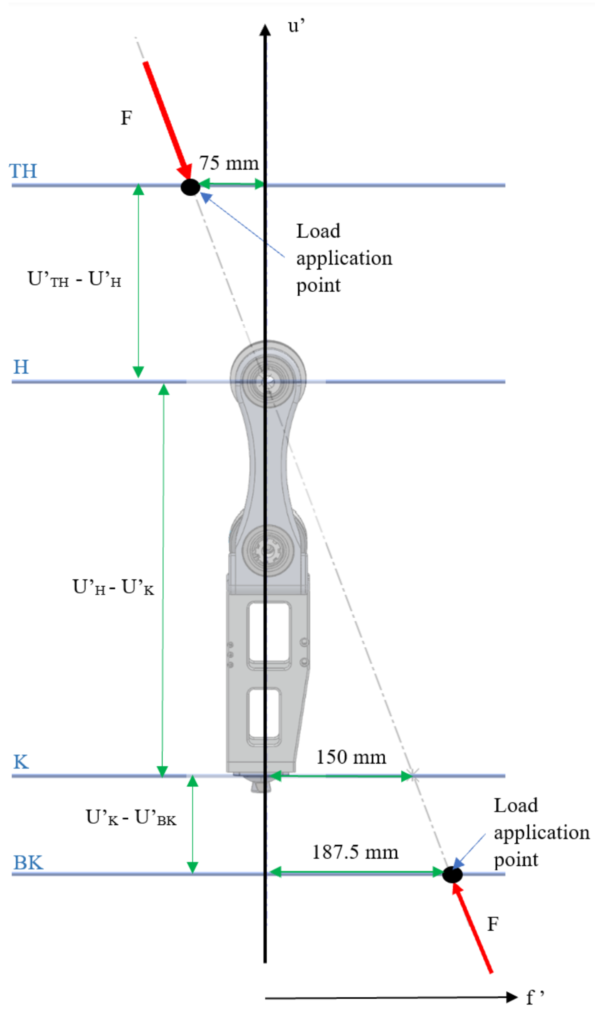

Figure 5-3: AP-extension loading condition for static load tests

5.2 Test Setups

Testing setups for each loading condition outlined in Sections 6.1.2 and 6.1.3 were developed. Before positioning the joint in the testing machine, the setups were mocked up on a workbench. Steel rods connected to the joint's proximal and distal ends achieved the vertical offset and were connected to adjustable load application fixtures to generate the required lever arms. Adjustable lever arms are frequently used in industry and connect directly to the loading apparatus.

The ISO Standard specifies the joint to be put in full extension, so the extension stop on front-mounted joints can be used to prevent rotation during static testing. Considering the LMPHJ lateral mounting orientation, a different means to prevent rotation was required. Many options were explored, including using the ropes or motor control settings to resist the torque; however, both options could not withstand the large moments generated in testing. Mechanical stops were introduced to prevent rotation and emulate an extension stop that will be introduced on the socket in future iterations.

A Servohydraulic Dynamic Low Force Testing System (Model LFV-5-ME, ID 4766) from walter+bai [93] was used for testing since it accommodated the adjustable adapters and is well suited for monotonic compression tests up to 5 kN. While there were no systems specific to prosthetic hip joints, this system is designed for lower-limb prosthetics testing and complies with prosthetic ankle (ISO 22675) and prosthetic knee (ISO 10328) testing standards. The customized setups to achieve the ML and AP-extension loading conditions (Figure 5-4) were secured into the machine using the connection between the adjustable fixtures and the loading points of the machine. A single compressive load is applied vertically; therefore, the joint was loaded into the machine at an angle to achieve the correct load line. For the ML test, the joint was positioned upside down to have the smaller lever arm closer to the load cell, decreasing the likelihood of damaging the joint.

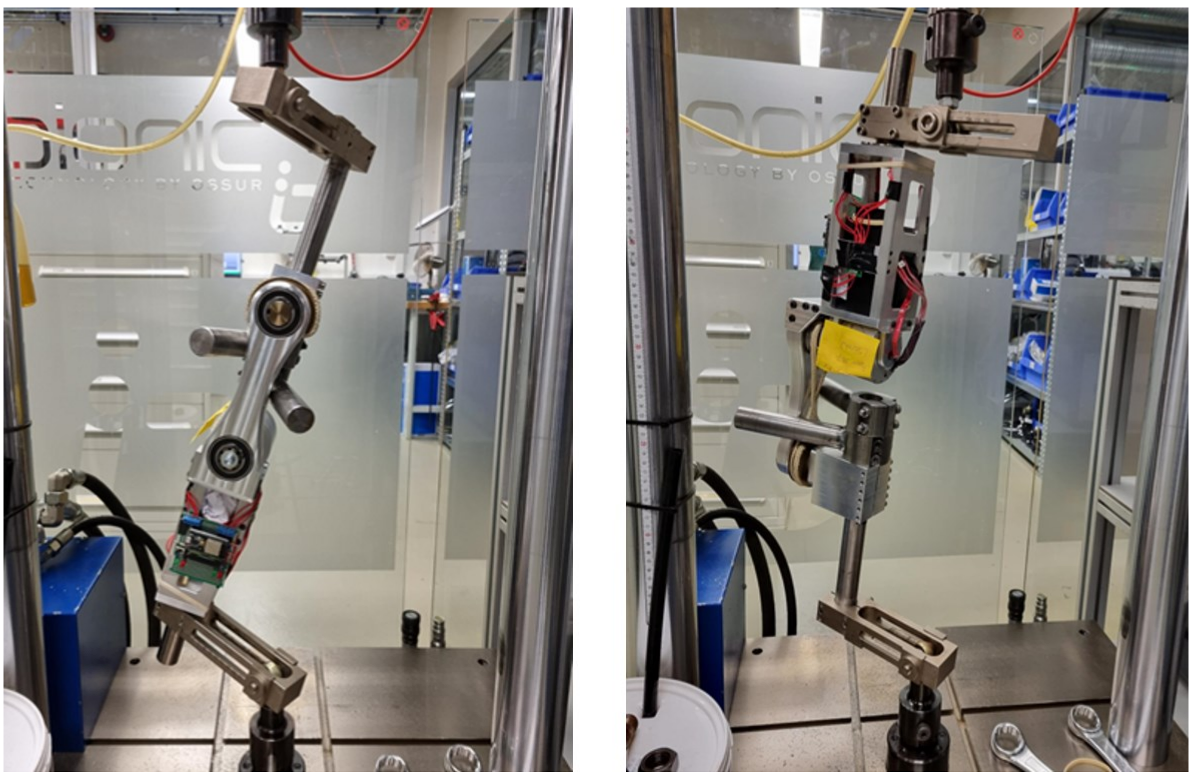

Figure 5-4: Static load test setups for AP-extension test (left) and ML test (right)

5.3 Static Loading Methodology

A static proof test followed by a static failure test was completed for each condition. Based on the low stresses and negligible displacement results from the torsional test simulations, this test was not executed. The procedure for each test was as follows:

1. Prepare and align the test sample following the loading conditions defined in Sections 6.1.2 and 6.1.3
2. Apply a 1024 N settling force for approximately 30s and then remove the force
3. Apply a 50 N stabilizing force
4. Increase the applied load incrementally to the test force at a rate of 200 N/s:
    - Proof test: 2240 N
    - Failure test: 3360 N (or until the sample fails)
5. Decrease the load at 200 N/s to the stabilizing force of 50 N
6. Zero the load and remove the LMPHJ from the testing machine
7. Inspect the sample for physical or functional defects

A test program in Dion 7 was created, and settings were specified to apply loading according to the testing methodology. Load limits of 2240 N for the proof test and 3560 N for the failure test were set. A displacement limit of 20 mm for all tests was specified to reduce the risk of severely damaging the joint if failure occurred. During testing, the load was incrementally applied until either limit was achieved, at which point the machine began unloading the joint.

5.4 Static Testing Results and Discussion

Data collection was completed using the Dion 7 software within the testing system. Time, applied force, and vertical displacement were recorded at 100Hz. For each test, the loading profile was the same; however, for the ML condition, the duration for when the settling force was applied was not recorded. Therefore, in Figure 5-5 and Figure 5-6, the peaks for each test occur at different times. The loads were applied consistently until the test force was reached and removed at the same rate, generating the symmetrical peaks in Figure 5-5. The LMPHJ withstood the 3360 N ultimate test force, satisfying this element of the ISO standard failure criteria (Section 4.12.1).

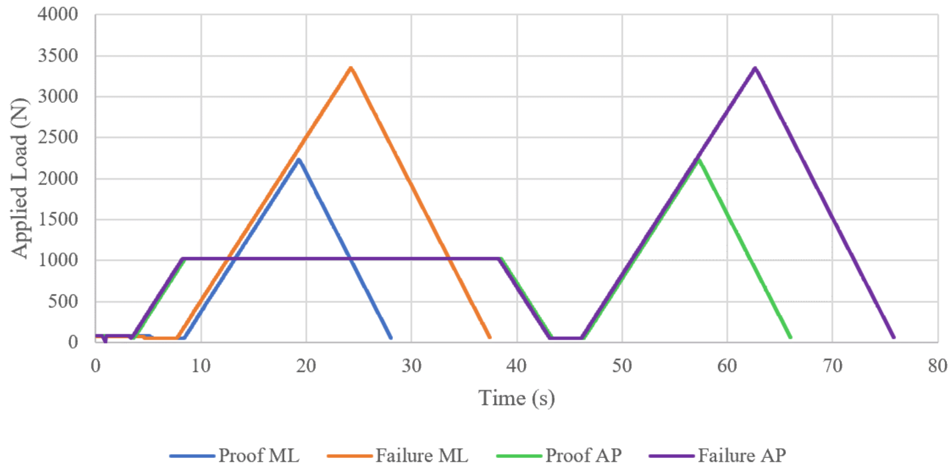

Figure 5-5: Loading profiles of static load tests

Vertical displacement recorded throughout the test was used to interpret LMPHJ deformation. This displacement is the difference in measured distance between the two application points throughout the test; therefore, a larger displacement indicates more joint deformation. Figure 5-5 and Figure 5-6 follow similar shapes, indicating that as the applied force increased, so did the vertical displacement, therefore, the deformation. Pearson Correlations between the applied load and displacement were computed for each test, and all resulted in correlation coefficients greater than 0.95, demonstrating high correlations between these variables.

While the applied loads throughout each test were the same, displacements in the ML setup were much larger (Figure 5-6). During the ML test, a maximum displacement of 18.43 mm was recorded compared to a 6.82 mm maximum displacement for the AP-ext test. The increased deformation during the ML test was likely due to the larger lever arms, hence greater moments applied, and the asymmetrical nature of this setup. While the experimental and simulated setups presented in Section 4.12.2 and 4.12.3 were slightly different, similar results were achieved, whereby the ML condition resulted in large deflections compared to the AP setup.

In the plot, the deflection looks greater at the test's end than toward the start, which could suggest permanent deformation. However, at the beginning of each test, the measured deflection was approximately the same as at the end. The lower deflection values between 5 s - 10 s of each test are likely a result of the programmed limits of the testing machine. The initial loads measured for each test were 70 N-85 N, which are greater than the 50 N stabilizing force. Therefore, to achieve this force specified in the program, the machine needed to unload the joint from its original position, changing the direction of the displacement. Comparing initial and final joint positions, there was no permeant deformation. Therefore, the LMPHJ satisfies each testing condition considering the failure criteria of 15 mm permanent deformation.

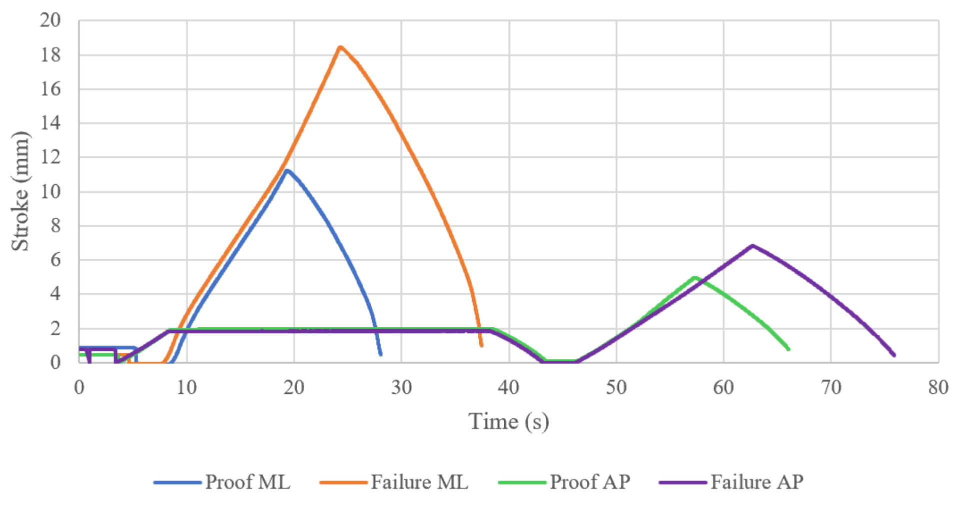

Figure 5-6: Vertical displacement results of static load tests

Following mechanical testing, the LMPHJ was removed from the testing setup and examined for any permanent deformation, signs of failure, and indications of functionality issues. The LMPHJ maintained its structural integrity and functionality, successfully meeting the applicable failure criteria from the ISO standard and validated its capabilities to withstand the loads during simulator testing.

Chapter 6: Functional Testing

Functional testing was executed using a simulator designed by members of the Power Hip Research team that enables able-bodied participants to walk with a HKAF prosthesis [94]. To assess the ability of the LMPHJ to enable a more natural walking pattern, biomechanical parameters were evaluated to characterize each participant's gait as a case series. A subjective comparison to the Helix^{3D} was made by participants regarding the LMPHJ functionality. The test protocol was approved by the University of Ottawa Office of Research Ethics and Integrity (Appendix C).

6.1 Test Setup

The test HKAF prosthesis (Figure 6-1) consisted of the LMPHJ, Össur Rheo 3 knee joint, and Össur Pro-Flex XC foot. A carbon fibre adapter was manufactured to connect the LMPHJ to the lateral side of the simulator's hip abduction orthosis. A running shoe was worn on the prosthetic limb, and a modified running shoe with an insole 3 cm thicker was worn on the participant's opposite limb. The thicker insole ensured the participant would have sufficient foot clearance on their non-loading limb (i.e., only the prosthesis and contralateral limb contacted the ground). Prosthetic leg length adjustments were required for each user to ensure approximately the same length as the contralateral side. The simulator was secured to the participant using a strap around the pelvic basket, two straps around the leg, and one underneath the right ischium. Smartphone sensor data were collected using an application [95] on a mobile device secured in a holster positioned in the middle of the lower back and worn around the waist. The option to use one or two walking canes was available to participants.

Figure 6-1: Test set-up for LMPHJ evaluation with able-bodied participants

Markings on the floor indicated a 10 m walkway (Figure 6-2) in a motion analysis laboratory. To maintain the same relative distance between the camera and the joint across data collection sessions, a distance of 1.5 m from the walkway was also indicated on the floor.

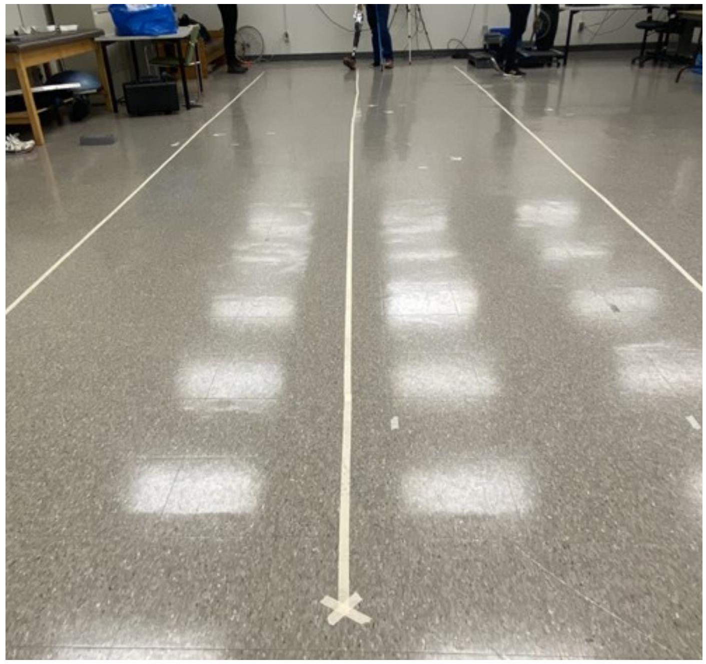

Figure 6-2: 10m walkway for LMPHJ functional testing

6.2 Methods

LMPHJ functional testing was completed for level ground walking. Biomechanical gait parameters were evaluated through 2D video analysis and smartphone sensor data collection to characterize participant's gait. Subjective feedback was noted when compared to walking with the simulator using the Helix^{3D}. Each participant required one training session and one testing session for data collection. Training sessions allowed participants to acclimate to the test set-up, the simulator, and the pre-determined gait pattern the control system enabled. For testing, each participant walked back and forth over the 10m walkway once, for a total distance of 20m. All training and testing were conducted in the Movement Performance Laboratory at the University of Ottawa.

6.2.1 Participants

For enhanced safety, only able-bodied individuals were considered for preliminary functional testing with the simulator. Future testing with amputees will better assess the functionality and usability based on the target population.

Three participants (Table 6-1) volunteered to assess the LMPHJ's functionality. All participants were male between the ages of 25 and 44 years old. Participants B and C used two canes for support, while Participant A was comfortable using only one cane. Each participant had previously learned to walk independently with the simulator using an OttoBock Helix^{3D} hip joint, Ossur Rheo knee joint, and Ossur Pro-Flex XC [94].

Table 6-1: Participant information

	Participant A	**Participant B**	**Participant C**
Sex	Male	Male	Male
Age (years)	44	28	25
Height (cm)	178	180	175
Weight (kg)	95	95	98

6.2.2 Control System: Predetermined Gait Profile

The LMPHJ intelligent control system is under development; therefore, to complete this testing, a predetermined gait profile (Figure 6-3) was tuned to enable level ground walking using the simulator. A relatively slow walking speed of 2.5 m/s was selected to ensure all participants could follow the prosthesis at this pace. The hip ROM was 45° degrees maximum flexion and 20° degrees maximum extension.

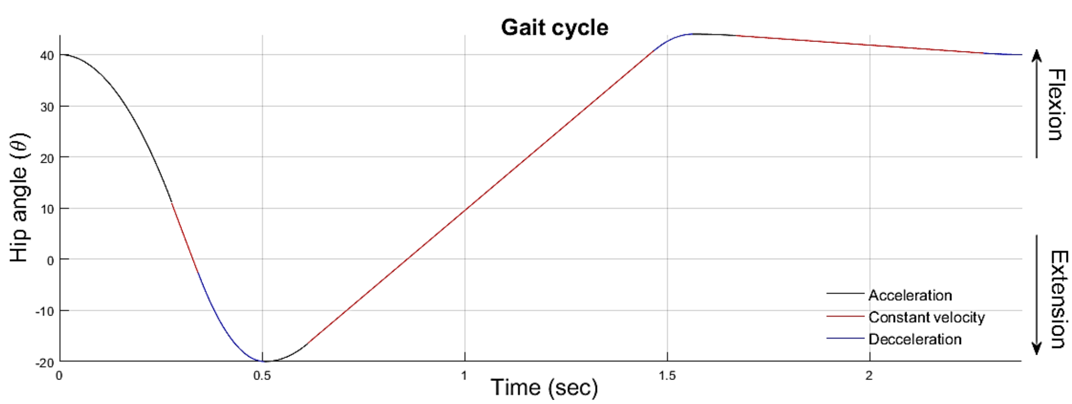

Figure 6-3: Gait profile used for functional testing of the LMPHJ

6.2.3 Data Procurement and Analysis

Video data was recorded to extract spatiotemporal gait parameters throughout each test session. The investigator secured an iPhone 11 (2019) in a handheld tripod to assist with stability, positioned the phone approximately 1.5 m from the LMPHJ, and followed the participant throughout the test session while keeping the phone parallel to the walkway. Videos were captured at 60 fps. A separate smartphone (Google Pixel 4a (2020)) was secured to a belt around the participant's waist to collect smartphone sensor data at a sampling rate of 100Hz. The TOHRC Data Logger app [95] generated reports on step parameters such as foot strikes, pelvic tilt, and pelvic accelerations.

Eight walking strides were evaluated for each participant. Video Editor software from Microsoft was used to crop the raw video files to isolate eight continuous strides. This software was also used to identify heel strike and toe-off for the prosthetic and intact limbs for all eight gait cycles. Kinovea [96] was used to obtain hip joint angles throughout each test by tracking points identified in the video frame-by-frame. The annotated videos were exported as MP4 files for reference, and the angular kinematics were exported as csv files for further analysis of hip ROM.

The TOHRC Data Logger app generated a csv file of the smartphone sensor data for each testing session. The data were cropped and synchronized in time with each participant's cropped video, based on heel strike. Peak pelvis acceleration in the anterior-posterior direction was analyzed since this is the maximum pelvis acceleration, followed by a rapid deceleration following heel strike. Across the eight gait cycles, pelvic tilt angles were measured and reported.

6.3 Functional Testing Results and Discussion

Throughout tuning, training, and testing sessions, the LMPHJ supported over 500 steps by participants weighing 95kg or more. Table 6-2 presents the spatiotemporal gait parameters for each participant, averaged across eight gait cycles. Stride time was similar for all participants, with an average of 2.35 +/- 0.06 s. On average, the cadence for participants was also relatively similar, with a mean of 46.99 +/- 3.34 steps/min. Since the gait profile implemented by the control system was consistent for each test session, these results were expected.

Step time variability occurred between participants for the prosthetic and intact limbs. Participant A had an average step time of 0.81 +/- 0.09 s on the prosthetic side and 1.58 +/- 0.14 s on the intact side, favouring the intact limb by 50% during stance. In comparison, Participant C achieved the same average step time of around 1.2 s for both the intact and prosthetic limbs, demonstrating a high degree of step time symmetry.

The swing phase duration for all participants was distinctly longer for the prosthetic limb (0.91 +/- 0.09 s) than the intact limb (0.30 +/- 0.06 s). Additionally, participants were in double support for nearly 50% of the gait cycle. These are common characteristics of prosthetic gait, whereby the time spent in single support on the prosthetic limb is minimized. Since participants were required to follow a predetermined gait pattern, it was evident during testing that the users advanced quickly through intact limb swing phase to ensure the prosthetic limb was not loaded for the actuation of swing phase for the prosthetic limb. With the implementation of the complete control system, it is expected that users could feel more confident that the LMPHJ would be in the correct position for weightbearing as they naturally vary their stride.

Table 6-2: Spatiotemporal gait parameters determined through 2D video analysis for eight strides. Percentages (%) represent the proportion of average stride time

Participant		A	B	C	**Average**
Stride Time (s)		2.39 +/- 0.11	2.28 +/- 0.13	2.38 +/- 0.15	2.35 +/- 0.06
Step Time (s)	**Prosthetic**	0.81 +/- 0.09 (33%)	0.98 +/- 0.10 (43%)	1.21 +/- 0.1 2 (52%)	1.0 +/-0.20 (46%)
	Intact	1.58 +/- 0.14 (66%)	1.30 +/- 0.09 (57%)	1.16 +/- 0.05 (48%)	1.35 +/- 0.21 (57%)
Swing Time (s)	**Prosthetic**	1.00 +/- 0.11 (42%)	0.83 +/- 0.05 (36%)	0.90 +/- 0.09 (38%)	0.91 +/- 0.09 (39%)
	Intact	0.38 +/- 0.09 (16%)	0.25 +/- 0.05 (11%)	0.29 +/- 0.06 (12%)	0.30 +/- 0.06 (13%)
Double Support (s)		1.00 +/- 0.12 (45%)	1.20 +/- 0.09 (53%)	1.19 +/- 0.16 (50%)	1.13+/- 0.10 (48%)
Cadence (steps/min)		44.15 +/- 2.00	46.16 +/- 2.9	50.67 +/- 2.90	46.99 +/- 3.34
Step Time Ratio		0.52	0.75	1.04	0.77

The LMPHJ mean ROM was 58.31 +/- 5.12° with a maximum flexion angle of 51.14 +/- 3.43° and a maximum extension angle of 24.53 +/- 4.33° (Table 6-3). Figure 6-4 shows each participant's ROM throughout the eight gait cycles analyzed. These results exceeded the ROM input by the control system (45° flexion - 20° extension), which could be a result of overshoot but is likely attributed to angular artifacts within the video recordings in the event the smartphone was not perfectly perpendicular to the joint (Figure 6-5). These results demonstrated a substantially larger ROM compared to other hip prostheses, suggesting the LMPHJ can enable improved hip mobility.

Table 6-3: LMPHJ range of motion averaged over eight gait cycles for each participant

Participant	**Maximum Hip Flexion Angle (deg)**	**Maximum Hip Extension Angle (deg)**	**Hip Range of Motion (deg)**
A	54.89	- 21.31	56.81 +/- 5.20
B	48.15	- 22.84	64.95 +/- 3.45
C	50.38	- 29.46	53.17 +/- 6.71
Average	51.14 +/- 3.43	24.53 +/- 4.33	58.31 +/- 5.12

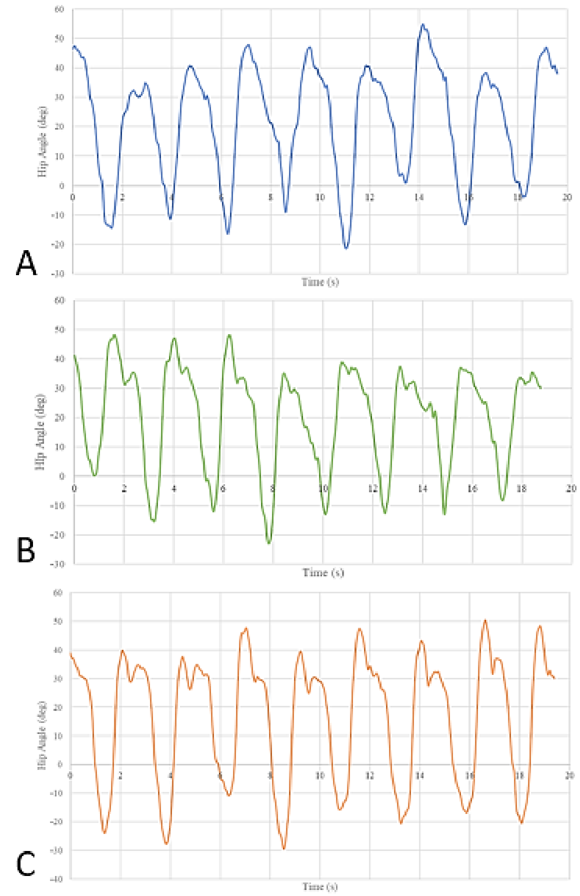

Figure 6-4: Hip angle (deg) vs time (s) of eight strides for Participant A (blue), B (green) and C (orange)

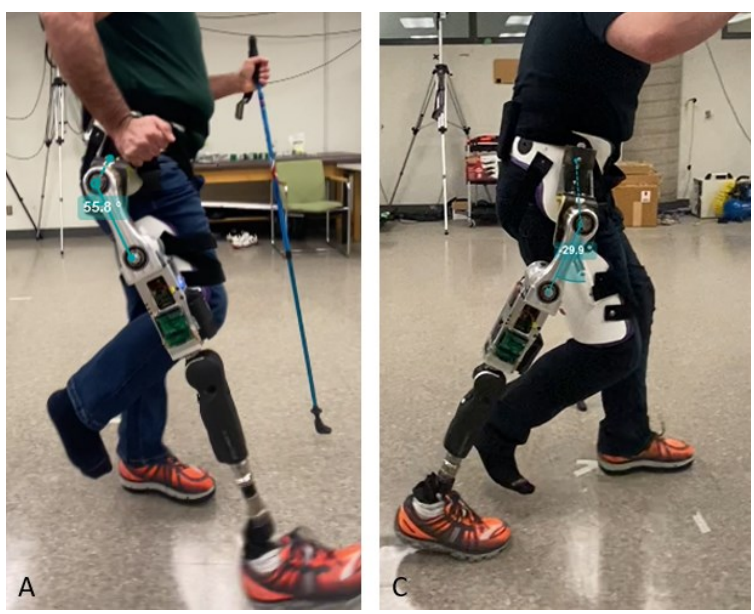

Figure 6-5: Maximum hip flexion angle demonstrated by Participant A (left) and maximum hip extension angle demonstrated by Participant C (right)

An average pelvic tilt of 12.23 +/- 5.62° was reported for participants (Table 6-4), which is considerably higher than expected. When visually analyzing the videos, there were no drastic pelvic movements. Additionally, it should be noted that during testing sessions, the participants expressed that they felt much less pelvic tilt was required to propel the prosthetic leg forward compared to previous testing sessions using the Helix^{3D}. These results were likely achieved because participants wore the belt containing the smartphone further up their lower back to clear the orthotic socket. Therefore, the angles reported would represent the trunk angle, and while using the canes to walk, participants tended to lean forward. It is recommended to secure a Velcro attachment to the orthosis pelvic basket for future testing to collect more consistent data on pelvic movement throughout gait.

Table 6-4: Pelvic tilt results for eight gait cycles for Participants A, B, and C

Participant	Maximum Pelvic Tilt (°)	Average Pelvic Tilt (°)
A	20.46	9.45 +/- 3.23
B	41.68	16.24 +/- 10.09
C	21.88	11.01 +/- 3.55
Average	28.01 +/- 11.86	12.23 +/- 5.62°

Throughout training and testing sessions, participants offered subjective feedback on the LMPHJ. All three participants agreed that, compared to the passive Helix^{3D}, the LMPHJ was easier to walk with and felt more stable while standing and walking. While additional testing will be required with the complete control system implemented to compare the LMPHJ to the current gold standard quantitatively, this initial feedback supports future research for a powered prosthesis solution for hip-level amputees.

Chapter 7: Conclusions and Future Work

In this thesis, a novel laterally mounted powered hip joint was designed and validated to provide a more functional solution for amputees who use a HKAF prosthesis. The new LMPHJ was designed to promote more natural gait patterns and offer safe and controlled movement across various daily activities. A full-scale prototype was designed, manufactured, and assembled with machined and commercially available components. Mechanical testing conditions were based on existing international standards and executed by industry professionals at Össur's headquarters in Reykjavik, Iceland. LMPHJ functionality and usability was assessed analytically and subjectively using a customized simulator at the University of Ottawa. Validation was completed by evaluating the design against the original requirements.

Table 7-1 revisits the design criteria defined in Chapter 3, along with the final evaluation of the LMPHJ against each requirement. All design criteria were met.

The mechanical design enabled the full range of motion in flexion and extension required for walking and other daily activities. However, an extension stop could be implemented in future revisions to limit joint extension to only the maximum required 15.0 degrees. The Össur actuator outputs a maximum angular velocity of 300.0 °/s and maximum torque of 96.0 Nm, corresponding to a speed of 220.0 °/s and torque of 130.9 Nm when considering the pulley size ratio. The maximum possible power generation for the system is the product of these parameters, resulting in a peak power generation of 502.5 W. Therefore, LMPHJ meets the requirements for each of the parameters required at the hip for level ground walking, stairs, and inclines. While the control system is currently configured for level walking only, more functionalities will be implemented in future iterations.

The LMPHJ weight in the scope of this thesis was equivalent to the maximum weight specified of 3.5 kg, fully meeting the design criteria. Although the joint was relatively heavy, the actuation system was able to compensate for the weight and augment participant gait. Therefore, this did not affect LMPHJ functionality. The LMPHJ, electronics chassis, and electrical components are all preliminary prototypes; therefore, future iterations should aim to decrease the overall weight and size.

Mechanical testing validated the 100.0 kg weight rating, with the LMPHJ showing no signs of failure and permanent deformation after subjecting the joint to the highest loading level specified in the ISO standard. There was a high correlation between the applied loads and displacement, with the largest displacements measured during the ML test, likely due to the joint geometry being less resistant to bending in the corresponding test plane.

Table 7-1: Summary of LMPHJ evaluation against design criteria

Requirement	Criteria	LMPHJ Outcome	Final Evaluation
Range of motion	130.0° flexion, 15.0° extension	Full range of motion (130.0° flexion, 15.0° extension) enabled by the mechanical system and constrained by the control system	Fully met
Hip angular velocity	150.0 °/second	Maximum speed is 220.0 °/second	Fully met
Supports user weight	Max 100.0 kg	LMPHJ successfully passed all static tests assuming a 100.0 kg user	Fully met
Hip torque	Peak moment: 125.0 Nm	Maximum torque at hip is 130.9 Nm	Fully met
Hip power	Peak power generation: 360.0 W	Maximum power at hip is 502.5 W	Fully met
Minimize weight	≤ 3.5 kg	3.5 kg (without electronics) 5.2 kg (with electronics)	Fully met
No sharp edges	Fillet exposed edges	Fillets applied to all exposed edges and notes made on each drawing to break sharp edges	Fully met
Laterally mounted	Lamination plate secured on lateral side of prosthetic socket	Design was configured and tested assuming a lateral mounting orientation	Fully met
Ease of manufacturing	Less than 20 machined components	16 machined parts	Fully met
Must fit under clothing	Lateral protrusion ≤ 5.5 cm	Lateral protrusion from lamination plate is 5.4 cm	Fully met
Does not interfere with sitting	Posterior protrusion from axis of rotation ≤ 6.5 cm	Posterior protrusion from axis of rotation is 4.1 cm	Fully met
Does not interfere with prosthetic socket	Motor positioned 130.0 mm distal to the axis of rotation	Motor positioned 130.0 mm distal to axis of rotation	Fully met

Geometric constraints were achieved so that the joint comfortably fits beneath pants, will not interfere with the prosthetic socket, and does not protrude in any direction beyond typical anthropometric measurements. Fillets were added to all exposed edges while modeling, and manufacturing instructions were specified to break sharp edges to ensure no risk of injury from the components would occur.

The joint was designed to be secured to the lateral side of the prosthetic socket and positioned at the anatomical hip joint axis of rotation. This mounting orientation could achieve more symmetrical loading across the prosthetic and intact limbs during ambulation with positive power generation compared to front-mounted joints.

Functional testing demonstrated that the LMPHJ enables controlled walking over level ground. Three participants could walk using the hip prostheses simulator for training and testing sessions. An average cadence of 2.35 +/- 0.06s, maximum flexion of 51.14 +/-3.43°, and a maximum extension of 24.53 +/- 4.33° were achieved. One participant demonstrated equal step times between the prosthetic and intact limbs, indicating that the LMPHJ could improve gait symmetry. Based on subjective feedback, the participants perceived that the LMPHJ required less energy and pelvic tilt to walk when compared to their previous experience with the Helix^{3D}. Additional testing will be required to quantify these claims.

7.1 Summary of Contributions

Throughout this thesis, an innovative powered hip joint was developed, providing novel contributions to prosthetic design and wearable robotics, specifically, the area of hip-level prosthetics, which is not as frequently studied. These contributions include:

- Designed a novel laterally mounted powered prosthetic hip joint
- Reintroduced a lateral mounting orientation since the motor-powered microprocessor joint can provide safe and controlled actuation of the hip joint.
- Designed, built and tested a pulley system drivetrain that enables the powered components to be positioned in the usable space beneath the prosthetic socket
- Maintained a simple, robust design to reduce the amount of machining required.
- Adapted existing ISO standard testing requirements to evaluate a laterally mounted system
- Demonstrated the designed hip joint has full ROM and can withstand loading in accordance with ISO standards
- Validated hip joint performance by walking on the new HKAF prosthesis with a customized simulator

7.2 Future work

While the LMPHJ met the design criteria, changes could be made, and further testing could be completed in future iterations to improve the overall design.

7.2.1 Outer Casing

A casing to enclose the LMPHJ will be required. Since a casing did not provide any functional advantage to the system, it was not included in the initial design. However, for safety reasons, all moving parts should be contained to expose no pinch points. A 2.0 cm clearance to the prosthetic socket was added to this design, considering a casing would be eventually added. Ideally, the casing would be low profile, lightweight, and integrated into the existing design. Initially, for a prototype, a 3D-printed solution could be fabricated. One solution would be to make the casing in two pieces that clip over the entire system.

7.2.2 Extension Stop Implementation

While the control system regulates safe ambulation, an extension stop should be implemented for safety reasons and to alleviate the load on the actuator. In the case when the motor loses power, an extension stop would mechanically block the joint from rotating to further extension angles, which could result in balance issues and fall risks. Additionally, by limiting the maximum extension the joint can achieve through a physical stop, the load from the actuator is lessened because the actuator alone will not have to limit this position.

A potential solution for this is to secure a plastic or rubber segment to the side of the prosthetic socket so that it contacts the outer casing of the joint at the user's maximum extension angle. The prosthetist could decide the stop's positioning based on the recommended amount of extension required by the user. A sufficient contact area will be necessary to function effectively; however, this component should be as low-profile as possible.

7.2.3 Supporting Link

The supporting link is a major component that, if optimized, could benefit the overall design considerably. The link's shape and size were determined through simulation; however, this part weighs 606.0 g and contributes 2.5 cm of lateral protrusion. There were no signs of deformation during testing, indicating that a smaller link is possible, reducing the overall weight. Mechanical testing could be performed on this component alone to determine the opportunity for size reduction. Much of the lateral protrusion is attributed to the large angular contact bearings that were required, so a lower profile option should be explored. In addition to geometric changes, a material change could facilitate weight and space savings. For instance, carbon fiber could considerably reduce this component's weight.

The link length for the LMPHJ prototype was based on pelvic radiograph measurements and the joint's geometry to ensure clearance between the joint and the prosthetic socket. This length will vary across users. To accommodate for this, an adjustable solution would be ideal. Alternatively, various link lengths will be required to fit various user height ranges.

7.2.4 Tensioning Solution

The current tensioning solution is simple and does not require additional lateral components. However, the pulley and shaft machining were complex, and assembly was awkward. To help alleviate these issues, a different solution to tension the system should be explored.

One idea is to introduce a one-way clutch bearing or mechanism between the pulley and the shaft that would only allow rotation in one direction. These would only need to be applied to the distal or proximal pulleys. Another concept that could be explored is implementing a rotating, rigid cam mechanism at the pulley opening to pull the rope through to tension the system. While this type of mechanism likely could not secure the rope under maximum operating conditions, it would allow a way to tension the system easily. The excess rope pulled through the cam could be secured inside the pulley with a spliced end. Like a one-way clutch mechanism, this solution would only need to be applied to one set of pulleys.

7.2.5 Slack Elimination

The LMPHJ incorporated Vectran ropes to actuate the pulley system drivetrain. While Vectran fibres have low stretch and creep, rope stretch occurred in the preliminary testing sessions and introduced slack into the system. The braided configuration and splicing likely caused stretch. This concern was eliminated once the ropes settled and reached a condition where they would no longer stretch; however, alternative methods or materials should be explored in future iterations.

If maintaining the use of rope, it is recommended to pre-stretch the spliced ropes prior to testing to remove any constructional stretch. Alternatively, the substitution of a steel cable with swaged connections at either end could be used in place of a rope. The cable solution would be easier to construct since rope splicing was completed by an industry professional for the LMPHJ design. Additionally, a steel cable solution could reduce the amount of tolerance for rope length. It is recommended to use a 1/8” steel wire coated in Nylon plastic to ensure the cable fit within the pulley grooves, and the Nylon plastic would eliminate metal-metal contact that could wear on the wire.

7.2.6 Testing

Although the LMPHJ performed well during the testing, further mechanical and clinical testing will be required. First, the cyclic strength tests outlined in ISO:15032 must be executed. The tests simulate the repetitive loads that occur during normal walking, determining the joint's resistance to fatigue loading. Functional testing with a complete intelligent control system will be an essential next step for evaluating the LMPHJ. With improved functionality, standardized tests such as the 2 Minute Walk Test [97] and the L-Test [98] could quantify functional differences compared to passive, front-mounted prosthetic hip joints such as the Helix^{3D}. In the future, LMPHJ testing is needed with hip-level amputees to verify prosthesis performance with the target population.

References

[1] M. T. Houdek *et al.*, “Functional outcome measures of patients following hemipelvectomy,” *Prosthet. Orthot. Int.*, vol. 40, no. 5, pp. 566–572, Oct. 2016, doi: 10.1177/0309364615574164.

[2] M. Nietert, N. Englisch, P. Kreil, and G. Alba-Lopez, “Loads in hip disarticulation prostheses during normal daily use,” *Prosthet. Orthot. Int.*, vol. 22, no. 3, pp. 199–215, Dec. 1998, doi: 10.3109/03093649809164485.

[3] F. Nowroozi, M. L. Salvanelli, and L. H. Gerber, “Energy expenditure in hip disarticulation and hemipelvectomy amputees,” *Arch. Phys. Med. Rehabil.*, vol. 64, no. 7, pp. 300–303, Jul. 1983.

[4] T. Chin, R. Kuroda, T. Akisue, T. Iguchi, and M. Kurosaka, “Energy consumption during prosthetic walking and physical fitness in older hip disarticulation amputees,” *J. Rehabil. Res. Dev.*, vol. 49, no. 8, pp. 1255–1260, 2012, doi: 10.1682/jrrd.2011.04.0067.

[5] T. Chin, S. Sawamura, R. Shiba, H. Oyabu, Y. Nagakura, and A. Nakagawa, “Energy expenditure during walking in amputees after disarticulation of the hip,” *J. Bone Joint Surg. Br.*, vol. 87-B, no. 1, pp. 117–119, Jan. 2005, doi: 10.1302/0301-620X.87B1.14617.

[6] M. T. Karimi and M. Kamali, “Evaluation of Gait Performance in Hemipelvectomy Amputation While Walking With a Prosthesis,” *USWR*, vol. 8, no. 1, pp. 75–61, Apr. 2018, doi: 10.32598/ptj.8.1.55.

[7] E. Ludwigs, M. Bellmann, T. Schmalz, and S. Blumentritt, “Biomechanical Differences between Two Exoprosthetic Hip Joint Systems during Level Walking,” *Prosthet. Orthot. Int.*, vol. 34, no. 4, pp. 449–460, Dec. 2010, doi: 10.3109/03093646.2010.499551.

[8] P. Yari, P. U. Dijkstra, and J. H. Geertzen, “Functional outcome of hip disarticulation and hemipelvectomy: a cross-sectional national descriptive study in the Netherlands,” *Clin. Rehabil.*, vol. 22, no. 12, pp. 1127–1133, Dec. 2008, doi: 10.1177/0269215508095088.

[9] S. K. Au, J. Weber, and H. Herr, “Powered Ankle–Foot Prosthesis Improves Walking Metabolic Economy,” *IEEE Trans. Robot.*, vol. 25, no. 1, pp. 51–66, Feb. 2009, doi: 10.1109/TRO.2008.2008747.

[10] Erik. J. Wolf, V. Q. Everding, A. A. Linberg, J. M. Czerniecki, and C. J. M. Gambel, “Comparison of the Power Knee and C-Leg during step-up and sit-to-stand tasks,” *Gait Posture*, vol. 38, no. 3, pp. 397–402, Jul. 2013, doi: 10.1016/j.gaitpost.2013.01.007.

[11] A. Brandt, W. Riddick, J. Stallrich, M. Lewek, and H. H. Huang, “Effects of extended powered knee prosthesis stance time via visual feedback on gait symmetry of individuals with unilateral amputation: a preliminary study,” *J. NeuroEngineering Rehabil.*, vol. 16, no. 1, p. 112, Sep. 2019, doi: 10.1186/s12984-019-0583-z.

[12] S. K. Au, J. Weber, and H. Herr, “Biomechanical Design of a Powered Ankle-Foot Prosthesis,” in *2007 IEEE 10th International Conference on Rehabilitation Robotics*, Jun. 2007, pp. 298–303. doi: 10.1109/ICORR.2007.4428441.

[13] Y. Ueyama, T. Kubo, and M. Shibata, “Robotic hip-disarticulation prosthesis: evaluation of prosthetic gaits in a non-amputee individual,” *Adv. Robot.*, vol. 34, no. 1, pp. 37–44, Jan. 2020, doi: 10.1080/01691864.2019.1705908.

[14] E. Gailledrat *et al.*, “Does the new Helix 3D hip joint improve walking of hip disarticulated amputees?,” *Ann. Phys. Rehabil. Med.*, vol. 56, no. 5, pp. 411–418, Jul. 2013, doi: 10.1016/j.rehab.2013.05.001.

[15] C. Jayaraman *et al.*, “Impact of Powered Knee-Ankle Prosthesis on Low Back Muscle Mechanics in Transfemoral Amputees: A Case Series,” *Front. Neurosci.*, vol. 12, 2018, doi: 10.3389/fnins.2018.00134

[16] F. H. Martini, J. L. Nath, and E. F. Bartholomew, *Fundamentals of Anatomy & Physiology*, 10th ed. Pearson, 2014.

[17] T. K. Uchida and S. L. Delp, *Biomechanics of Movement*. MIT Press, 2021.

[18] S. R. Chaudhry, A. Nahian, and K. Chaudhry, “Anatomy, Abdomen and Pelvis, Pelvis,” in *StatPearls*, Treasure Island (FL): StatPearls Publishing, 2021. Accessed: Dec. 17, 2021. [Online]. Available: http://www.ncbi.nlm.nih.gov/books/NBK482258/

[19] R. K. Kotarinos, “Chapter Three - Musculoskeletal Pelvic Anatomy,” in *Biomechanics of the Female Pelvic Floor*, L. Hoyte and M. Damaser, Eds., Academic Press, 2016, pp. 53–87. doi: 10.1016/B978-0-12-803228-2.00003-9.

[20] M. Gold, A. Munjal, and M. Varacallo, “Anatomy, Bony Pelvis and Lower Limb, Hip Joint,” in *Anatomy, Bony Pelvis and Lower Limb, Hip Joint*, Treasure Island (FL): StatPearls Publishing, 2017.

[21] M. Bozkurt, Ç. Işık, M. Akkaya, and S. Gürsoy, “Functional Anatomy of the Hip Joint,” in *Musculoskeletal Research and Basic Science*, F. Korkusuz, Ed., Cham: Springer International Publishing, 2016, pp. 735–739. doi: 10.1007/978-3-319-20777-3_46.

[22] T. R. Dillingham, L. E. Pezzin, and E. J. MacKenzie, “Limb amputation and limb deficiency: epidemiology and recent trends in the United States,” *South. Med. J.*, vol. 95, no. 8, pp. 875–884, 2002.

[23] H. Gholizadeh, N. Baddour, M. Botros, K. Brannen, F. Golshan, and E. D. Lemaire, “Hip disarticulation and hemipelvectomy prostheses: A review of the literature,” *Prosthet. Orthot. Int.*, vol. 45, no. 5, pp. 434–439, Oct. 2021, doi: 10.1097/pxr.0000000000000029.

[24] L. M. Silva and N. Stergiou, “Chapter 7 - The basics of gait analysis,” in *Biomechanics and Gait Analysis*, N. Stergiou, Ed., Academic Press, 2020, pp. 225–250. doi: 10.1016/B978-0-12-813372-9.00007-5.

[25] B. L. Schnall, B. S. Baum, and A. M. Andrews, “Gait Characteristics of a Soldier With a Traumatic Hip Disarticulation,” *Phys. Ther.*, vol. 88, no. 12, pp. 1568–1577, Dec. 2008, doi: 10.2522/ptj.20070337.

[26] “Hip prosthesis with: Helix 3D | Ottobock CA.” https://www.ottobock.ca/en/prosthetics/lower-limb-prosthetics/solution-overview/helix-hip-system/ (accessed May 03, 2021).

[27] R. D. McAnelly, M. Refaeian, D. G. O’Connell, G. D. Powell, and N. E. Walsh, “Successful prosthetic fitting of a 73-year-old hip disarticulation amputee patient with cardiopulmonary disease,” *Arch. Phys. Med. Rehabil.*, vol. 79, no. 5, pp. 585–588, May 1998, doi: 10.1016/s0003-9993(98)90078-8.

[28] L. M. Nelson and N. T. Carbone, “Functional Outcome Measurements of a Veteran With a Hip Disarticulation Using a Helix 3D Hip Joint: A Case Report,” *Jpo J. Prosthet. Orthot.*, vol. 23, no. 1, pp. 21–26, Jan. 2011, doi: 10.1097/JPO.0b013e318209777c.

[29] A. D. Segal *et al.*, “Kinematic and kinetic comparisons of transfemoral amputee gait using C-Leg and Mauch SNS prosthetic knees,” *J. Rehabil. Res. Dev.*, vol. 43, no. 7, pp. 857–870, Dec. 2006, doi: 10.1682/jrrd.2005.09.0147.

[30] M. J. Highsmith *et al.*, “Kinetic asymmetry in transfemoral amputees while performing sit to stand and stand to sit movements,” *Gait Posture*, vol. 34, no. 1, pp. 86–91, May 2011, doi: 10.1016/j.gaitpost.2011.03.018.

[31] T. Schmalz, S. Blumentritt, and B. Marx, “Biomechanical analysis of stair ambulation in lower limb amputees,” *Gait Posture*, vol. 25, no. 2, pp. 267–278, Feb. 2007, doi: 10.1016/j.gaitpost.2006.04.008.

[32] V. Nalam and H. (Helen) Huang, “Empowering prosthesis users with a hip exoskeleton,” *Nat. Med.*, vol. 27, no. 10, pp. 1677–1678, Oct. 2021, doi: 10.1038/s41591-021-01529-w.

[33] E. J. Wolf, V. Q. Everding, A. L. Linberg, B. L. Schnall, J. M. Czerniecki, J. M. Gambel, "Assessment of transfemoral amputees using C-Leg and Power Knee for ascending and descending inclines and steps," *J Rehabil Res Dev*, vol. 49, no. 6, pp. 831-842, 2012, doi: 10.1682/jrrd.2010.12.0234.

[34] ISO 15032:2000, “Prostheses - Structural testing of hip joints,” 2000.

[35] M. Omasta, D. Paloušek, T. Návrat, and J. Rosický, “Finite element analysis for the evaluation of the structural behaviour, of a prosthesis for trans-tibial amputees,” *Med. Eng. Phys.*, vol. 34, no. 1, pp. 38–45, Jan. 2012, doi: 10.1016/j.medengphy.2011.06.014.

[36] J. E. Akin, *Finite element analysis concepts: via SolidWorks*. World Scientific, 2010.

[37] S. Phanphet, S. Dechjarern, S. Jomjanyong "Above-knee prosthesis design based on fatigue life using finite element method and design of experiment," *Med. Eng Phys*., vol. 43, pp.86-91, Mar. 2017, doi: 10.1016/j.medengphy.2017.01.001

[38] M. W. Legro, G. D. Reiber, D. G. Smith, M. del Aguila, J. Larsen, and D. Boone, “Prosthesis evaluation questionnaire for persons with lower limb amputations: Assessing prosthesis-related quality of life,” *Arch. Phys. Med. Rehabil.*, vol. 79, no. 8, pp. 931–938, Aug. 1998, doi: 10.1016/S0003-9993(98)90090-9.

[39] L. Xinwei, X. Yixuan, H. Chen, H. Bingshan, and Y. Hongliu, “A Gait Simulation and Evaluation System for Hip Disarticulation Prostheses,” *IEEE Trans. Autom. Sci. Eng.*, vol. 18, no. 2, pp. 448–457, Apr. 2021, doi: 10.1109/TASE.2020.3035438.

[40] C. McLaurin, “The Evolution of the Canadian-Type Hip-Disarticulation Prosthesis.”

[41] L. Gillis, “A new prosthesis for disarticulation at the hip,” *J. Bone Joint Surg. Br.*, vol. 50, no. 2, pp. 389–391, 1968.

[42] C. W. Radcliffe, “The biomechanics of the Canadian-type hip-disarticulation prosthesis,” *Artif. Limbs*, vol. 4, no. 2, pp. 29–38, 1957.

[43] A. C. Bell, “Canadian Hip Disarticulation Prosthesis,” *Orthop. Prosthet. Appl. Joural*, vol. 10, pp. 35–39, 1956.

[44] S. E. Solomonidis, A. J. Loughran, J. Taylor, and J. P. Paul, “Biomechanics of the hip disarticulation prosthesis,” *Prosthet. Orthot. Int.*, vol. 1, no. 1, pp. 13–18, Apr. 1977, doi: 10.3109/03093647709164599.

[45] J. Michael, “Component Selection Criteria: Lower Limb Disarticulations,” *Clin. Prosthet. Orthot.*, vol. 12, no. 3, pp. 99–108, 1988.

[46] S. Blumentritt, E. Ludwigs, M. Bellmann, and H. Boiten, “The New Helix3D Hip Joint,” *Orthop. Tech.*, vol. 5, pp. 1–5, 2008.

[47] P. Cherelle, G. Mathijssen, Q. Wang, B. Vanderborght, and D. Lefeber, “Advances in Propulsive Bionic Feet and Their Actuation Principles,” *Adv. Mech. Eng.*, vol. 6, p. 984046, Jan. 2014, doi: 10.1155/2014/984046.

[48] J. R. Montgomery and A. M. Grabowski, “Use of a powered ankle–foot prosthesis reduces the metabolic cost of uphill walking and improves leg work symmetry in people with transtibial amputations,” *J. R. Soc. Interface*, vol. 15, no. 145, p. 20180442, Aug. 2018, doi: 10.1098/rsif.2018.0442.

[49] H. M. Herr and A. M. Grabowski, “Bionic ankle–foot prosthesis normalizes walking gait for persons with leg amputation,” *Proc. R. Soc. B Biol. Sci.*, vol. 279, no. 1728, pp. 457–464, Feb. 2012, doi: 10.1098/rspb.2011.1194.

[50] S. Au, M. Berniker, and H. Herr, “Powered ankle-foot prosthesis to assist level-ground and stair-descent gaits,” *Neural Netw.*, vol. 21, no. 4, pp. 654–666, May 2008, doi: 10.1016/j.neunet.2008.03.006.

[51] D. H. Gates, J. M Aldridge, J. M Wilken, “Kinematic comparison of walking on uneven ground using powered and unpowered prostheses," *Clin Biomech*., vol. 28, no. 4, pp. 467-472, Apr. 2013, doi: 10.1016/j.clinbiomech.2013.03.005.

[52] N. Hata, T. Kubo, and T. Inoue, “Development of a powered hip disarticulation prosthesis with swing phase controller,” *Nihon Kikai Gakkai Ronbunshu C HenTransactions Jpn. Soc. Mech. Eng. Part C*, vol. 75, pp. 404–412, Feb. 2009, doi: 10.1299/kikaic.75.404.

[53] M. K. Ishmael, D. Archangeli, and T. Lenzi, “Powered hip exoskeleton improves walking economy in individuals with above-knee amputation,” *Nat. Med.*, vol. 27, no. 10, pp. 1783–1788, Oct. 2021, doi: 10.1038/s41591-021-01515-2.

[54] H. Naito, “Gait Analysis of Newly Developed Hip Disarticulation Prosthesis Walking - Rotation Axis of Hip Joint is on the Side of Socket,” presented at the 13th ISPO World Congress, 2010.

[55] X. Li, Z. Deng, Q. Meng, S. Bai, W. Chen, and H. Yu, “Design and optimization of a hip disarticulation prosthesis using the remote center of motion mechanism,” *Technol. Health Care*, vol. 29, no. 2, pp. 269–281, Jan. 2021, doi: 10.3233/THC-192088.

[56] T. Kobayashi *et al.*, “Effects of walking speed on magnitude and symmetry of ground reaction forces in individuals with transfemoral prosthesis,” *J. Biomech.*, vol. 130, p. 110845, Jan. 2022, doi: 10.1016/j.jbiomech.2021.110845.

[57] W. Cao, W. Zhao, W. Chen, H. Yu, and Q. Meng, “The comparison of transfemoral amputees using mechanical and microprocessor- controlled prosthetic knee under different walking speeds: A randomized cross-over trial,” *Technol. Health Care*, vol. 26, no. 4, pp. 581–592, Jul. 2018, doi: 10.3233/THC-171157.

[58] M. Grimmer and A. Seyfarth, “Mimicking Human-Like Leg Function in Prosthetic Limbs,” in *Neuro-Robotics: From Brain Machine Interfaces to Rehabilitation Robotics*, P. Artemiadis, Ed., in Trends in Augmentation of Human Performance. Dordrecht: Springer Netherlands, 2014, pp. 105–155. doi: 10.1007/978-94-017-8932-5_5.

[59] F. B. Rodrigues, A. O. Andrade, and M. F. Vieira, “Effects of inclined surfaces on gait variability and stability in unilateral lower limb amputees,” *Med. Biol. Eng. Comput.*, vol. 57, no. 11, pp. 2337–2346, Nov. 2019, doi: 10.1007/s11517-019-02042-6.

[60] C. J. Lamoth, E. Ainsworth, W. Polomski, H. Houdijk, "Variability and stability analysis of walking of transfemoral amputees," *Med Eng Phys*., vol. 32, no. 9, pp. 1009-1014, Nov. 2010, doi: 10.1016/j.medengphy.2010.07.001.

[61] M. Haggerty, D. C. Dickin, J. Popp, and H. Wang, “The influence of incline walking on joint mechanics,” *Gait Posture*, vol. 39, no. 4, pp. 1017–1021, Apr. 2014, doi: 10.1016/j.gaitpost.2013.12.027.

[62] CMHC, “Accessible Housing by Design — Ramps,” Canada Mortgage and Housing Corporation, Canada, 2016.

[63] H. Bombaci, B. Simsek, M. Soyarslan, and M. Murat Yildirim, “Determination of the hip rotation centre from landmarks in pelvic radiograph,” *Acta Orthop. Traumatol. Turc.*, vol. 51, no. 6, pp. 470–473, Dec. 2017, doi: 10.1016/j.aott.2017.09.004.

[64] Man-Systems Integration Standards, “Volume I, Section 3: Anthromopetry and Biomechanics,” NASA, Standard, Aug. 2020.

[65] “Power Knee™. Ossur.com.” https://www.ossur.com/en-us/prosthetics/knees/power-knee (accessed Feb. 09, 2022).

[66] “Exoskeleton joint actuator.” http://www.maxongroup.us/maxon/view/news/Exoskeleton-joint-actuator (accessed Jun. 17, 2022).

[67] B. Chen, B. Zi, L. Qin, and Q. Pan, “State-of-the-art research in robotic hip exoskeletons: A general review,” *J. Orthop. Transl.*, vol. 20, pp. 4–13, Jan. 2020, doi: 10.1016/j.jot.2019.09.006.

[68] “Honda Global | honda walking assist device.” https://global.honda/products/power/walkingassist.html (accessed Mar. 02, 2022).

[69] D. Langlois, A. V. Clausen, and Á. Einarsson, “Powered prosthetic hip joint,” US9044346B2, Jun. 02, 2015

[70] “ASM Material Data Sheet.” https://asm.matweb.com/search/SpecificMaterial.asp?bassnum=ma2024t4 (accessed Apr. 18, 2022).

[71] “Kinetics MIM 17-4PH Stainless Steel (H900 Condition).” https://www.matweb.com/search/datasheet.aspx?matguid=346e4ed0aeae4a7ab69a81e62491c3f1&n=1&ckck=1 (accessed Apr. 18, 2022).

[72] J. Ramirez, A. Rubiano, and P. Castiblanco, “Soft Driving Epicyclical Mechanism for Robotic Finger,” *Actuators*, vol. 8, no. 3, Art. no. 3, Sep. 2019, doi: 10.3390/act8030058.

[73] D. E. Beers and J. E. Ramirez, “Vectran High-performance Fibre,” *J. Text. Inst.*, vol. 81, no. 4, pp. 561–574, Jan. 1990, doi: 10.1080/00405009008658729.

[74] “Marlow Excel V12 4mm 12-Strand Vectran The Chandlery.” https://www.thechandleryonline.com/product_info.php?products_id=2489 (accessed Mar. 15, 2022).

[75] C. Aka and G. Basal, “Mechanical and fatigue behaviour of artificial ligaments (ALs),” *J. Mech. Behav. Biomed. Mater.*, vol. 126, p. 105063, Feb. 2022, doi: 10.1016/j.jmbbm.2021.105063.

[76] N. L. Pedersen, “Stress concentrations in keyways and optimization of keyway design,” *J. Strain Anal. Eng. Des.*, vol. 45, no. 8, pp. 593–604, Nov. 2010, doi: 10.1177/030932471004500804.

[77] R. G. Budynas, *Shigley’s Mechanical Engineering Design*, 10th edition. New York, NY: McGraw Hill, 2014.

[78] “Össur 3-Prong Socket Adapter.” https://www.ossur.com/en-ca/prosthetics/adapters/3-prong-socket-adapter (accessed Mar. 02, 2022).

[79] “‘Q’ Angle,” *Physiopedia*. https://www.physio-pedia.com/%27Q%27_Angle (accessed Feb. 24, 2022).

[80] E. Oberg, F. Jones, H. Horton, and H. Ryffel, *Machinery’s Handbook*, 29th ed. New York, NY: Industrial Press, 2012.

[81] G. H. Majzoobi and N. Daemi, “The effects of notch geometry on fatigue life using notch sensitivity factor,” *Trans. Indian Inst. Met.*, vol. 63, no. 2, pp. 547–552, Apr. 2010, doi: 10.1007/s12666-010-0080-3.

[82] “Topology Optimization Comes to SOLIDWORKS,” *Engineers Rule*, Oct. 25, 2017. https://www.engineersrule.com/topology-optimization-comes-solidworks/ (accessed Mar. 03, 2022).

[83] “Working with Teflon Washers and Spacers,” *New Process Fibre Company, Inc.* https://www.newprocess.com/general-info/ (accessed Feb. 04, 2022).

[84] H. Wen and H. Mahmoud, “New Model for Ductile Fracture of Metal Alloys. II: Reverse Loading,” *J. Eng. Mech.*, vol. 142, no. 2, p. 04015089, Feb. 2016, doi: 10.1061/(ASCE)EM.1943-7889.0001010.

[85] E. L. Grimsmo, A. Aalberg, M. Langseth, and A. H. Clausen, “Failure modes of bolt and nut assemblies under tensile loading,” *J. Constr. Steel Res.*, vol. 126, pp. 15–25, Nov. 2016, doi: 10.1016/j.jcsr.2016.06.023.

[86] ISO 898-1, “Mechanical properties of fasteners made of carbon steel and alloy steel - Part 1: Bolts, screws and studs with specified property classes — Coarse thread and fine pitch thread,” 2013.

[87] FED-STD-H28/2B, “Screw-Thread Standards for Federal Services,” 1991.

[88] EN 1993-1-8, “Design of joints,” European Committee for Standardization, 2005.

[89] EN 1993-1-1, “General rules for building,” European Committee for Standardization, 2005.

[90] “Ultimaker S3: Easy-to-use 3D printing starts here,” *https://ultimaker.com*. https://ultimaker.com/3d-printers/ultimaker-s3 (accessed May 18, 2022).

[91] ISO 10328:2016, “Prostheses - Structural testing of lower-limb prostheses - Requirements and test methods,” 2016.

[92] J. Dudok - van Velzen, H. Houdijk, W. Polomski, and C. Van Bennekom, “Usability of gait analysis in the alignment of trans-tibial prostheses: A clinical study,” *Prosthet. Orthot. Int.*, vol. 29, pp. 255–67, Jan. 2006, doi: 10.1080/03093640500238857.

[93] “Servohydraulic Dynamic Low Force Testing System Type LFV 5 kN.” https://www.walterbai.com/page/Testing_Solutions/Servohydraulic_Dynamic_Low_Force_Testing_System_Type_LFV_5_kN.php (accessed Jun. 28, 2022).

[94] A. Fanous, M. Botros, H. Gholizadeh, N. Baddour, and E. Lemaire, “Design and evaluation of a hip prosthesis simulator: A technical note,” *Prosthet. Orthot. Int.*, 2022.

[95] E. Lemaire, “TOHRC Data Logger.” The Ottawa Hospital Rehab Centre, Aug. 05, 2015.

[96] J. Charmant, “Kinovea.” 2021.

[97] L. Frlan-Vrgoc, T. S.-L. Vrbanić, D. Kraguljac, and M. Kovacević, “Functional outcome assessment of lower limb amputees and prosthetic users with a 2-minute walk test,” *Coll. Antropol.*, vol. 35, no. 4, pp. 1215–1218, Dec. 2011.

[98] A. B. Deathe and W. C. Miller, “The L Test of Functional Mobility: Measurement Properties of a Modified Version of the Timed ‘Up & Go’ Test Designed for People With Lower-Limb Amputations,” *Phys. Ther.*, vol. 85, no. 7, pp. 626–635, Jul. 2005, doi: 10.1093/ptj/85.7.626.

Appendix A: Bill of Materials

Item No.	Part Description	Material	Machined/ Purchased/ Modified	Quantity
1	Pronged Lamination Plate	2024-T4 Aluminum	Machined	1
2	Proximal Pulley	17-4 PH Stainless Steel	Machined	2
3	Proximal Pulley Plate	17-4 PH Stainless Steel	Machined	2
4	Proximal Shaft	17-4 PH Stainless Steel	Machined	1
5	Supporting Link	2024-T4 Aluminum	Machined	1
6	Distal Shaft	17-4 PH Stainless Steel	Machined	1
7	Top Plate	2024-T4 Aluminum	Machined	1
8	Motor Mounting Ring	2024-T4 Aluminum	Machined	1
9	Medial Attachment	2024-T4 Aluminum	Machined	1
10	Distal Pulley	17-4 PH Stainless Steel	Machined	2
11	Distal Pulley Plate	17-4 PH Stainless Steel	Machined	2
12	Distal Shaft	17-4 PH Stainless Steel	Machined	1
13	Anterior Brace	2024-T4 Aluminum	Machined	1
14	Posterior Brace	2024-T4 Aluminum	Machined	1
15	Double Eye Spliced Rope	Vectran®	Purchased	2
16	4mm x 4mm Key	8360 Alloy Steel	Purchased	1
17	6mm x 6mm Key	8360 Alloy Steel	Purchased	1
18	4mm x 4mm Key Rounded	8360 Alloy Steel	Purchased/Modified	1
19	6mm x 6mm Key Rounded	8360 Alloy Steel	Purchased/Modified	1
20	25mm Angular-Contact Double Row Ball Bearings	N/A	Purchased	2
21	25mm Washers	PTFE Plastic	Purchased	2
22	25mm Ring Shims	PTFE Plastic	Purchased	6
23	0.984” Wave Disk Springs	High-Carbon Steel	Purchased	4
24	O-Ring	Buna-N Rubber	Purchased	1
25	25mm External Retaining Rings	1060-1090 Spring Steel	Purchased	2
26	Socket Head M3 x 0.5 mm, 8mm	Alloy Steel	Purchased	16
27	Button Head M4 x 0.7mm, 8mm	Alloy Steel	Purchased	2
28	Socket Head M5 x 0.8mm, 16mm	Alloy Steel	Purchased	1
29	Socket Head M5 x 0.8mm, 12mm	Alloy Steel	Purchased	2
30	Socket Head M5 x 0.8mm, 14mm	Alloy Steel	Purchased	6
31	Button Head M5 x 0.8mm, 10mm	Alloy Steel	Purchased	8
32	Socket Head M6 x 1mm, 18mm	Alloy Steel	Purchased	1
33	Össur Power Knee™ Actuator	N/A	Modified	1

Appendix B: Engineering Drawings for Machined Components

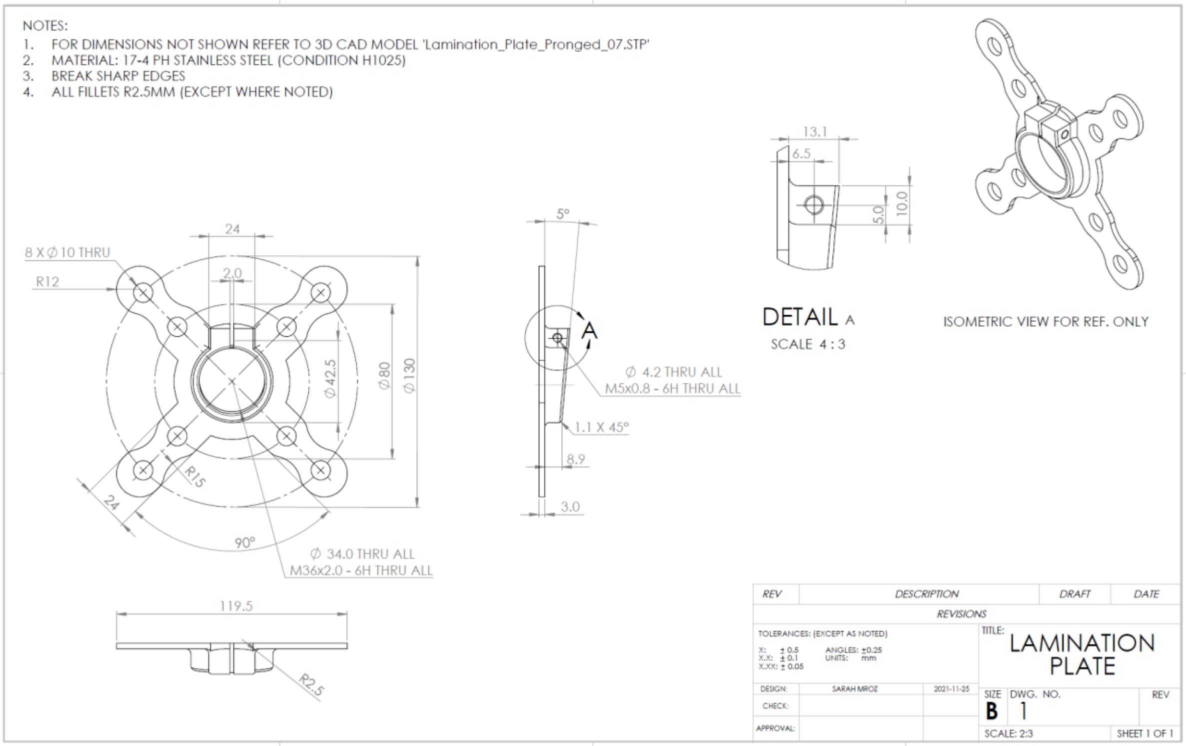

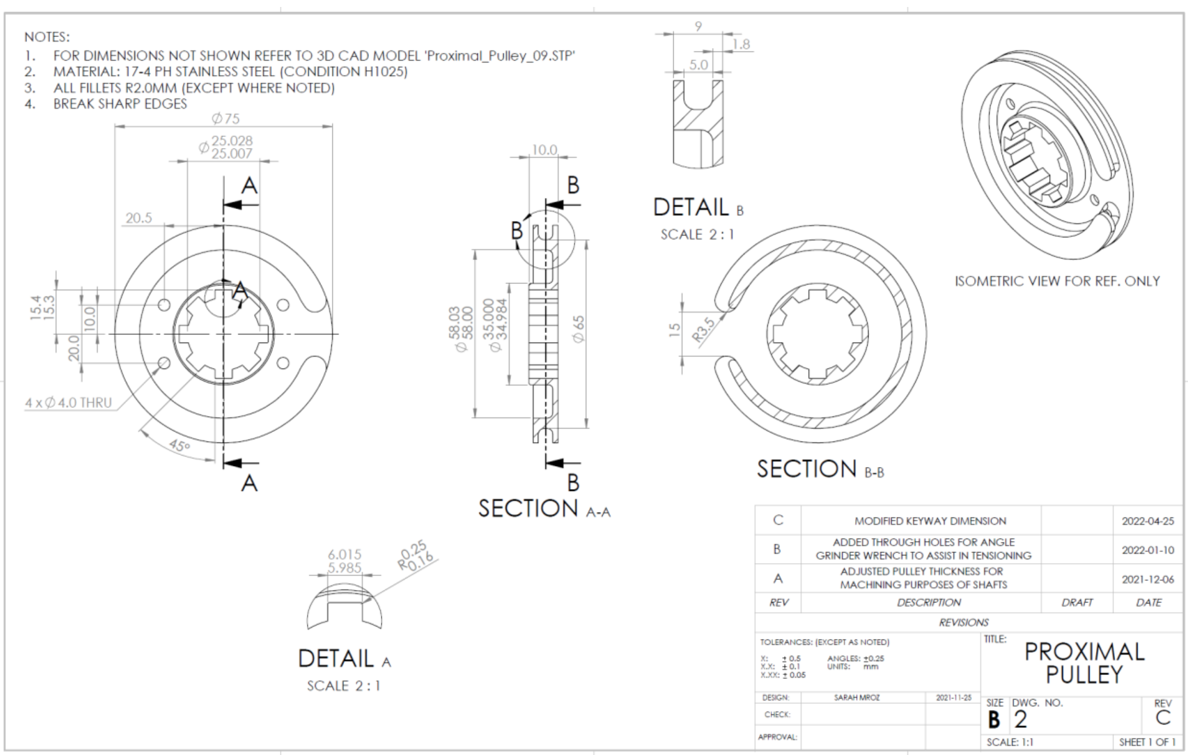

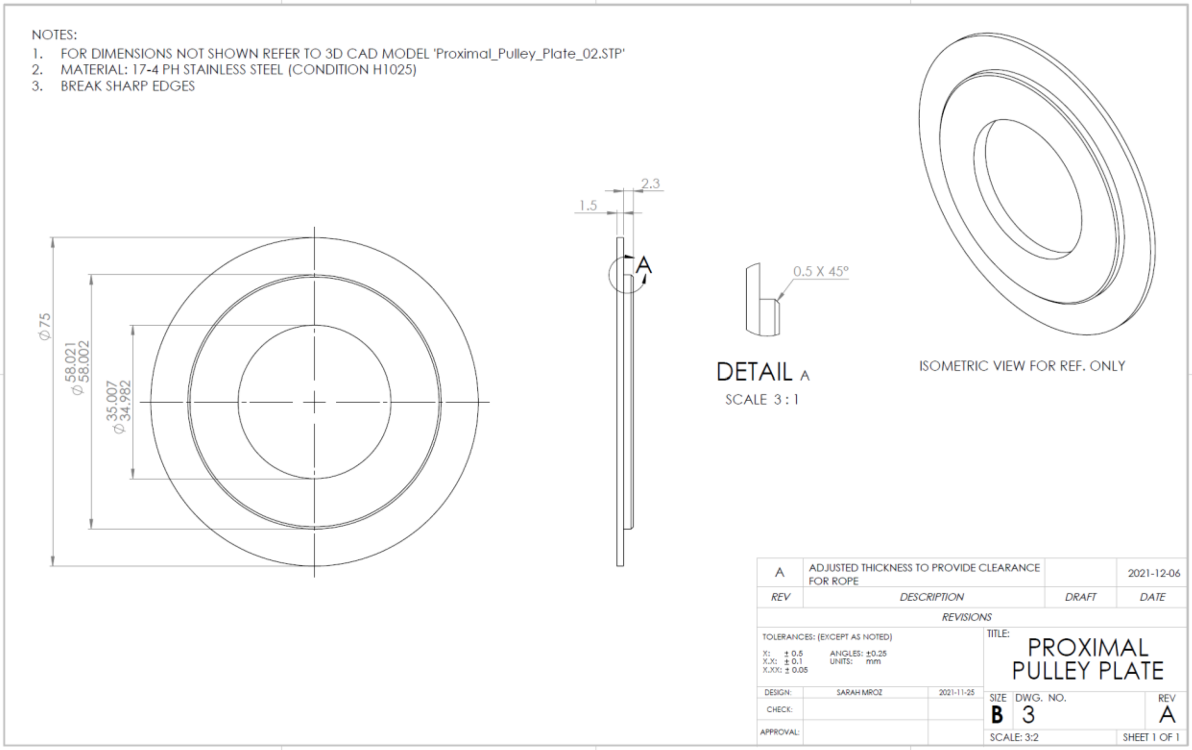
NOTES:
1. FOR DIMENSIONS NOT SHOWN REFER TO 3D CAD MODEL 'Proximal_Pulley_Plate_02.STP'
2. MATERIAL: 17-4 PH STAINLESS STEEL (CONDITION H1025)
3. BREAK SHARP EDGES
Ø75
Ø 58.021
58.002
Ø 35.007
34.982
1.5
2.3
A
0.5 X 45°
DETAIL A
SCALE 3 : 1
ISOMETRIC VIEW FOR REF. ONLY
A
ADJUSTED THICKNESS TO PROVIDE CLEARANCE FOR ROPE
2021-12-06
REV
DESCRIPTION
DRAFT
DATE
REVISIONS
TOLERANCES: (EXCEPT AS NOTED)
X: ± 0.5
X.X: ± 0.1
X.XX: ± 0.05
ANGLES: ±0.25
UNITS: mm
TITLE:
PROXIMAL PULLEY PLATE
DESIGN:
SARAH MROZ
2021-11-25
CHECK:
APPROVAL:
SIZE B
DWG. NO. 3
REV A
SCALE: 3:2
SHEET 1 OF 1

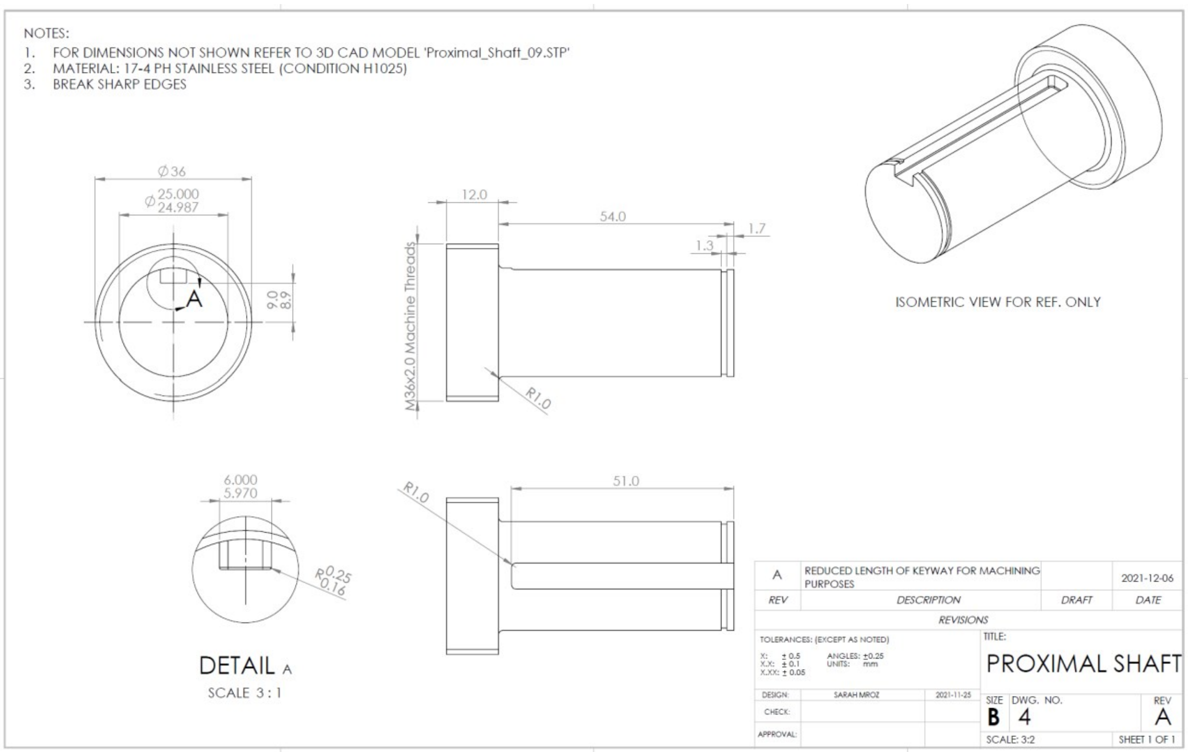
NOTES:
1. FOR DIMENSIONS NOT SHOWN REFER TO 3D CAD MODEL 'Proximal_Shaft_09.STP'
2. MATERIAL: 17-4 PH STAINLESS STEEL (CONDITION H1025)
3. BREAK SHARP EDGES
Ø36
Ø 25.000
24.987
9.0
8.9
A
12.0
54.0
1.7
1.3
M36x2.0 Machine Threads
R1.0
ISOMETRIC VIEW FOR REF. ONLY
6.000
5.970
R0.25
R0.16
DETAIL A
SCALE 3 : 1
R1.0
51.0
A
REDUCED LENGTH OF KEYWAY FOR MACHINING PURPOSES
2021-12-06
REV
DESCRIPTION
DRAFT
DATE
REVISIONS
TOLERANCES: (EXCEPT AS NOTED)
X: ± 0.5
X.X: ± 0.1
X.XX: ± 0.05
ANGLES: ±0.25
UNITS: mm
TITLE:
PROXIMAL SHAFT
DESIGN:
SARAH MROZ
2021-11-25
CHECK:
APPROVAL:
SIZE B
DWG. NO. 4
REV A
SCALE: 3:2
SHEET 1 OF 1

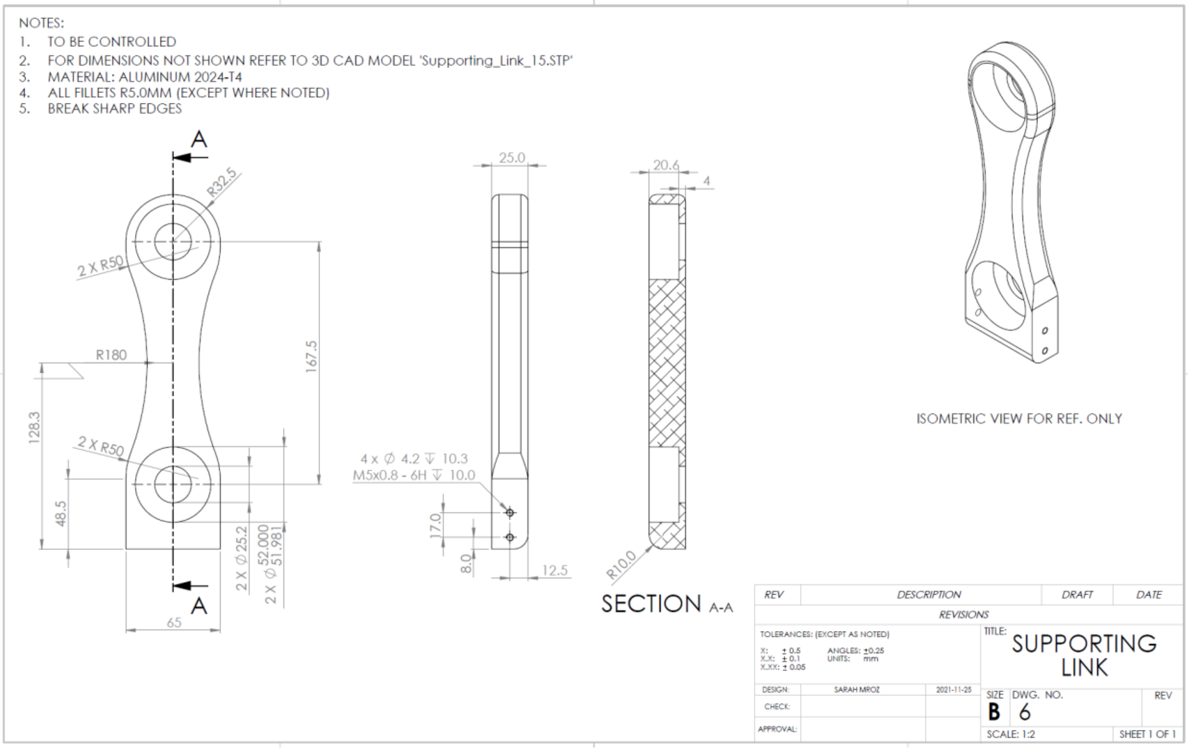
NOTES:
1. TO BE CONTROLLED
2. FOR DIMENSIONS NOT SHOWN REFER TO 3D CAD MODEL 'Supporting_Link_15.STP'
3. MATERIAL: ALUMINUM 2024-T4
4. ALL FILLETS R5.0MM (EXCEPT WHERE NOTED)
5. BREAK SHARP EDGES
A
R32.5
2 X R50
R180
167.5
128.3
48.5
2 X Ø 25.2
2 X Ø 52.000 51.981
65
25.0
4 x Ø 4.2 ↧ 10.3
M5x0.8 - 6H ↧ 10.0
17.0
8.0
12.5
20.6
4
R10.0
SECTION A-A
ISOMETRIC VIEW FOR REF. ONLY
REV
DESCRIPTION
DRAFT
DATE
REVISIONS
TOLERANCES: (EXCEPT AS NOTED)
X: ± 0.5
X.X: ± 0.1
X.XX: ± 0.05
ANGLES: ±0.25
UNITS: mm
TITLE:
SUPPORTING LINK
DESIGN:
SARAH MROZ
2021-11-25
CHECK:
APPROVAL:
SIZE
B
DWG. NO.
6
REV
SCALE: 1:2
SHEET 1 OF 1

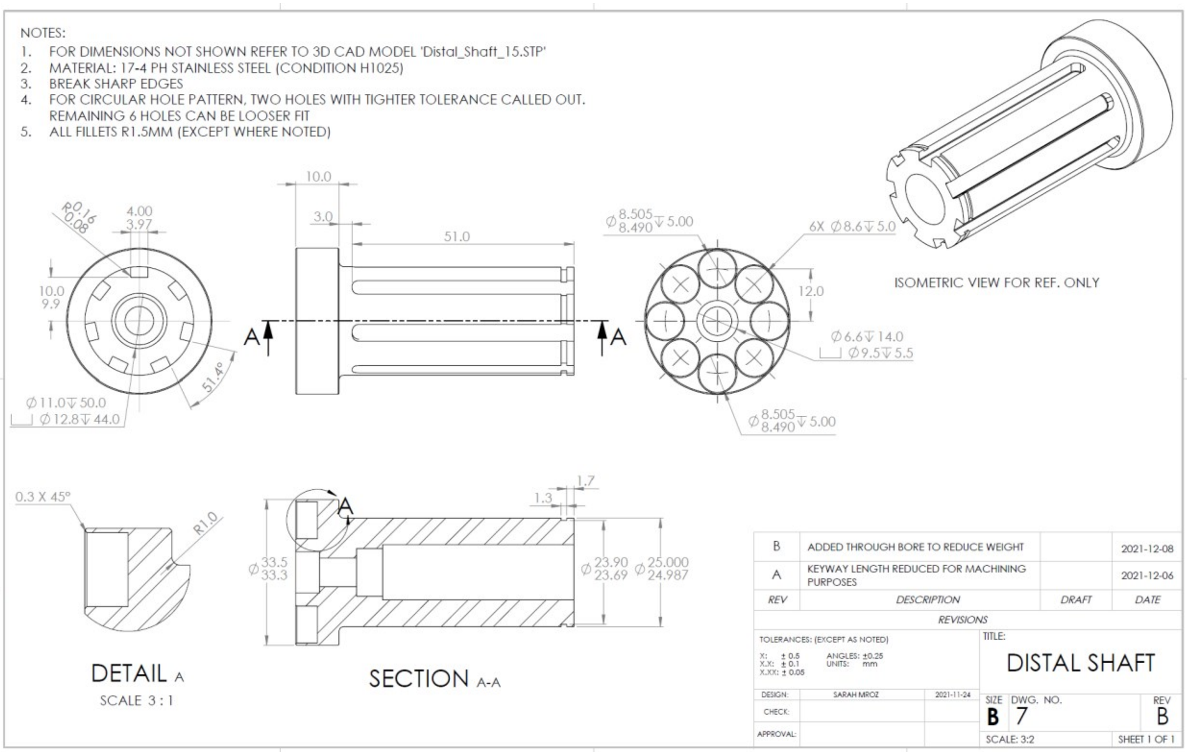
NOTES:
1. FOR DIMENSIONS NOT SHOWN REFER TO 3D CAD MODEL 'Distal_Shaft_15.STP'
2. MATERIAL: 17-4 PH STAINLESS STEEL (CONDITION H1025)
3. BREAK SHARP EDGES
4. FOR CIRCULAR HOLE PATTERN, TWO HOLES WITH TIGHTER TOLERANCE CALLED OUT. REMAINING 6 HOLES CAN BE LOOSER FIT
5. ALL FILLETS R1.5MM (EXCEPT WHERE NOTED)
R0.16 R0.08
4.00 3.97
10.0 9.9
51.4°
Ø 11.0 ↧ 50.0
⌴ Ø 12.8 ↧ 44.0
10.0
3.0
51.0
A
Ø 8.505 8.490 ↧ 5.00
6X Ø 8.6 ↧ 5.0
12.0
Ø 6.6 ↧ 14.0
⌴ Ø 9.5 ↧ 5.5
Ø 8.505 8.490 ↧ 5.00
ISOMETRIC VIEW FOR REF. ONLY
0.3 X 45°
R1.0
DETAIL A
SCALE 3 : 1
1.7
1.3
Ø 33.5 33.3
Ø 23.90 23.69
Ø 25.000 24.987
SECTION A-A
B
ADDED THROUGH BORE TO REDUCE WEIGHT
2021-12-08
A
KEYWAY LENGTH REDUCED FOR MACHINING PURPOSES
2021-12-06
REV
DESCRIPTION
DRAFT
DATE
REVISIONS
TOLERANCES: (EXCEPT AS NOTED)
X: ± 0.5
X.X: ± 0.1
X.XX: ± 0.05
ANGLES: ±0.25
UNITS: mm
TITLE:
DISTAL SHAFT
DESIGN:
SARAH MROZ
2021-11-24
CHECK:
APPROVAL:
SIZE
B
DWG. NO.
7
REV
B
SCALE: 3:2
SHEET 1 OF 1

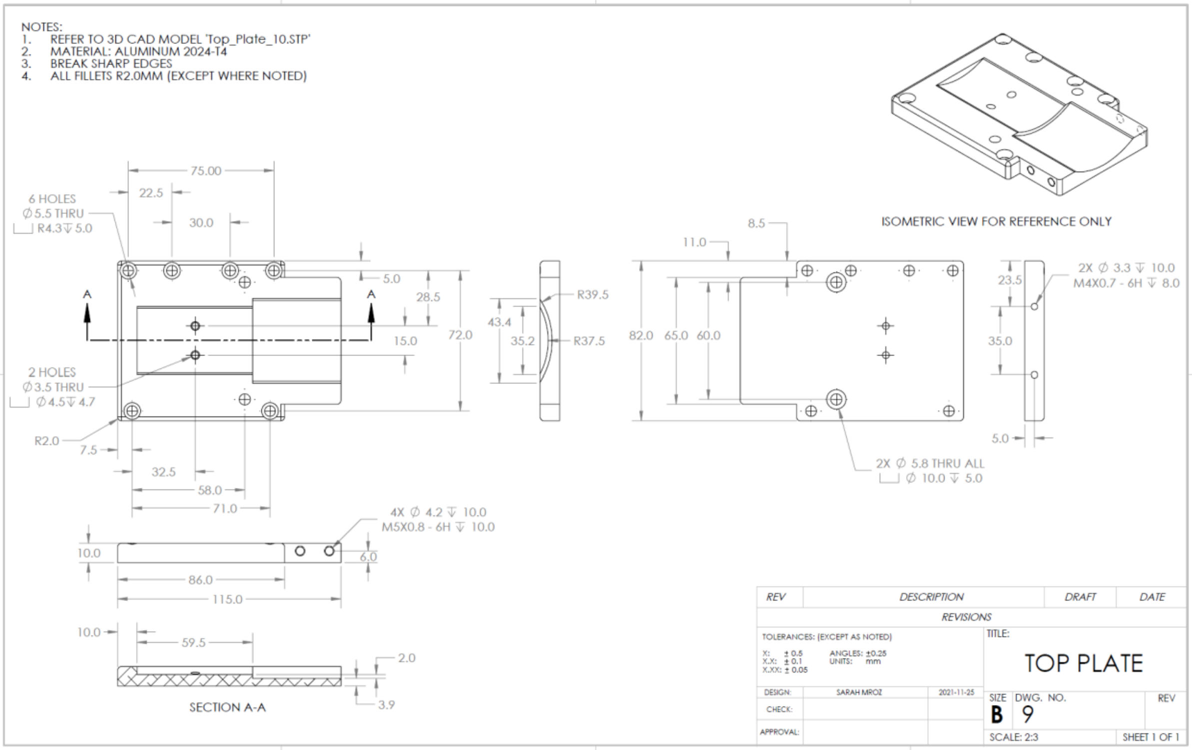
NOTES:
1. REFER TO 3D CAD MODEL 'Top_Plate_10.STP'
2. MATERIAL: ALUMINUM 2024-T4
3. BREAK SHARP EDGES
4. ALL FILLETS R2.0MM (EXCEPT WHERE NOTED)
ISOMETRIC VIEW FOR REFERENCE ONLY
6 HOLES
∅5.5 THRU
R4.3 ↧ 5.0
2 HOLES
∅3.5 THRU
∅4.5 ↧ 4.7
2X ∅ 3.3 ↧ 10.0
M4X0.7 - 6H ↧ 8.0
2X ∅ 5.8 THRU ALL
∅ 10.0 ↧ 5.0
4X ∅ 4.2 ↧ 10.0
M5X0.8 - 6H ↧ 10.0
SECTION A-A
REV
DESCRIPTION
DRAFT
DATE
REVISIONS
TOLERANCES: (EXCEPT AS NOTED)
X: ± 0.5
X.X: ± 0.1
X.XX: ± 0.05
ANGLES: ±0.25
UNITS: mm
DESIGN: SARAH MROZ 2021-11-25
CHECK:
APPROVAL:
TITLE:
TOP PLATE
SIZE B
DWG. NO. 9
REV
SCALE: 2:3
SHEET 1 OF 1

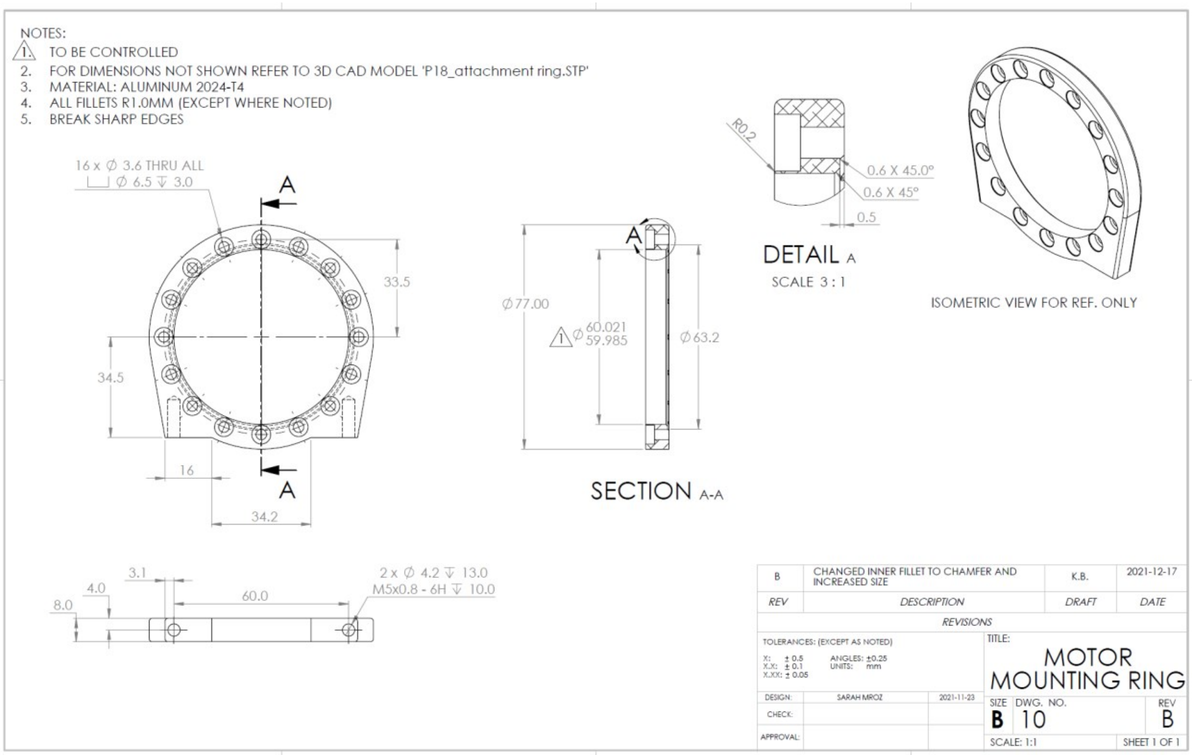
NOTES:
1. TO BE CONTROLLED
2. FOR DIMENSIONS NOT SHOWN REFER TO 3D CAD MODEL 'P18_attachment ring.STP'
3. MATERIAL: ALUMINUM 2024-T4
4. ALL FILLETS R1.0MM (EXCEPT WHERE NOTED)
5. BREAK SHARP EDGES
16 x ∅ 3.6 THRU ALL
∅ 6.5 ↧ 3.0
0.6 X 45.0°
0.6 X 45°
DETAIL A
SCALE 3 : 1
ISOMETRIC VIEW FOR REF. ONLY
SECTION A-A
2 x ∅ 4.2 ↧ 13.0
M5x0.8 - 6H ↧ 10.0
B
CHANGED INNER FILLET TO CHAMFER AND INCREASED SIZE
K.B.
2021-12-17
REV
DESCRIPTION
DRAFT
DATE
REVISIONS
TOLERANCES: (EXCEPT AS NOTED)
X: ± 0.5
X.X: ± 0.1
X.XX: ± 0.05
ANGLES: ±0.25
UNITS: mm
DESIGN: SARAH MROZ 2021-11-23
CHECK:
APPROVAL:
TITLE:
MOTOR MOUNTING RING
SIZE B
DWG. NO. 10
REV B
SCALE: 1:1
SHEET 1 OF 1

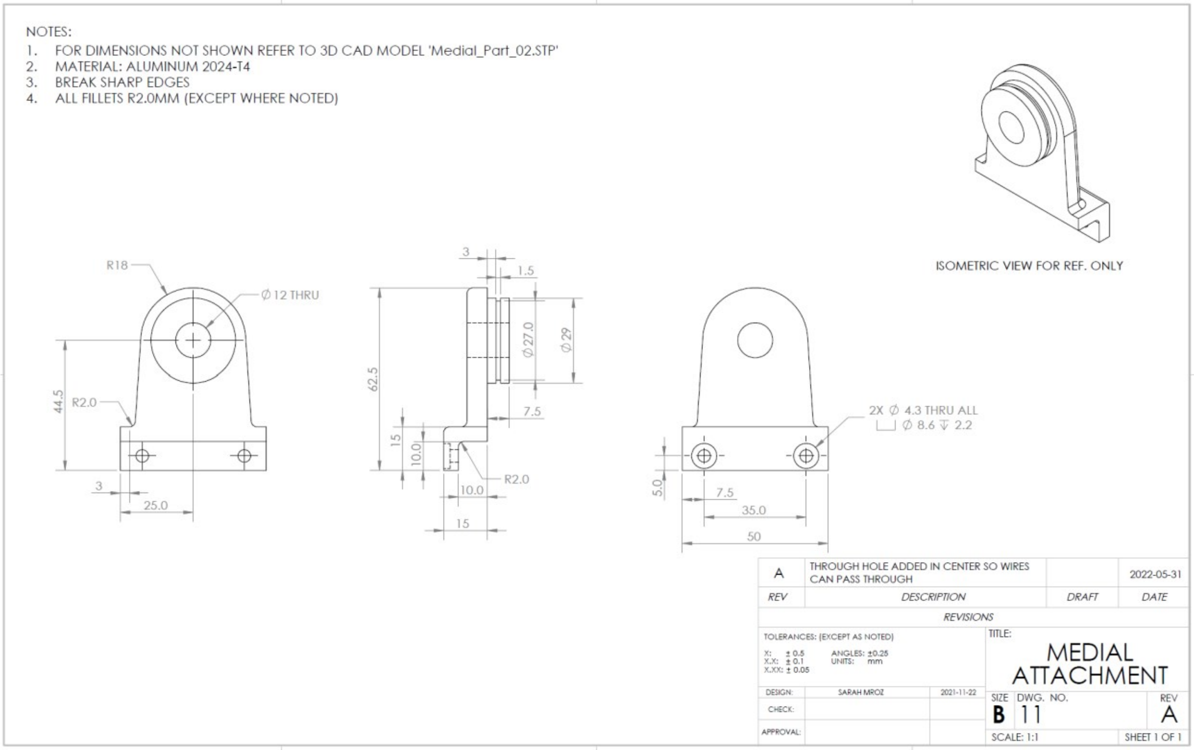
NOTES:
1. FOR DIMENSIONS NOT SHOWN REFER TO 3D CAD MODEL 'Medial_Part_02.STP'
2. MATERIAL: ALUMINUM 2024-T4
3. BREAK SHARP EDGES
4. ALL FILLETS R2.0MM (EXCEPT WHERE NOTED)
ISOMETRIC VIEW FOR REF. ONLY
R18
Ø 12 THRU
44.5
R2.0
3
25.0
62.5
1.5
Ø27.0
Ø29
7.5
15
10.0
R2.0
2X Ø 4.3 THRU ALL
⌴ Ø 8.6 ↧ 2.2
5.0
35.0
50
A
THROUGH HOLE ADDED IN CENTER SO WIRES CAN PASS THROUGH
2022-05-31
REV
DESCRIPTION
DRAFT
DATE
REVISIONS
TOLERANCES: (EXCEPT AS NOTED)
X: ± 0.5
X.X: ± 0.1
X.XX: ± 0.05
ANGLES: ±0.25
UNITS: mm
TITLE:
MEDIAL ATTACHMENT
DESIGN:
SARAH MROZ
2021-11-22
CHECK:
APPROVAL:
SIZE
B
DWG. NO.
11
REV
A
SCALE: 1:1
SHEET 1 OF 1

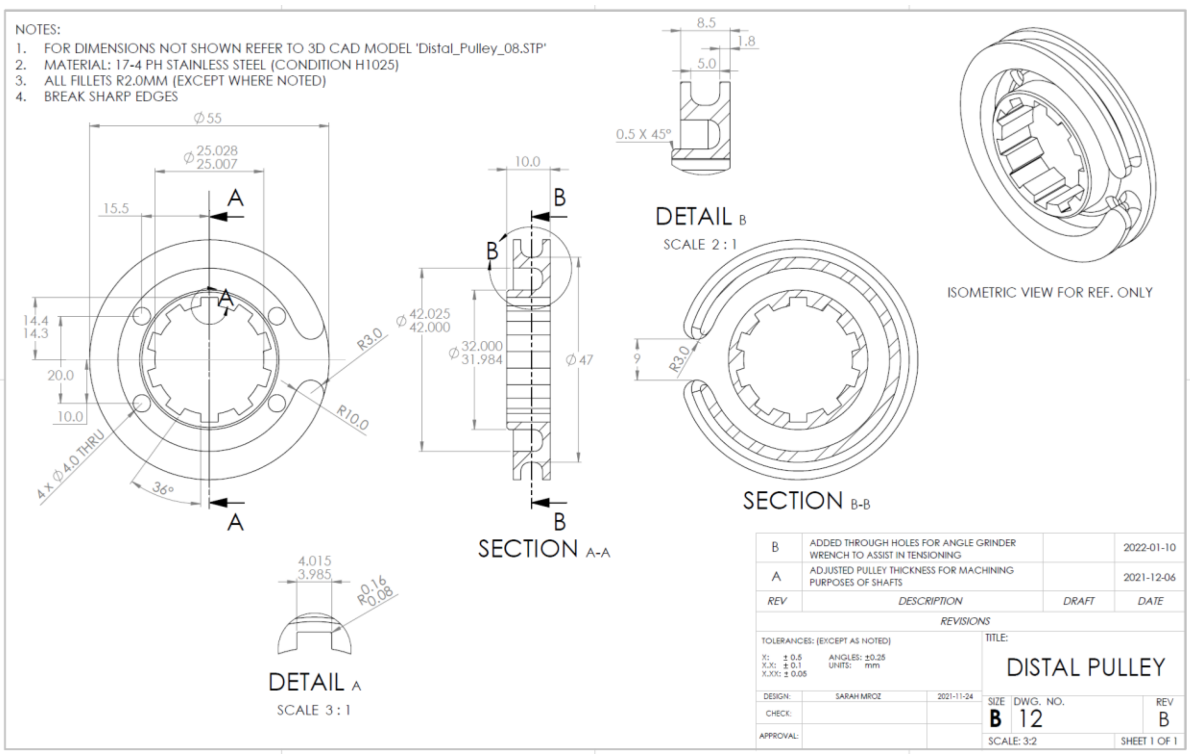
NOTES:
1. FOR DIMENSIONS NOT SHOWN REFER TO 3D CAD MODEL 'Distal_Pulley_08.STP'
2. MATERIAL: 17-4 PH STAINLESS STEEL (CONDITION H1025)
3. ALL FILLETS R2.0MM (EXCEPT WHERE NOTED)
4. BREAK SHARP EDGES
Ø55
Ø 25.028
25.007
15.5
14.4
14.3
20.0
10.0
4 x Ø4.0 THRU
36°
R3.0
R10.0
A
10.0
B
Ø 42.025
42.000
Ø 32.000
31.984
Ø47
SECTION A-A
8.5
1.8
5.0
0.5 X 45°
DETAIL B
SCALE 2 : 1
9
R3.0
SECTION B-B
ISOMETRIC VIEW FOR REF. ONLY
4.015
3.985
R0.16
0.08
DETAIL A
SCALE 3 : 1
B
ADDED THROUGH HOLES FOR ANGLE GRINDER WRENCH TO ASSIST IN TENSIONING
2022-01-10
A
ADJUSTED PULLEY THICKNESS FOR MACHINING PURPOSES OF SHAFTS
2021-12-06
REV
DESCRIPTION
DRAFT
DATE
REVISIONS
TOLERANCES: (EXCEPT AS NOTED)
X: ± 0.5
X.X: ± 0.1
X.XX: ± 0.05
ANGLES: ±0.25
UNITS: mm
TITLE:
DISTAL PULLEY
DESIGN:
SARAH MROZ
2021-11-24
CHECK:
APPROVAL:
SIZE
B
DWG. NO.
12
REV
B
SCALE: 3:2
SHEET 1 OF 1

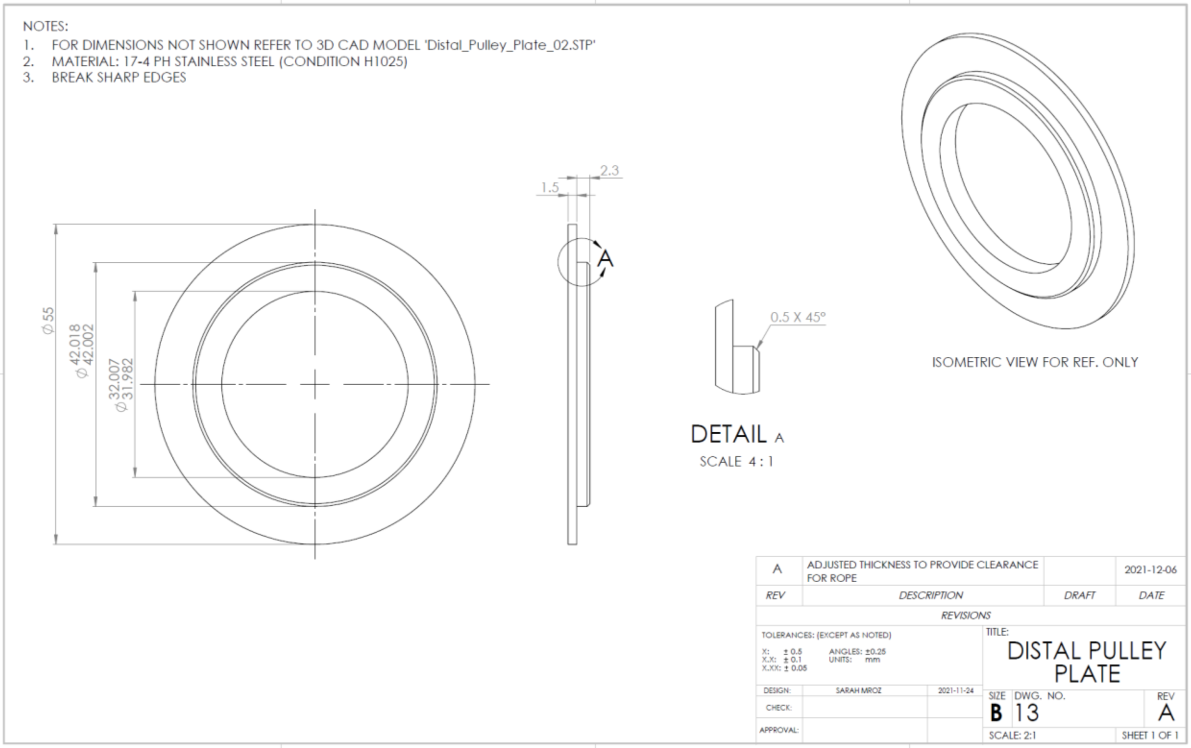
NOTES:
1. FOR DIMENSIONS NOT SHOWN REFER TO 3D CAD MODEL 'Distal_Pulley_Plate_02.STP'
2. MATERIAL: 17-4 PH STAINLESS STEEL (CONDITION H1025)
3. BREAK SHARP EDGES
Ø 55
Ø 42.018
Ø 42.002
Ø 32.007
Ø 31.982
1.5
2.3
A
0.5 X 45°
DETAIL A
SCALE 4 : 1
ISOMETRIC VIEW FOR REF. ONLY
A
ADJUSTED THICKNESS TO PROVIDE CLEARANCE FOR ROPE
2021-12-06
REV
DESCRIPTION
DRAFT
DATE
REVISIONS
TOLERANCES: (EXCEPT AS NOTED)
X: ± 0.5
X.X: ± 0.1
X.XX: ± 0.05
ANGLES: ±0.25
UNITS: mm
TITLE:
DISTAL PULLEY PLATE
DESIGN:
SARAH MROZ
2021-11-24
CHECK:
APPROVAL:
SIZE
B
DWG. NO.
13
REV
A
SCALE: 2:1
SHEET 1 OF 1

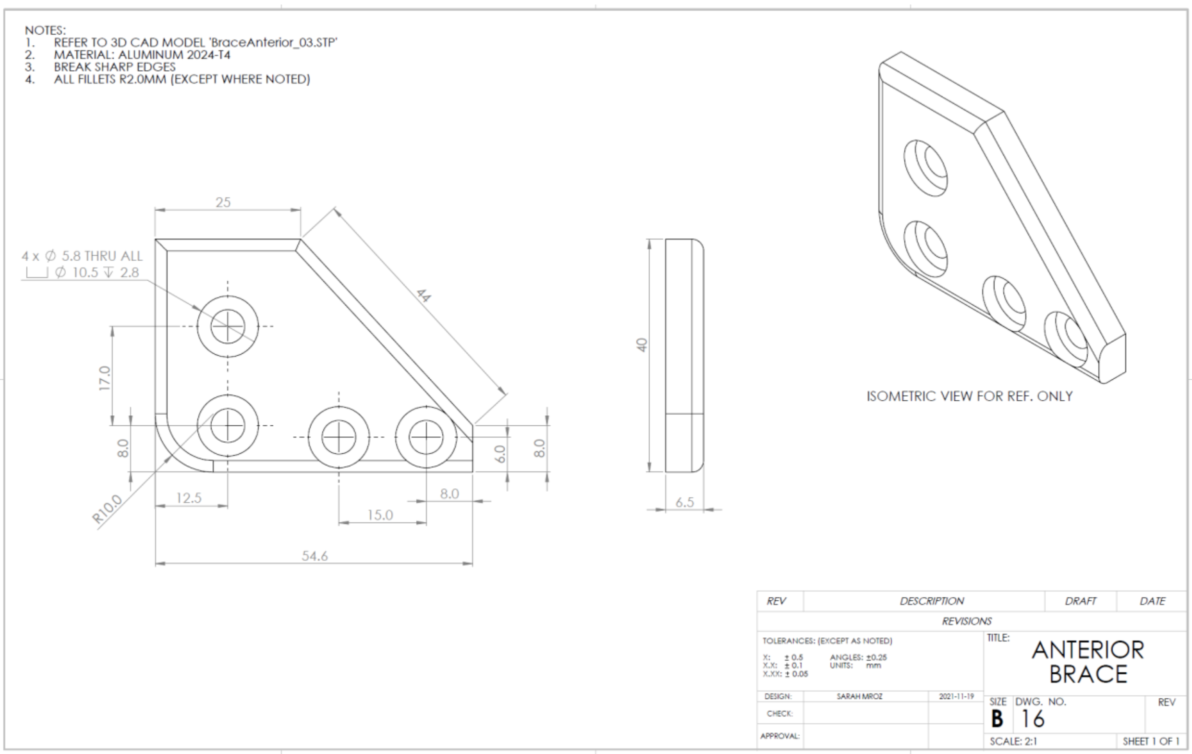
NOTES:
1. REFER TO 3D CAD MODEL 'BraceAnterior_03.STP'
2. MATERIAL: ALUMINUM 2024-T4
3. BREAK SHARP EDGES
4. ALL FILLETS R2.0MM (EXCEPT WHERE NOTED)
25
44
4 x Ø 5.8 THRU ALL
⌴ Ø 10.5 ↧ 2.8
17.0
8.0
R10.0
12.5
15.0
8.0
6.0
8.0
54.6
40
6.5
ISOMETRIC VIEW FOR REF. ONLY
REV
DESCRIPTION
DRAFT
DATE
REVISIONS
TOLERANCES: (EXCEPT AS NOTED)
X: ± 0.5
X.X: ± 0.1
X.XX: ± 0.05
ANGLES: ±0.25
UNITS: mm
TITLE:
ANTERIOR BRACE
DESIGN:
SARAH MROZ
2021-11-19
CHECK:
APPROVAL:
SIZE
B
DWG. NO.
16
REV
SCALE: 2:1
SHEET 1 OF 1

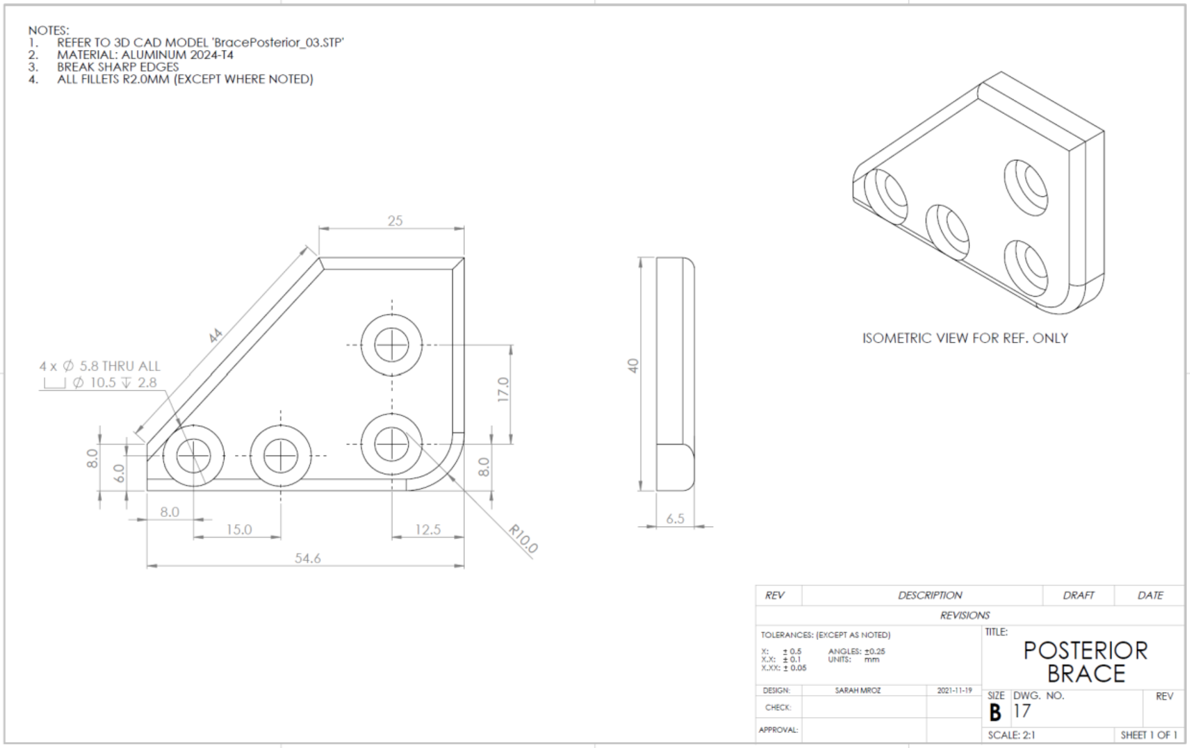
NOTES:
1. REFER TO 3D CAD MODEL 'BracePosterior_03.STP'
2. MATERIAL: ALUMINUM 2024-T4
3. BREAK SHARP EDGES
4. ALL FILLETS R2.0MM (EXCEPT WHERE NOTED)
25
44
4 x ∅ 5.8 THRU ALL
⌴ ∅ 10.5 ↧ 2.8
17.0
8.0
6.0
8.0
8.0
15.0
12.5
54.6
R10.0
40
6.5
ISOMETRIC VIEW FOR REF. ONLY
REV
DESCRIPTION
DRAFT
DATE
REVISIONS
TOLERANCES: (EXCEPT AS NOTED)
X: ± 0.5
X.X: ± 0.1
X.XX: ± 0.05
ANGLES: ±0.25
UNITS: mm
TITLE:
POSTERIOR BRACE
DESIGN: SARAH MROZ 2021-11-19
CHECK:
APPROVAL:
SIZE B
DWG. NO. 17
REV
SCALE: 2:1
SHEET 1 OF 1

Appendix C: Certificate of Ethics Approval

25/08/2021

Université d'Ottawa | University of Ottawa

Bureau d'éthique et d'intégrité de la recherche | Office of Research Ethics and Integrity

CERTIFICAT D'APPROBATION ÉTHIQUE | CERTIFICATE OF ETHICS APPROVAL

Numéro du dossier / Ethics File Number	H-04-21-6811
Titre du projet / Project Title	DESIGNING AND EVALUATION OF A HIP DISARTICULATION PROSTHESIS SIMULATOR
Type de projet / Project Type	Recherche de professeur / Professor's research project
Statut du projet / Project Status	Approuvé / Approved
Date d'approbation (jj/mm/aaaa) / Approval Date (dd/mm/yyyy)	25/08/2021
Date d'expiration (jj/mm/aaaa) / Expiry Date (dd/mm/yyyy)	24/08/2022

Équipe de recherche / Research Team

Chercheur / Researcher	Affiliation	Role
Edward LEMAIRE	Département de médecine / Department of Medicine	Chercheur Principal / Principal Investigator
Amir FANOUS	Département de génie mécanique / Department of Mechanical Engineering	Étudiant-chercheur / Student-researcher
Michael BOTROS	Département de génie mécanique / Department of Mechanical Engineering	Assistant de recherche / Research Assistant
Natalie BADDOUR	Département de génie mécanique / Department of Mechanical Engineering	Co-chercheur principal / Co-principal investigator
Hossein GHOLIZADEH	Département de génie mécanique / Department of Mechanical Engineering	Co-chercheur / Co-investigator

Conditions spéciales ou commentaires / Special conditions or comments

550, rue Cumberland, pièce 154 | 550 Cumberland Street, Room 154
Ottawa (Ontario) K1N 6N5 Canada | Ottawa, Ontario K1N 6N5 Canada

613-562-5387 • 613-562-5338 • ethique@uOttawa.ca / ethics@uOttawa.ca
www.recherche.uottawa.ca/deontologie | www.recherche.uottawa.ca/ethics

25/08/2021

Université d'Ottawa | University of Ottawa

Bureau d'éthique et d'intégrité de la recherche | Office of Research Ethics and Integrity

Le Comité d'éthique de la recherche (CÉR) de l'Université d'Ottawa, opérant conformément à l'*Énoncé de politique des Trois conseils* (2014) et toutes autres lois et tous règlements applicables, a examiné et approuvé la demande d'éthique du projet de recherche ci-nommé.

L'approbation est valide pour la durée indiquée plus haut et est sujette aux conditions énumérées dans la section intitulée "Conditions Spéciales ou Commentaires". Le formulaire « Renouvellement ou Fermeture de Projet » doit être complété quatre semaines avant la date d'échéance indiquée ci-haut afin de demander un renouvellement de cette approbation éthique ou afin de fermer le dossier.

Toutes modifications apportées au projet doivent être approuvées par le CÉR avant leur mise en place, sauf si le participant doit être retiré en raison d'un danger immédiat ou s'il s'agit d'un changement ayant trait à des éléments administratifs ou logistiques du projet. Les chercheurs doivent aviser le CÉR dans les plus brefs délais de tout changement pouvant augmenter le niveau de risque aux participants ou pouvant affecter considérablement le déroulement du projet, rapporter tout évènement imprévu ou indésirable et soumettre toute nouvelle information pouvant nuire à la conduite du projet ou à la sécurité des participants.

The University of Ottawa Research Ethics Board, which operates in accordance with the *Tri-Council Policy Statement* (2014) and other applicable laws and regulations, has examined and approved the ethics application for the above-named research project.

Ethics approval is valid for the period indicated above and is subject to the conditions listed in the section entitled "Special Conditions or Comments". The "Renewal/Project Closure" form must be completedfour weeks before the above-referenced expiry date to request a renewal of this ethics approval or closure of the file.

Any changes made to the project must be approved by the REB before being implemented, except when necessary to remove participants from immediate endangerment or when the modification(s) only pertain to administrative or logistical components of the project. Investigators must also promptly alert the REB of any changes that increase the risk to participant(s), any changes that considerably affect the conduct of the project, all unanticipated and harmful events that occur, and new information that may negatively affect the conduct of the project or the safety of the participant(s).

Germain ZONGO
Responsable d'éthique en recherche / Protocol Officer
Pour/For **Daniel LAGAREC** Président(e) du/ Chair of the **Comité d'éthique de la recherche en sciences de la santé et sciences / Health Sciences and Sciences Research Ethics Board**

550, rue Cumberland, pièce 154 | 550 Cumberland Street, Room 154
Ottawa (Ontario) K1N 6N5 Canada | Ottawa, Ontario K1N 6N5 Canada

613-562-5387 • 613-562-5338 • ethique@uOttawa.ca / ethics@uOttawa.ca
www.recherche.uottawa.ca/deontologie | www.recherche.uottawa.ca/ethics